Heinz-Nixdorf Lehrstuhl für Medizinische Elektronik

# Analysis of Biological Signals with Multifunctional Bioelectronic Sensor Chips on Living Cells

Roza Elena Motrescu

Vollständiger Abdruck der von Fakultät für Elektrotechnik und Informationstechnik der Technische Universität München zur Erlangung des akademischen Grades eines Doktors der Naturwissenschaften genehmigten Dissertation.

| | |
|---|---|
| **Vorsitzender:** | **Univ.- Prof. Dr. - Ing. habil. A.W. Koch** |
| **Prüfer der Dissertation:** | |
| | **1. Univ.- Prof. Dr. rer. nat. habil. B. Wolf** |
| | **2. Univ.- Prof. Dr. agr., Dr. rer. nat. habil. A. Melzer** |

Die Dissertation wurde am 30.06.2004 bei der Technischen Universität München eingereicht und durch die Fakultät für Elektrotechnik und Informationstechnik am 12.10.2004 angenommen.

**Analysis of Biological Signals with Multifunctional Bioelectronic Sensor Chips on Living Cells**

Multifunktionale bioelektronische Sensorchips (auf Glas- Keramik- und Siliziumsubstraten) ermöglichen eine neuartige dynamische Messung des zellulären Signalverhaltens anhand mikrophysiologischer Parameter (Veränderungen im Zellmetabolismus und der Zellmorphologie). Vergleiche zwischen zellulären Assays auf Sensorchip-Basis und biochemischen Standard-Assays ergaben neue Erkenntnisse über Wirkungsmechanismen von Stoffen aus verschiedenen Substanzklassen. In einem weiteren Forschungsansatz wurde gezielt an der Entwicklung eines Assays für ein dynamisches Monitoring des invasiven Verhaltens von Tumorzellen gearbeitet.

**Analysis of Biological Signals with Multifunctional Bioelectronic Sensor Chips on Living Cells**

Multifunctional bioelectronic Sensorchips (on glass- ceramic- and silicon substrate) allow a dynamic analysis of cellular signalling behaviour based on microphysiological parameters (changes in cell metabolism and cell morphology). A comparison between cell assays based on sensor chips and biochemical standard assays yielded new knowledge about the action mechanism of different substances. In an additional approach the development of an assay for a dynamic monitoring of the invasive behaviour of tumor cells was pursued.

# Acknowledgements

Firstly I would like to thank Prof. Dr. Bernhard Wolf, my supervisor, for all his help and motivation during my Ph.D. studies, without which this work would not have been possible.
I am also very grateful to Dr. Martin Brischwein and Dr. habil. Angela M. Otto for many informative discussions and for their professional help in organising the experimental work as well as proof reading this thesis.

I would also like to thank:

Dr. Stefan Zahler for his prompt and skilled help in explaining and performing various experiments.

Mr. Alfred Michelfelder and Mrs. Gudrun Teschner for their technical support in the laboratory and for the friendly atmosphere that they helped to create.

Mrs. Margarethe Remm for her support with the production of the glass chips.

Miss Eléonore Cabala for her professional and friendly collaboration concerning the cell monitoring system and for the many useful discussions.

Mr. Johann Ressler for his support with all things concerning computers and computer networks.

Mr. Robert Arbogast and Mr. Wolfgang Ruppert for their support with the constructions and modifications on sensor chip system.

To Sabine Drechsler and all my other colleagues from Rostock, where I began this work, and who introduced me to Germany. Especially I want to thank my family, Martin and my friends in Germany and Romania for their continued support and understanding. Finally to all those people, I've inevitably not mentioned, and who have helped me along the way – Thank you.

# Abreviations

| | |
|---|---|
| cAMP | cyclic adenosine monophosphate |
| 5´-AMP | adenosine 5´-monophosphate |
| ATP | adenosine triphosphate |
| $C_{par}$ | capacitance component of impedance |
| CAA | chloroacetaldehyde |
| CB | cytochalasin B |
| CMS | cell monitoring system |
| $c^i$ | concentration of ions inside of membrane |
| $c^o$ | concentration of ions outside of membrane |
| DMSO | Dimethyl sulfoxide |
| EBS | Earle`s balanced salts |
| f | frequency |
| F | Faraday constant |
| FCS | fetal calf serum |
| $FADH_2$ | flavin adenine dinucleotide |
| $H_2$DCFDA | 2`,7`-dichlorodihydro fluorescein diacetate, indicator for intracellular reactive oxygen species |
| IDES | interdigital electrode structures |
| $I_{eff}$ | RMS (root mean square) current |
| Ig-like CAMs | immunoglobulin superfamily of proteins |
| ISFET | ion sensitive field effect transistors |
| j | imaginary number |
| JAK | Janus kinase |
| JC-1 | fluorescence dye 15,5`,6,6`-tetrachloro-1,1`,3,3`-tetraethylbenzimidazolylcarbocianine, iodide indicator for mitochondrial membrane potential |
| ln | natural logharitm |
| MAP-kinase | mitogen-activated protein kinase |
| $NADH^+$ | nicotinamide adenine dinucleotide |
| P | permeability coefficient |
| PBS | phosphate buffered saline |

| | |
|---|---|
| PDK | phosphoinositide-dependent protein kinase |
| PKA | protein kinase A |
| PKB | protein kinase B |
| PKC | protein kinase C |
| R | gas constant |
| RTKs | tyrosine kinase receptors |
| ROS | reactive oxygen species |
| STAT | signal transducers and activators of transcription |
| T | absolute temperature |
| $U_{eff}$ | RMS (root mean square) voltage |
| $\underline{Z}$ | complex impedance |
| Z` | real part of the impedance |
| Z`` | imaginary part of the impedance |
| Φ | phase angle |
| $\Delta\psi$ | difference of the electric potential across the cell membrane |
| $\Delta\mu(H^+)$ | difference between the electrochemical potential of a proton inside and outside of the inner mitochondrial membrane |
| ΔpH | difference of the pH values across the membrane |
| ν | index for cations |
| μ | index for anions |

# Contents

# 1. Introduction

## 1.1 Cell signalling

Cells are systems with a complex nanostructural organisation (Figure 1.1). They are involved in a continuous exchange with their environment leading to adaptive responses in cellular activity. The barrier between the external and the intracellular environment is formed by the cell membrane. A cell membrane is a dynamic, fluid structure containing lipid molecules organised into a lipid bilayer (about 5 nm thick) with embedded protein molecules. This structure is described by the so called fluid mosaic model (Alberts, et al., 2002).

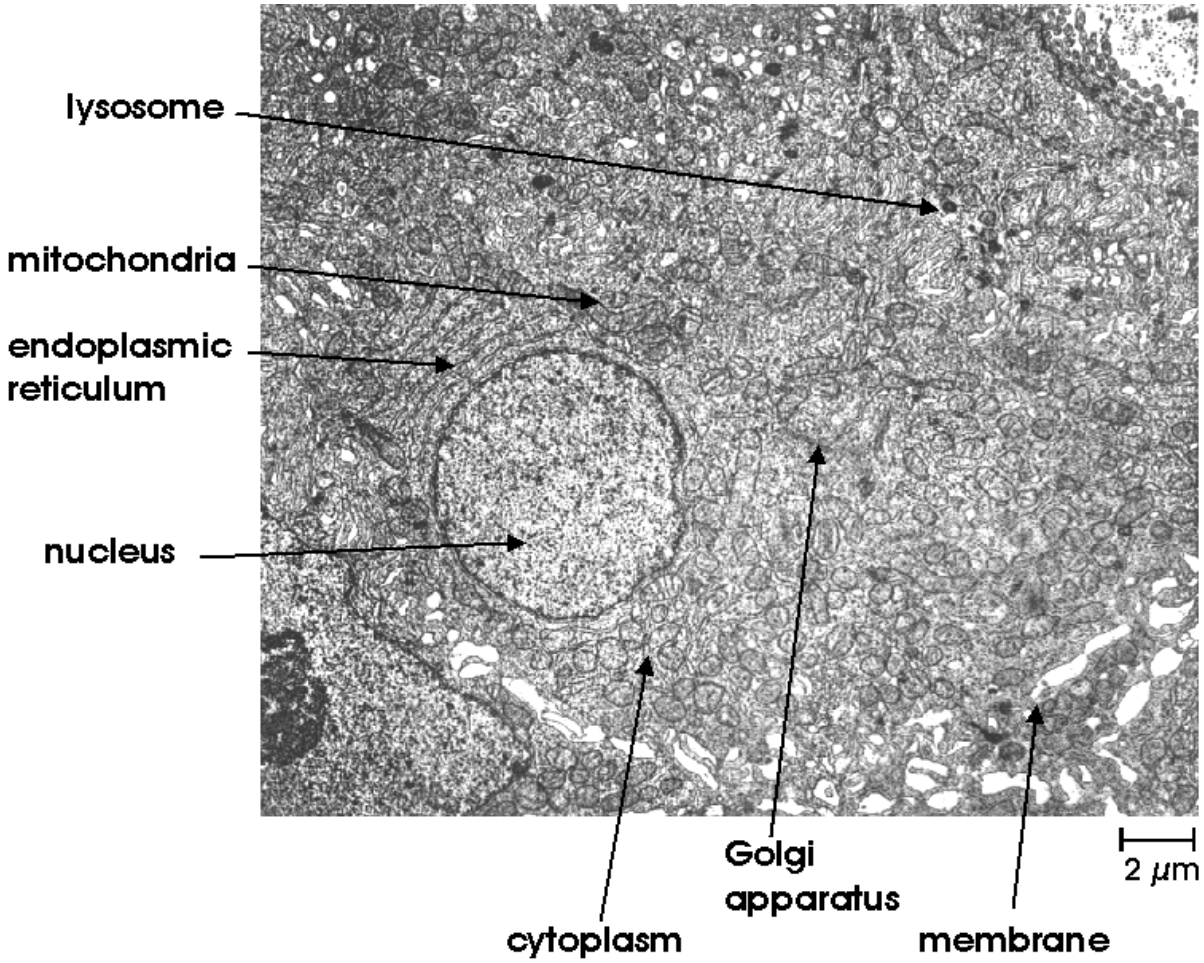


**Figure 1.1:** Electron micrograph of an epithelial cell from colon tissue demonstrating the high degree of compartmentation and the diversity of ultra-structural patterns (Wolf, et al., 1998).

Cell membranes contribute to the maintenance of the cytosol (intracellular fluid) composition which is different to that of the extracellular fluid. The lipid bilayer is impermeable to most water soluble molecules.

For a selective sensing of input signals from the outside the cell uses specific receptor proteins. These transmit, integrate and amplify the signals to elicit an immediate response or to change gene activities in the cell nucleus. There are three categories of cell surface receptors: (1) Ion-channel-linked receptors are transmitter-gated ion channels able to enhance the passive transport of different ions ($Ca^{2+}$, $K^+$, $Na^+$, $H^+$, $Cl^-$) across the cell membrane; (2) G-protein-linked receptors regulate the activity of a separate cell membrane-bound target protein; (3) Enzyme-linked receptors which itself have enzyme activity or are associated with enzymes. The data processing capabilities of the cellular signalling network are illustrated in Figure 1.2.

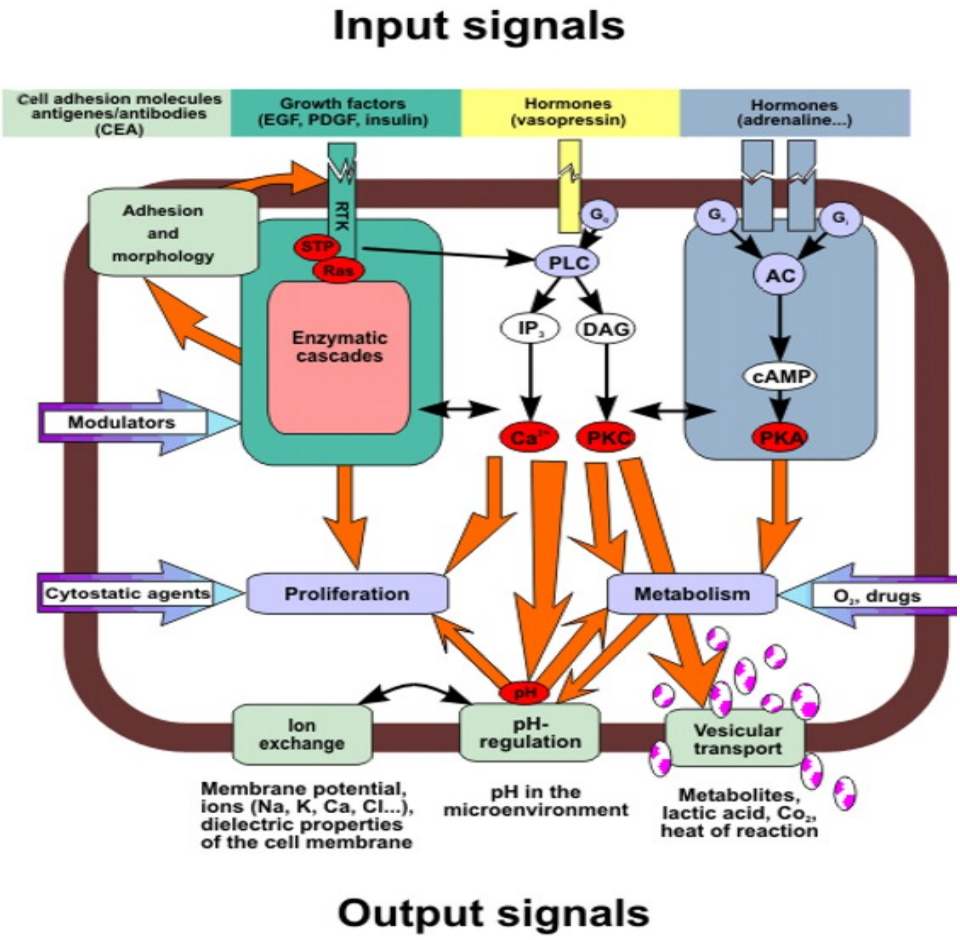


**Figure 1.2:** Cell signalling (Kraus & Wolf, 1995). From these studies we found out that multiparametric planar microsensor arrays might be ideal tools for a online and real time acquisition of complex cellular reaction patterns.

The response to input signals from the environment, i.e. the cellular "output signals", are usually accompanied by a change in the rates of energy metabolism, by changes in electric activity and/or by cell morphological alterations. To investigate cellular signalling properties for diagnostic or screening approaches, these changes can be monitored in real time and non-

invasively by allowing cells and tissues to be in contact with adequate microsensors. This coupling is usually achieved by growing cells directly on the surface of silicon- or glass-based sensor chips.

In the case of signalling via G-protein-linked receptors, numerous G-proteins couple the receptors to different enzymes, activating a chain of events resulting in the alteration of intracellular second messenger levels. Second messengers transmit information from the receptor to intracellular target segments and thus play a major role in cellular signalling. The most important second messengers are $Ca^{2+}$ ions and cyclic adenosine monophosphate (cAMP). Changes in the intracellular concentration of these two second messengers are usually stimulated by distinct pathways. In order to use $Ca^{2+}$ ions as an intracellular signal, the cells have to keep the concentration of cytosolic free $Ca^{2+}$ ions at a low level (approximately $10^{-7}$ M) in comparison to the extracellular free $Ca^{2+}$ ion concentration which is about $10^{-3}$ M. Intracellular $Ca^{2+}$ ions are stored in the endoplasmic reticulum, in mitochondria and in other cytoplasmic vesicles. $Ca^{2+}$ ions can enter or exit the cell through voltage dependent channels, specific carrier protein (G-protein-) receptors and ATP driven pumps. Some G-protein-linked receptors activate the inositol phospholipid signalling pathway.

To use cyclic AMP as a second messenger, the cell must be able to rapidly change the intracellular concentration of this substance. Normally, the concentration of intracellular cyclic AMP is maintained at approximately $10^{-7}$ M. Cyclic AMP concentration can, for example, be increased twenty-fold within seconds after hormonal stimulation. Cyclic AMP is synthesised from ATP by adenylyl cyclase, a plasma membrane bound enzyme, and is hydrolysed by cyclic AMP phosphodiesterases to give adenosine 5´-monophosphate (5´-AMP). Different signalling molecules are able to act on receptors. Some receptors activate a common pool of adenylyl cyclase leading to an increase in the intracellular level of cyclic AMP. They are coupled to this pool by the so-called stimulatory G-protein (Gs). Other receptors inhibit the activity of the adenylyl cyclase enzyme, leading to a decrease in the intracellular level of cyclic AMP via the inhibitory G-protein (Gi). The effects of cyclic AMP in the cell are mediated by activation of the cyclic-AMP-dependent protein kinase-A. This enzyme is known to catalyse the transfer of the terminal phosphate group from ATP to specific serines and threonines of selected proteins.

Another cellular signalling pathway is represented by enzyme-linked cell-surface receptors which are transmembrane proteins having a domain on both the outer surface of the plasma membrane and the cytoplasmic surface. Their cytosolic domain has either an intrinsic enzymatic activity or is directly associated with an enzyme. Numerous receptors stimulate

tyrosine kinase activity and are called tyrosine kinase receptors (RTKs). These receptors phosphorylate their own cytoplasmic domains, which not only activates the kinases but also leads to the production of phosphotyrosines, which serve as docking sites for other intracellular signalling proteins. Some docked proteins are adaptors between receptors and small proteins with GTP-ase activity (Ras). This again activates a cascade of serine/threonine phosphorylations that converges in mitogen-activated protein kinase (MAP-kinase) transmitting the signal to the nucleus.

These enzyme-linked receptors are also involved in signalling to the cytoskeleton and can thereby modulate cell movement and cell shape. Any dysfunction in cellular signalling via enzyme-linked receptors can lead to abnormal cellular proliferation, differentiation, and survival, which are abnormalities typically found in cancers. The various cell signalling pathways are interconnected and may work in parallel (Figure 1.3).

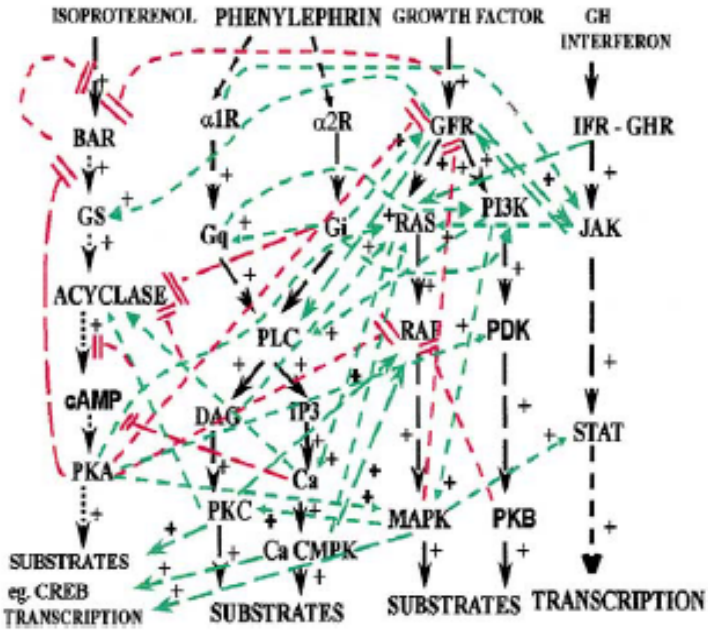


**Figure 1.3:** Example for cross signalling between five signal transduction cascades; black arrows represent the linear cascades; red lines represent negative control mechanisms (inhibitions) and green lines represent positive control mechanisms (stimulations) (Dumont, et al., 2001). The complexity of parallel and interacting signal pathways is supposed to limit the success of approaches to the understanding of cellular signalling and to therapeutic measures, which are directed to the manipulation of isolated molecular entities.

## 1.2 Cell adhesion

Cells are in contact with each other and with the culture substratum by cell-cell and cell-substratum adhesion (Figure 1.4). Animal cells secrete an extracellular matrix (ECM) which is a complex mixture of proteins and polysaccharides, mostly consisting of collagen, elastin, fibronectin, laminin and glycosaminoglycans. The structure of the ECM is organised by the cells. For example, the orientation of the cytoskeleton influences the orientation of the ECM produced outside. The ECM structure depends on the type of tissue. In epithelial tissues, for example, the ECM forms a thin layer (basal lamina) underlying the cellular sheet on the basolateral cell side. In contrast, in connective tissues the ECM is abundant, having only a few cells distributed within it. The ECM helps to bind the cells to the substratum and is able to influence cell behaviour by activating receptor-coupled signal pathways. The components of the ECM can be degraded by enzymes such as matrix metalloproteases and serine proteases.

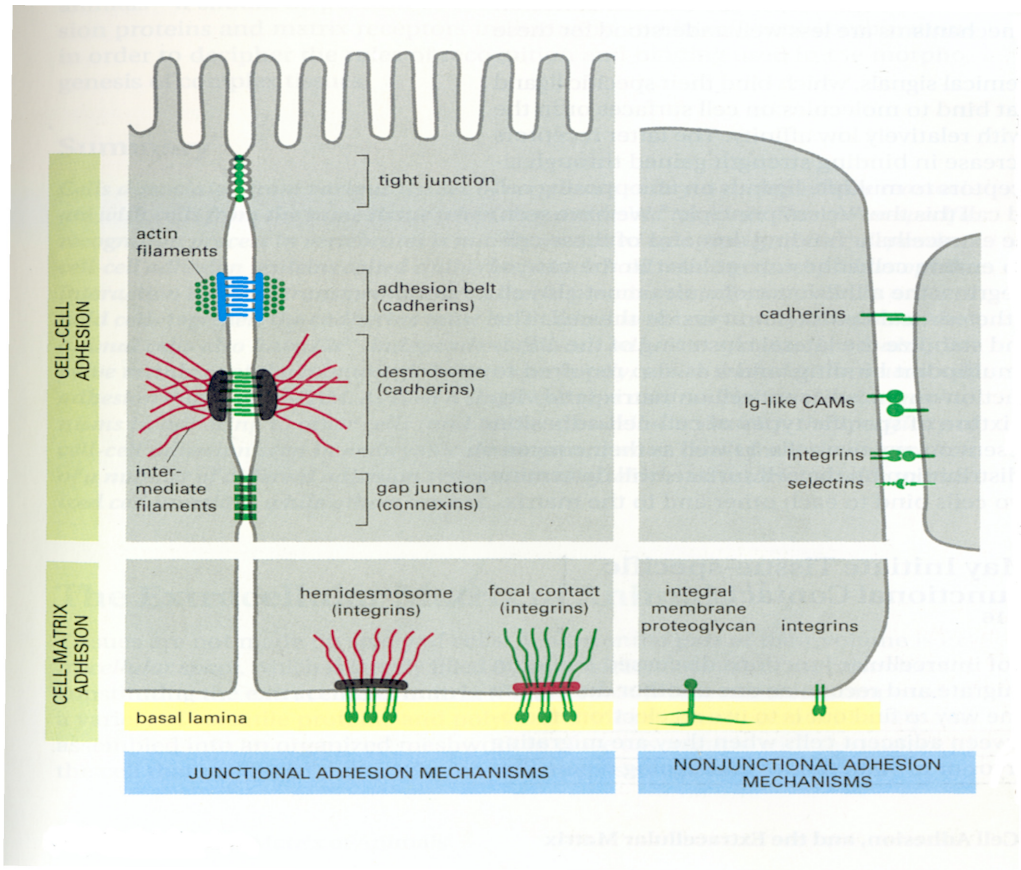


**Figure 1.4:** The different mechanisms of cell-cell and cell-substratum adhesion (Alberts, et al., 1994).

Cell-cell and cell-matrix adhesion is mediated by adhesion proteins: cadherins, the immunoglobulin superfamily of proteins (Ig-like CAMs), selectins and integrins. Cadherins form a family of transmembrane, $Ca^{2+}$ binding proteins, connecting adjacent cells. For efficient cell-cell adhesion, the cytoplasmic part of most cadherins has to be connected to the cytoskeleton by anchor proteins (catenins). The main types of cadherins are: E-cadherins in epithelial cells, N-cadherins in nerve and muscle cells and P-cadherins in cells from the placenta and epidermis. Molecules belonging to the Ig-like CAMs superfamily are $Ca^{2+}$ independent proteins involved in cell-cell adhesion and are important during neuronal development. Selectins are $Ca^{2+}$ dependent cell-surface oligosaccharide binding proteins (lectins) and mediate transient cell-cell and cell-matrix adhesion of endothelial cells. Selectins bind to a specific oligosaccharide on the surface of another cell. Three types of selectins have been discovered: L-selectins on blood white cells, P-selectins on blood platelets and endothelial cells, and E-selectins on activated endothelial cells. Integrins are another group of transmembrane proteins responsible for cell-matrix adhesion. Their activity depends on extracellular divalent cations such as $Ca^{2+}$ or $Mg^{2+}$. Integrins connect the extracellular matrix to the actin cytoskeleton. Upon specific binding of extracellular matrix components, all these proteins can also activate signalling pathways involved in cell growth, survival and proliferation.

The mechanisms of adhesion can be junctional and non-junctional. Junctional cell-cell adhesion mechanisms include (1) tight junctions (sealing neighbouring cells together in an epithelial sheet in order to prevent the leakage of molecules between cells); (2) gap junctions (allowing the passage of water, small molecules and ions between cells); (3) desmosomes (joining intermediate filaments in one cell to those of another cell) and (4) adhesion belts (an actin bundle in one cell is linked to a similar actin bundle in a neighbouring cell).

Junctional cell-matrix adhesion is organised in hemidesomsomes (the intermediate filaments from one cell are anchored to the basal lamina) and focal contacts (the bundles of actin filaments are connected to the extracellular matrix). Integrins, cadherins and selectins are involved in non-junctional cell-cell adhesion, whereas integral membrane proteoglycans and integrins are involved in non-junctional cell-matrix adhesion. The selective adhesion of different types of cells plays an important role in the development of different tissues and in some pathologic phenomena such as cancer metastasis, where cell migration and invasion are central cellular activities.

## 1.3 Membrane potential

Another important factor in cellular communication is the membrane potential. The cell membrane is positively polarised on the outside and negatively polarised on the inside (resting potential). This potential difference is caused by the different distribution of cations, anions and charged molecular groups between the outside and the inside of the cell membrane. Generally, the equilibrium difference of the electric potential at the cell membrane $\Delta\Psi$ is described by the Goldman equation (Adam, et al., 1988):

$$\Delta\psi = \frac{RT}{F} \ln \frac{\sum P_\nu c_\nu^o + \sum P_\mu c_\mu^i}{\sum P_\nu c_\nu^i + \sum P_\mu c_\mu^o}$$

This equation takes into account the different permeability of the cell membrane for the various ion species which have to be considered ($Na^+$, $K^+$, $Cl^-$). The numerator of the equation summarizes the extracellular concentrations of the cations and the intracellular concentrations of the anions (the denominator: vice versa). Since the permeability for chloride and natrium ions is considerably smaller than the permeability for potassium ions, the calculated membrane potential usually approaches the equilibrium potential for potassium ions. The equilibrium potential is then approximately given by the Nernst-equation (Glaser, 2001):

$$\Delta\psi = \frac{RT}{F} \ln \frac{c^o(K^+)}{c^i(K^+)}$$

where:

$\Delta\psi$: difference of the electric potential across the cell membrane

R: gas constant

T: absolute temperature

F: Faraday constant

ln: natural logarithm

P: permeability coefficient

$c^o$: concentration of ions outside of membrane

$c^i$: concentration of ions inside of membrane

ν: index for cations

μ: index for anions

External or internal stimuli may lead to changes in the membrane potential. In nerve and muscle cells, these changes called "action potentials" propagate as spatio-temporal waves along the cell membrane and play an important role in signalling between cells. The distribution of different ions outside and inside the cell membrane is regulated by a variety of ion pumping proteins. The most important of these pumps is the $Na^+$-$K^+$ pump, which acts as an antiporter actively transporting $Na^+$ out of the cell and $K^+$ into the cell against the electrochemical gradient. The energy required to transport these ions is provided by ATP hydrolysis.

The value of the membrane potential varies from cell type to cell type and is also dependent on the cell status (Figure 1.5). Values between -20 and -200 mV are commonly found. Tumor cells often have values in the range of -6 to -35 mV and normal cells in a quiescent state between -40 and -90 mV.

Changes in cellular activity are frequently reflected by changes in the membrane potential (Laris & Henius, 1982; Pulselli, et al., 1996). Such changes can be measured with optical or electrical methods. However, both types of measurement have their distinct drawbacks and at the moment it is hardly possible to monitor slow variations of the membrane potential for extended time periods (several hours) with high reliability. Electrical methods for measuring the cellular membrane potential include the patch clamp technique and microelectrode arrays. The patch clamp technique is an invasive method which was developed for studying ion channel proteins: microelectrodes are placed in contact with the intracellular environment allowing the measurement of an open circuit potential, which can be used to calculate absolute values of the cellular membrane potential (Hamill, et al., 1981). Recently, the invention of patch clamp chips (from glass) with μm apertures paved the way for a simplified instrumentation, for automation and thus for considerable increases of experimental throughput in electrophysiological screening (Fertig, 2002).

The microelectrode array technique is a non-invasive method used for extracellular measurements of action potentials generated in cultured networks of nerve cells (Gross, et al., 1994). In this case, electrically excitable cells are cultivated on surfaces containing an array of photo-etched electrodes which allow the simultaneous monitoring of spike activity from many neurons. Only relative changes of membrane potential are monitored.

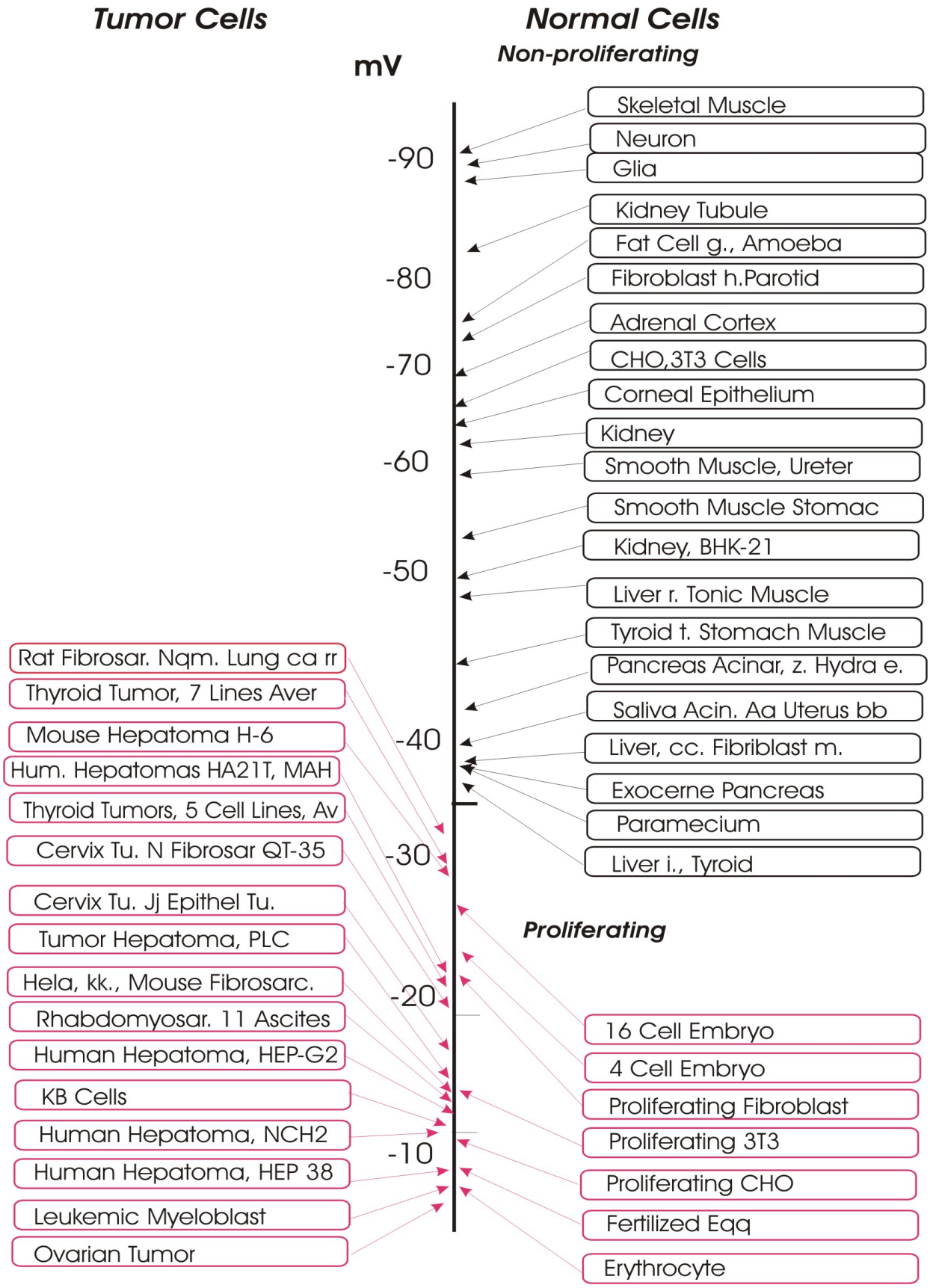


**Figure 1.5:** The transmembrane potential of normal animal cells and transformed tumor cells (Bingeli & Weinstein, 1986).

## 1.4 Cellular metabolism

In most cells, glucose is the central metabolite fuelling the ATP-generating pathways of metabolism. Glucose metabolism can proceed with or without consumption of oxygen. In both cases, glucose is decomposed into pyruvate in the multistep process of glycolysis. The pathway in which lactic acid is produced from pyruvate without oxygen consumption occurs both under hypoxic conditions (the partial pressure of oxygen is less than about 40 mmHg), for example in working skeletal muscle or some poorly vascularised areas in tumors) and under normoxic conditions (e.g. well vascularised areas in tumors). In the respiratory pathway, pyruvate is transported into mitochondria and introduced into the citric acid cycle. The reducing equivalents resulting from the reactions occurring in the citric acid cycle (i.e. nicotinamide adenine dinucleotide, $NADH^+$ and flavin adenine dinucleotide, $FADH_2$) are fed into the multi-enzyme complex of the respiratory chain located on the inner mitochondrial membrane. The reducing equivalents are ultimately used to reduce dissolved oxygen to $H_2O$. The energy yield (difference of the redox potential between the two redox couples $NADH^+/NAD^+$ and $O_2/H_2O$) is stored in an electrochemical gradient of protons across the inner mitochondrial membrane (Adam, et al., 1988):

$$\Delta\mu(H^+) = -2{,}3RT\Delta pH + F\Delta\Psi$$

where:

$\Delta\mu(H^+)$: difference between the electrochemical potential of a proton inside and outside of the inner mitochondrial membrane

R: gas constant

T: absolute temperature

$\Delta$pH: difference of the pH values across the membrane

F: Faraday constant

$\Delta\Phi$: difference of the electric potential across the membrane

This gradient in turn serves as the energy source of the $F_oF_1$ATP-ase system, also located in the inner mitochondrial membrane. The free energy of protons passing along their electrochemical gradient through this system is coupled to the formation of ATP from ADP and inorganic phosphate. About 30 molecules of ATP are generated from one molecule of glucose in oxidative phosphorylation, while only 2 ATP per glucose result from the non-

oxidative anaerobic pathway. In addition to glucose, the cell can use other substrates such as different amino acids and fatty acids as sources of energy (Alberts, et al., 2002; Dang & Semenza, 1999).

Oxygen is not only the terminal electron acceptor of the normal respiratory chain. In a pathophysiological process in mitochondria it can also be the source for the generation of reactive oxygen species (ROS) (Esposti, et al., 2002; Lee, et al., 2001). ROS are involved in carcinogenesis (Halkar, et al., 2001) as well as in the induction of apoptosis (Cortopassi & Wong, 1999; Wen, et al., 2002).

## 1.5 Tumor growth

Cancer cells have an abnormal metabolism and proliferation rate. They have acquired genetic mutations as a result of several, independent accidents occurring sequentially in individual cells changing the cellular phenotype in a characteristic way. This phenotype as well as interdependent changes in the tumor microenvironment gives rise to a clonal selection of tumor cells with the highest proliferative (and invasive) capacity. Intra- and extracellular signal transmission pathways are disturbed, leading to an aberrant rate of cellular metabolism and proliferation. A group of cells, the primary tumor, arises as a clone from a single cell. A tumor can be **benign**, with the cells remaining in an enclosed mass or **malign,** with the cells being able to infiltrate the surrounding tissue, to invade the blood and lymphatic ducts, to migrate in the organism through vessels and to form secondary tumors (Figure 1.6).

Genetic mutations alone, without an adequate microenvironment, would not be sufficient for tumor metastasis (invasion, migration and formation of secondary tumors). The tumor microenvironment also plays a decisive role in tumor progression (Cuvier, et al., 1997). Characteristics of tumors are: abnormal vascularisation, abundant areas of hypoxia, an increased rate of glycolysis and extracellular acidification. Alterations in metabolic regulation not only affect the extracellular microenvironment and cellular communication but are also an adaptive response to adverse microenvironmental conditions. Under these circumstances a positive selection for malignant cells adapted to extreme microenvironmental conditions occurs (Kraus & Wolf, 1996). The abnormal metabolism of tumor tissues is increasingly taken into account for diagnostic purposes, e.g. positron emission tomography (Pfister et al., 2002), nuclear magnetic resonance tomography (Griffiths, et al., 2002; Gillies, et al., 2002) and for radiotherapeutic treatment (Tacev, et al., 2002; Peters, et al., 1983). It is assumed that

tumor metabolism not only affects the activity of different drugs (Gerweck et al., 1999) but the action of different drugs also influences tumor metabolism and microenvironment.

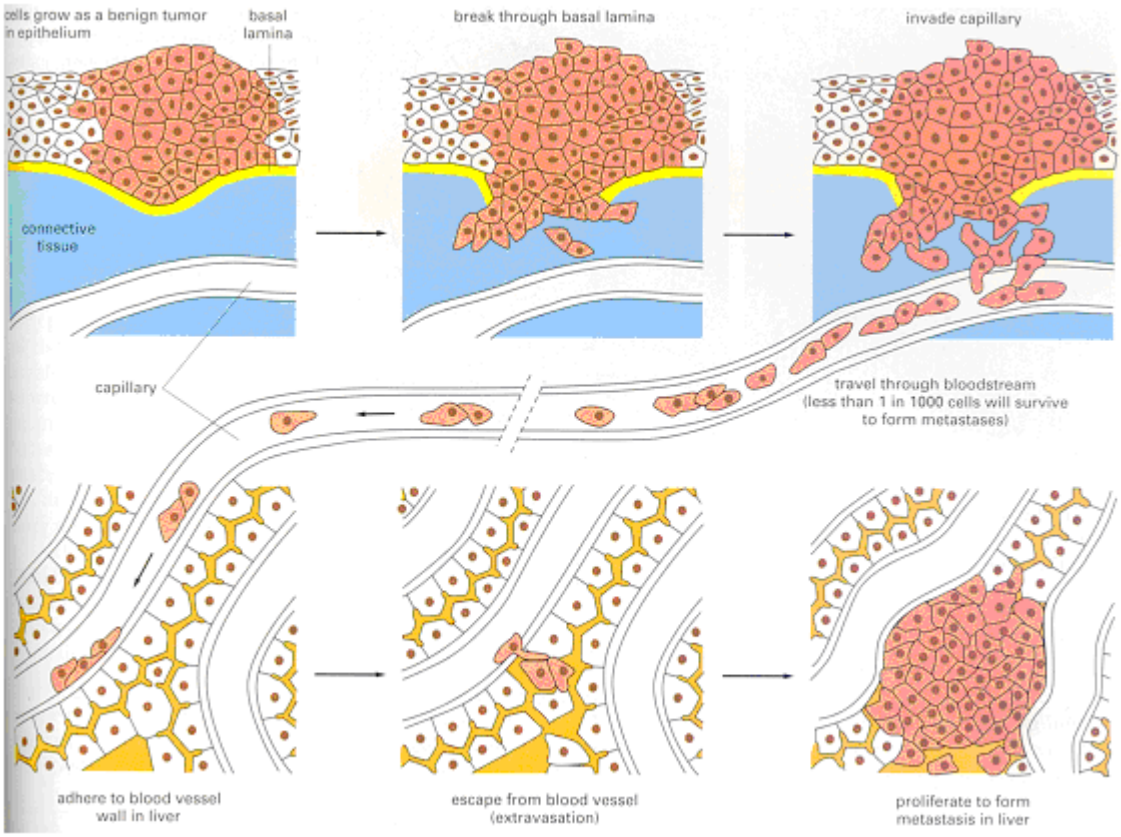


**Figure 1.6:** Different steps in the process of metastasis: spreading of a tumor from the primary site in an organ (lung or bladder) to the liver (Alberts, et al., 2002).

Extracellular acidification plays an important role in cancer invasion in view of the fact that enzymes responsible for degradation of the extracellular matrix have an optimum of activity at low pH. For example, matrix degrading enzymes of the cathepsin group have an optimum at between pH 4.5 and 5.5 (Briozzo et al., 1988; Rozhin, et al., 1994).

Even though the extracellular pH may be rather low, tumor cells maintain normal intracellular values of pH ~7.2 (Stubbs et al., 1999). The intracellular pH is regulated by different transport systems: $Ca^{2+}/H^+$ exchanger, ATP-driven $H^+$ pump, $H^+$/lactate symporter, $Cl^-/HCO_3^-$ and $Na^+/H^+$ antiporter exchanger. The latter system has been shown to play a major role in pH regulation in tumor cells (Harguindey, et al., 1995) with an activity regulated by several hormones (Thomas, 1989).

Hypoxic conditions induce genetic instability in tumor cells and can thereby facilitate the development of malignancy and metastasis (Acker & Plate, 2002; Vaupel & Hoeckel, 2000). In tumors the architecture of vascularisation is often chaotic (Secomb et al., 1995; Denekamp

et al., 1998), and thus hypoxic tissue regions can be commonly found in tumors (Burgman, et al., 2001; Ivanov, et al., 2001). Due to the increasing lack of oxygen in the center of a tumor mass, a growth to more than 1-2 $mm^3$ tumor volume in absence of neo-angiogenesis is not possible. It has been shown that hypoxia regulates not only the induction of angiogenesis, for example by up-regulating the production of vascular endothelial growth factor (VEGF) but also the expression and activity of some isoenzymes of the glycolytic pathway (e.g. lactate dehydrogenase A) (Blancher, et al., 2000; Semenza, et al., 2000). Hypoxia has to be considered in the treatment of many solid tumors. In contrast to cells under normoxia, cells in hypoxic parts of the tumor show an increased resistance to radiotherapy as well as to many chemotherapeutic drugs, e.g. 5-fluoruracil (Teicher, 1994; Vaupel, 1997; Brown, 1999; Vaupel et al., 2001).

## 1.6 Sensor chip system

Even though a lot of assays are available for the analysis of cellular output signals, most of them only allow the analysis of a single cell-related parameter. Moreover, since optical assays are based on staining cells with toxic or phototoxic dyes, a dynamic analysis of cellular behaviour for more than a few minutes is difficult to perform. This is particularly valid for central aspects of cellular life such as cell metabolic activity or cell morphology. Cell metabolism and cytoskeleton are involved in nearly all signal transducing pathways and due to this coupling, they may serve as sensitive indicators of any perturbation of the cellular signalling apparatus. Thus, it would be helpful to analyse dynamically cellular activity in the context of experimentally controlled cellular microenvironments. For example, tumor microenvironment is a major determinant for altered behaviour of cancer cells. Abnormalities in oxygen supply, an impaired exchange of nutrients and metabolic wastes as well as an acidic extracellular pH are main features of solid tumors, which combine to form adverse growth conditions, to which tumor cells can adapt. The most relevant primary phenotypic alteration appears to be a change in the metabolic profile (Dang & Semenza, 1999).

Cellular activity can be investigated with optical or electrical methods. Optical methods are now widespread in pharmaceutical high throughput screening of cells. Cells are stained with fluorescent dyes specifically binding to cellular compartments, and then light emission or light absorption is measured with a microplate reader (Manning & Sontheimer, 1999; Lin, et al., 1999) or with automated, imaging camera systems coupled to light microscope optics (Vanek & Tunon, 2002; Ghosh, et al., 2000). Cellular assays based on the green fluorescent

protein (GFP) and the aeqorin protein, allowing the intensity of protein expression and the intracellular localisation of proteins to be monitored, have become important applications of fluorescence technologies (Chiesa, et al., 2001; Zimmer, 2002). Furthermore, multicolor labelling allows concomitant analysis of more than one cellular segment.

For analysis of cell metabolism only a few optical methods are available. For tests on global metabolic activity and cell proliferation, tetrazolium dyes are sometimes used (Berridge, et al., 1996). Fluorescent dyes which are quenched by dissolved oxygen are employed (in a microplate format) for studies of cellular respiration. It appears however, that problems with low sensitivity are still present (Slater, et al., 2001; Wodnicka, et al., 2000).

The disadvantage of working with fluorescence dyes is that adverse side effects on cellular physiology cannot be completely avoided. It is difficult for example to test the reversibility of drug effects within the same cell or tissue culture. This problem becomes particularly serious, when the amount of the available cellular material is limited, as for example in chemo-sensitivity testing on freshly prepared human tumor specimens. Moreover, the toxicity of intracellular dyes is greatly enhanced under illumination: photobleaching or photooxidation leads to the formation of reactive oxygen species which may seriously affect cellular vitality. Taken together, these factors limit the applicability of fluorescence techniques for monitoring purposes.

Sensor chip systems belong to the group of electrical methods. Cells are cultured on bioelectronic sensor chips which allow changes in the rate of oxygen consumption, the rate of extracellular acidification, cell-cell and cell-substratum adhesion to be monitored over several days. At present, two versions of sensor chips can be used: glass or silicon chips. With the glass chip system, changes in the rate of oxygen consumption or extracellular acidification are measured by discrete microelectrodes while the correspondent planar sensors are currently developed. With the silicon chip system, extracellular acidification rates are measured with Ion Sensitive Field Effect Transistors (ISFET) and cellular oxygen consumption with amperometric electrode structures. In both sensor chip systems, Interdigitated Electrode Structures (IDES) are used to record electric impedance which is influenced by morphologic changes of adherently growing cells. A short comparison of the sensors in the glass chip system versus the silicon chip system is given in Table 1.1.

| Sensor for: | Glass Chips | Silicon Chips |
|---|---|---|
| pH | glass microelectrodes, planar metal-oxide-based sensors (in development) | planar ISFETs |
| $pO_2$ | Clark-type microelectrodes, planar amperometric electrode structures (in development) | planar amperometric electrode structures |
| Impedance | platinum IDES | palladium IDES |

**Table 1.1:** Comparison of sensors used in glass and silicon chip sensor systems.

The experimental studies with the glass chip system are performed in a double chamber setup allowing a parallel monitoring of two chips. The silicon chip system allows six chips with cell cultures to be monitored in parallel (Brischwein et al., 2003; Otto, et al., 2003). Glass chips offer the possibility of (microscope-) optical control during the experiment. Current work is directed at an improved integration of optical imaging tools into the glass chip system (see part 5.1). Both chip systems allow the online monitoring of cellular activity over several days. A detailed description of the glass sensor chip system is presented in part 2.2.
A summary of basic properties of optical and electrical methods for cell based assays is presented in Table 1.2.

| Electrical methods | Optical methods |
|---|---|
| non-toxic and non-invasive monitoring of cellular activity | (photo-) toxic properties of intracellular dyes, dynamic monitoring in the range of minutes |
| parameters analysed currently are: cell metabolism, cell morphology, electric activity, different ions | versatility, many dyes available for different cellular parameters, use of the same type of reader equipment |
| high sensitivity possible due to immediate contact between cell and microsensor | sensitivity often insufficient due to high signal backgrounds (low signal/ noise ratio) |
| online, dynamic analysis for extended time periods (several days) | end point analysis; dynamic analysis restricted to short time periods |

**Table 1.2:** Comparison between optical und electrical methods used for analysis of cellular activity.

## 1.7. Aim of the thesis

The goal of the this work was the analysis of cellular output signals using multifunctional bioelectronic sensor chips. Electric biosensors amenable to cellular signals were used: namlely pH, oxygen consumption and electric impedance. These sensors are integrated on a chip and thus allow to analyse these output signals in parallel.

The **first part** of this investigation is focussed:

(1) on monitoring of the cellular outputs signals under different biological conditions employing the bioelectronic sensor chips

(2) on the interpretation of sensor signals in the biochemical context, with the aid of different parameters measured using standard biochemical assays.

Cellular model systems having different intracellular signalling networks and exposed to various types of input signals are used:

(1) Hela cervix cancer cells stimulated with histamine as a model for calcium signalling

(2) LS174T colon cancer cells stimulated with a chemotherapeutic agent, chloro-acetaldehyde, which is known to affect the mitochondrial activity

(3) LS174T colon cancer cells stimulated with cytochalasin B which is known to distort components of the cytoskeleton and to inhibit glucose uptake

In the **second part** of this work the focus was on developing a sensor-based invasion assay for analysis of cellular invasion through an extracellular matrix. Toward this aim the human breast cancer cells MDA-MB 231 were used as model for cells with a metastatic potential.

In the **third part** the performance of different types of sensor chips in detecting cellular output signals was characterised.

The results of this study are examples for the application of multifunctional chip systems in monitoring cell activities and provide a basis for adapting the system for further types of cellular application.

# 2. Materials and Methods

## 2.1 Description of optical techniques

### 2.1.1 Fluorescence

Fluorescence is used to detect different components of biomolecular assemblies and to analyse certain cell-physiologic parameters. It is a physical process which only occurs in specific molecules called fluorescence dyes or fluorophores. Fluorescence dyes absorb light at one wavelength and emit light at a different, longer wavelength within the visible spectrum (Figure 2.1). The process of excitation/emission can be repeated many times until the dye is irreversibly destroyed (photobleaching).

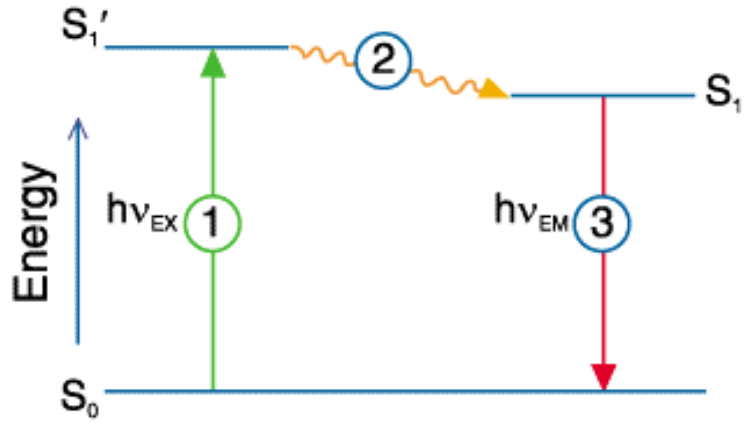


**Figure 2.1:** A simplified Jablonski diagram illustrating the processes involved in photon absorption and subsequent emission of fluorescence photons (Molecular Probes).
where:
$S_0$ = electronic ground state
$S_1$`= excited electronic singlet state
$S_1$ = relaxed singlet excited state

A photon of energy $h\nu_{EX}$ supplied by an external source (e.g. mercury lamp) transforms the fluorophore into an excited electronic singlet state ($S_1$'). This excited state exists for a time period of about 1 to 10 nanoseconds. During this time, the energy of the $S_1$' state is partially dissipated as thermal energy resulting in a relaxed singlet excited state ($S_1$), from which fluorescence emission originates. A photon of energy $h\nu_{EM}$ is emitted, returning the fluorophore to its ground state $S_0$. Due to the energy dissipation during the lifetime of the

excited state the energy of this photon is lower, and thus the photon has a longer wavelength than the excitation photon $h\nu_{EX}$ (Lottspeich & Zorbas, 1998).

### 2.1.1.1 Fluorescence microscope

In this study fluorescence microscopy was used in order to analyse the mitochondrial activity and the level of reactive oxygen species in LS174T cells incubated for different time periods with chloroacetaldehyde or cytochalasin B containing media (see parts 3.1.2.3, 3.1.2.4).
The microscope is an important tool to analyse cellular structures and cell-physiologic parameters. The ability to magnify images depends on the combined effect of different lenses (for example, if the objective lens magnifies 100-fold and the eyepiece 10-fold the final magnification will be 1000-fold). The most important property of a microscope objective lens however, is its power of resolution, which is the ability to distinguish between two objects positioned very closely to each other. The resolution of an objective lens is numerically equivalent to D (minimum distance between two distinguishable objects). The smaller the value of D, the better the resolution. D is a function of three parameters and can be expressed as follows:

$$D = \frac{\lambda}{n \sin \alpha}$$

where:
$\alpha$ = the angular aperture (half-angle of the cone of light entering the lens from the specimen)
n = refractive index of the air or fluid medium between the specimen and the objective lens
$\lambda$ = wavelength of incident light

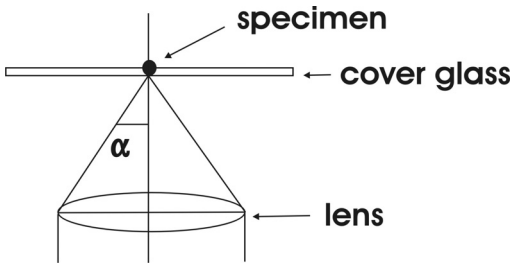


**Figure 2.2:** The path of light rays passing through a specimen in a microscope.

The *angular aperture* depends on the width of the objective lens and its distance from the specimen. The *refractive index* measures the degree to which a medium bends a ray of light

that passes through it. In order to improve the resolution, a medium with a higher refractive index can be placed between the specimen and the objective lens (e.g. immersion oil with a refractive index of N = 1.5 improves the resolution by a factor of 1.5 in comparison to air with N = 1). A short wavelength of incident light leads to a low value of D and thus to a better resolution (Lodish et al., 1996).

In a fluorescence microscope the illuminating light is passed through a filter (excitation filter) before reaching the specimen. Similarly the light obtained from the specimen is passed through another filter (emission filter). A beam splitting mirror in the light path prevents scattered excitation light from entering the eyepiece (Figure 2.3).

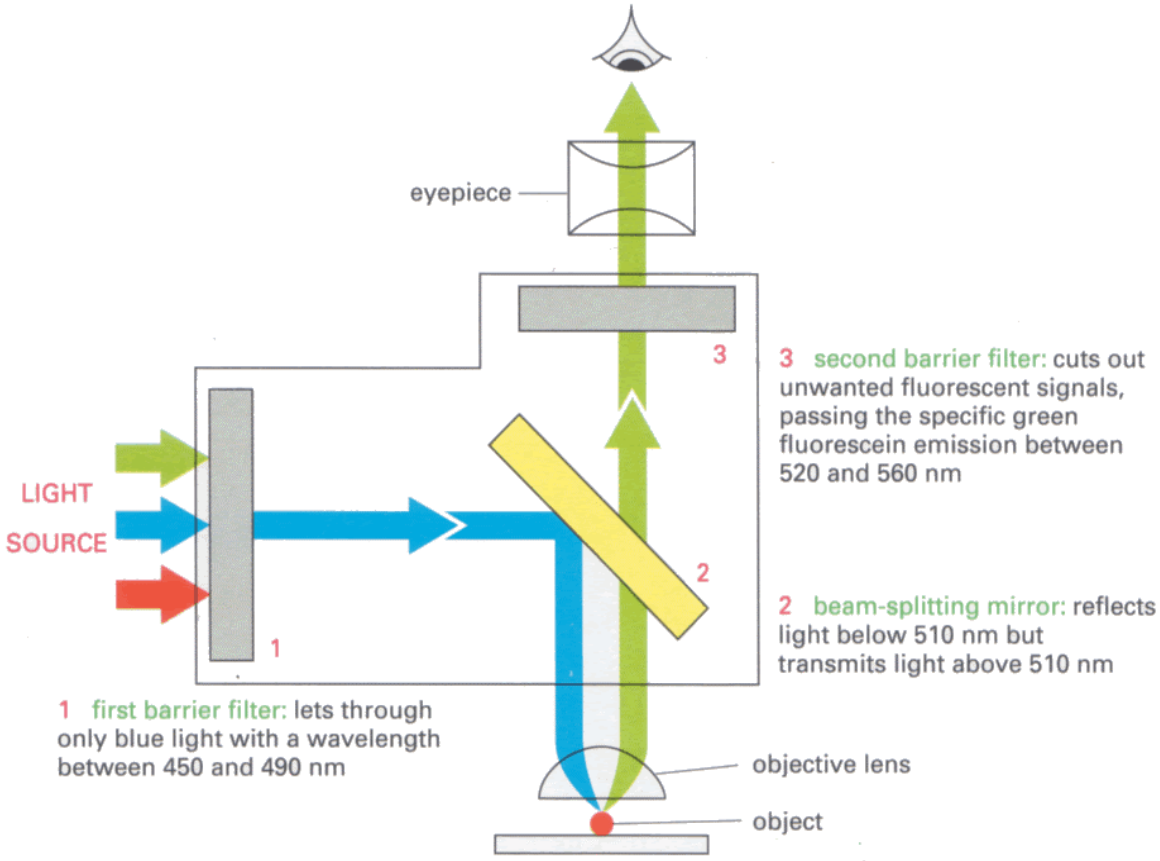


**Figure 2.3:** The optical system of a fluorescence microscope; detection of fluorescein, a fluorescent molecule (Alberts, et al., 1994).

This optical configuration effectively maintains a dark background and thus provides a high sensitivity of detection. The sensitivity of detection is improved by fluorescence microscopy in comparison to normal optical microscopy. A great variety of fluorescence dyes selectively staining different components of the cell have been developed: for example, Fura-2-AM, Fluo 4-AM are used for analysis of intracellular free calcium ions concentration, rhodamine for

staining the mitochondria, BCECF-AM for analysis of intracellular pH. Some dyes such as Fura-2 (a calcium indicator), BCECF (a pH indicator) and JC-1 (used for the analysis of the mitochondrial membrane potential) have emission or excitation spectra with bands both increasing and decreasing upon binding (e.g. upon binding of calcium ions to Fura-2). This allows a "ratiometric" evaluation of fluorescence intensities and enables the elimination of any distortion generated by photobleaching, unequal loading and retention of the dye, or different optical path lengths.

Not only spatial resolution is improved by high numerical aperture objectives, but also the sensitivity in detection of low intensity fluorescence signals. Moreover, the visual inspection of the fluorescent specimen is increasingly replaced by highly sensitive imaging cameras with digital image acquisition capabilities. At the heart of such a camera is a CCD (Charge Coupled Device) chip, containing an array of "pixel elements" and collecting light for a given time period. The longer this time period is, the higher the sensitivity will be, but at the cost of time resolution. A typical pixel size is 6.5 µm x 6.5 µm. A high quality camera may contain an array of 1376 x 1040 pixels. The collected light intensity is stored for each pixel and then evaluated using the appropriate software.

Fluorescence methods offer the potential to stain different cellular segments with a variety of dyes simultaneously, which can be advantageous from an analytical point of view.

### 2.1.1.2 Plate reader

In order to analyse the effect of histamine on Hela cells a fluorescence plate reader ("Fluostar", BMG, Lab Technologies, Offenburg, Germany, Figure 2.4) was used. A detailed description of the experiments is done in part 3.1.1.2.

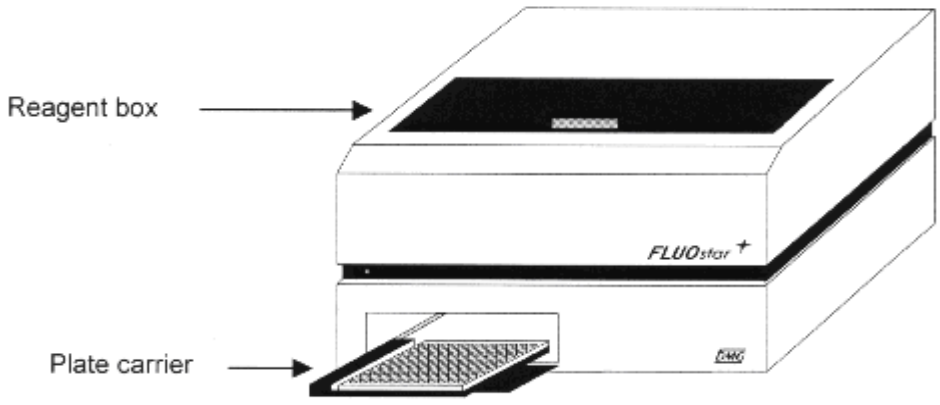


**Figure 2.4:** Front view of the Fluostar plate reader (BMG, Fluostar handbook).

To measure fluorescence intensity, the stained specimen is placed in a multi-well plate (e.g. 6, 12, 24, 96, 384 well plates). The plate is then introduced by a plate carrier into the apparatus. The light provided by a xenon lamp is passed through the excitation filter to the sample. The emission light from the sample is collected by the measurement head and passed through the emission filter to the photo-detector (Figure 2.5).

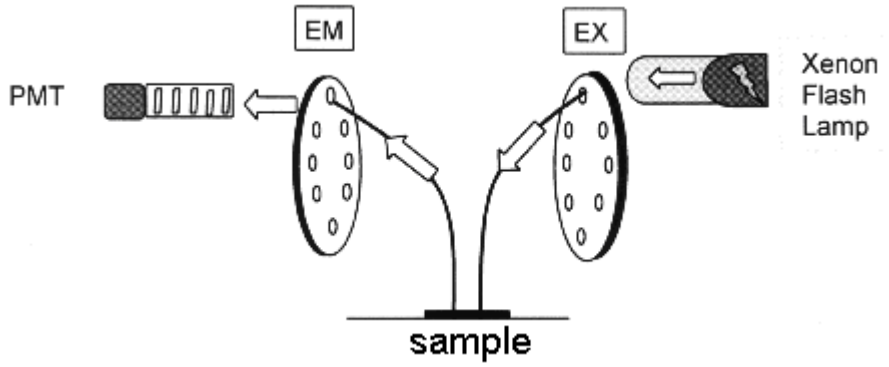


**Figure 2.5:** The light path of a fluorescence reader Fluostar (from BMG, Fluostar Handbook).
where:
EX = excitation filter
EM = emission filter
PMT = photomultiplier tube

The spectral range for fluorescence intensity (excitation and emission) is between 240-740 nm. An filter combination appropriate for the dye used must be selected. As there is no beam splitting mirror in the light path, the spectral selectivity of the filter combination is particularly important to keep the background at a low level. The apparatus allows an incubation temperature range from 5 °C to 45 °C to be selected in 0.1 °C steps. The shortest time necessary for reading a 96 well plate is 15 seconds.
It is possible to choose between two different optic configurations:
● *Top optic:* Excitation and the detection of emitted light is provided by a measurement head at the top of the plate (Figure 2.6).

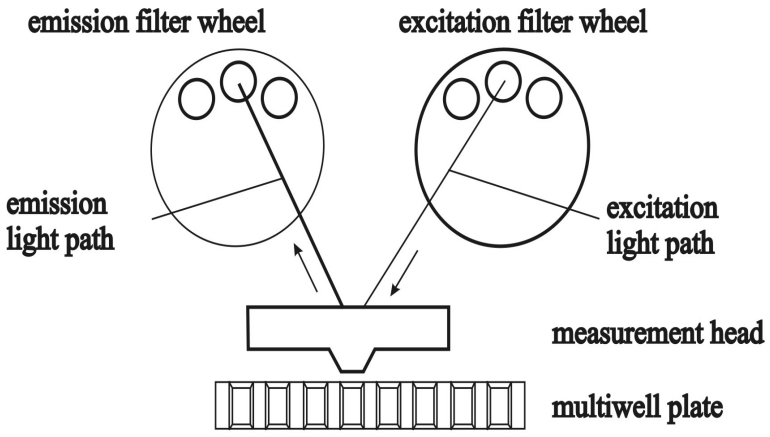


**Figure 2.6:** The top optic measurement mode by Fluostar.

● *Bottom optic:* Excitation and the detection of emitted light is provided by a measurement head placed at the bottom of the plate. In this case plates with a transparent bottom must be used (Figure 2.7). This configuration is preferable for measurements in plates with adherent cells.

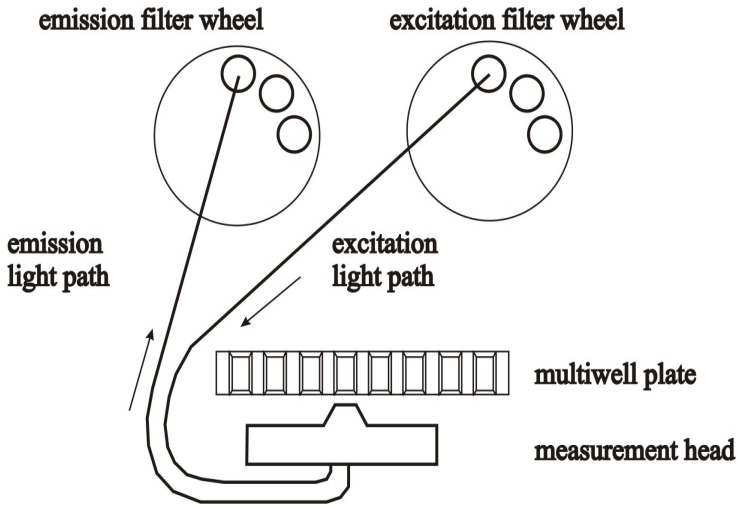


**Figure 2.7:** The bottom optic measurement mode by Fluostar.

Apart from these optic configurations, Fluostar allows an adequate measurement mode to be chosen for the experiment:

● *The Well Mode* is used for reactions with fast kinetics. A certain number of measurement intervals is assigned to each well. In this mode, each well is measured one after the other. The reader then switches to the next well.

● *The Plate Mode* is used for reactions with slow kinetics. A number of cycles is defined and within each cycle all individual wells of a plate are measured once.

The addition of a solution or a test substance is possible during an experiment via automatic piston pumps in combination with an injection needle. Fluostar can be equipped with a maximum of two pumps.
The sensitivity of the apparatus is up to 2 fmol/well fluorescein for fluorescence intensity. Before an experiment is started a gain adjustment must be done in order to adjust the sensitivity of the photomultiplier tube to the well with the highest fluorescence intensity.

## 2.1.2 Luminescence

The ATP level in LS174T cells incubated for different time periods with chloroacetaldehyde and cytochalasin B containing media (described in part 3.1.2.2) was analysed using a luminescence plate reader (Lumistar, BMG, Lab Technologies, Offenburg, Germany).
Luminescence is a three stage process in which light is emitted as a result of a chemical reaction. An example is the luciferin-luciferase reaction. This reaction is used to measure ATP concentrations in biological specimens:

$$\text{ATP + D-Luciferin + } O_2 \xrightarrow[Mg^{2+}]{\text{Luciferase}} \text{Oxyluciferin + AMP + } PP_i + \ CO_2 + \text{Light}\uparrow$$

Luciferase obtained from the firefly Photinus pyralis reacts with luciferin and ATP forming inorganic pyrophosphate ($PP_i$) and luciferase-luciferyl-AMP. This complex dissociates in the presence of oxygen into luciferase, oxyluciferin, AMP and $CO_2$, a process which is accompanied by the emission of a photon with a wavelength of 560 nm (Manfredi, et, al. 2002). In contrast to fluorescence, each luciferin molecule is able to cause the emission of only a single photon. Since there is no external light source, the emitted luminescence light can be measured in a dark box against a zero background, which allows single photons to be counted.
To measure the luminescence the samples are placed in a plate reader similar to Fluostar ("Lumistar"). The measurement head positioned on the top of the plate collects the light emitted by the sample, and this light is directed along the emission light path to the detector (Figure 2.8). White plates are used to increase the quantum yield of the measurement.

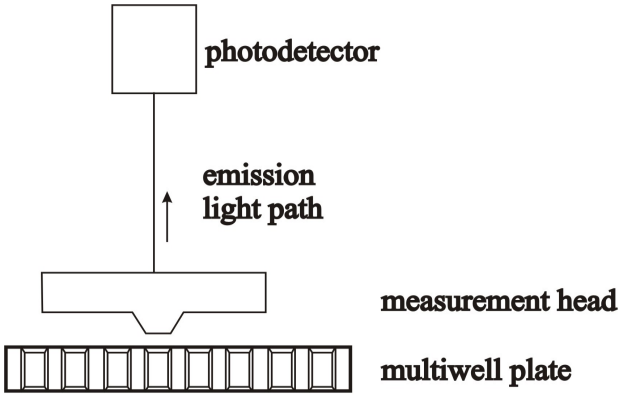


**Figure 2.8:** Luminescence measurement with the Lumistar plate reader.

The sensitivity of the device is 0.2 amol/well recombinant aequorin (calcium indicator). A 96 well plate can be read in 23 seconds. The spectral range of the device is between 290 and 700 nm. Lumistar can be equipped with up to three injection pumps.

## 2.2 Cell monitoring system (CMS)

The Cell Monitoring System (CMS, Brischwein, et al., 1996; Figure 2.9) was designed to allow a dynamic online analysis of living cells over long time periods (several days). Sensor measurements provide information about cell-cell and cell-substratum adhesion, the rates of oxygen consumption and extracellular acidification. Since the cells grow on a glass chip, simultaneous (microscope-) optic access is possible.

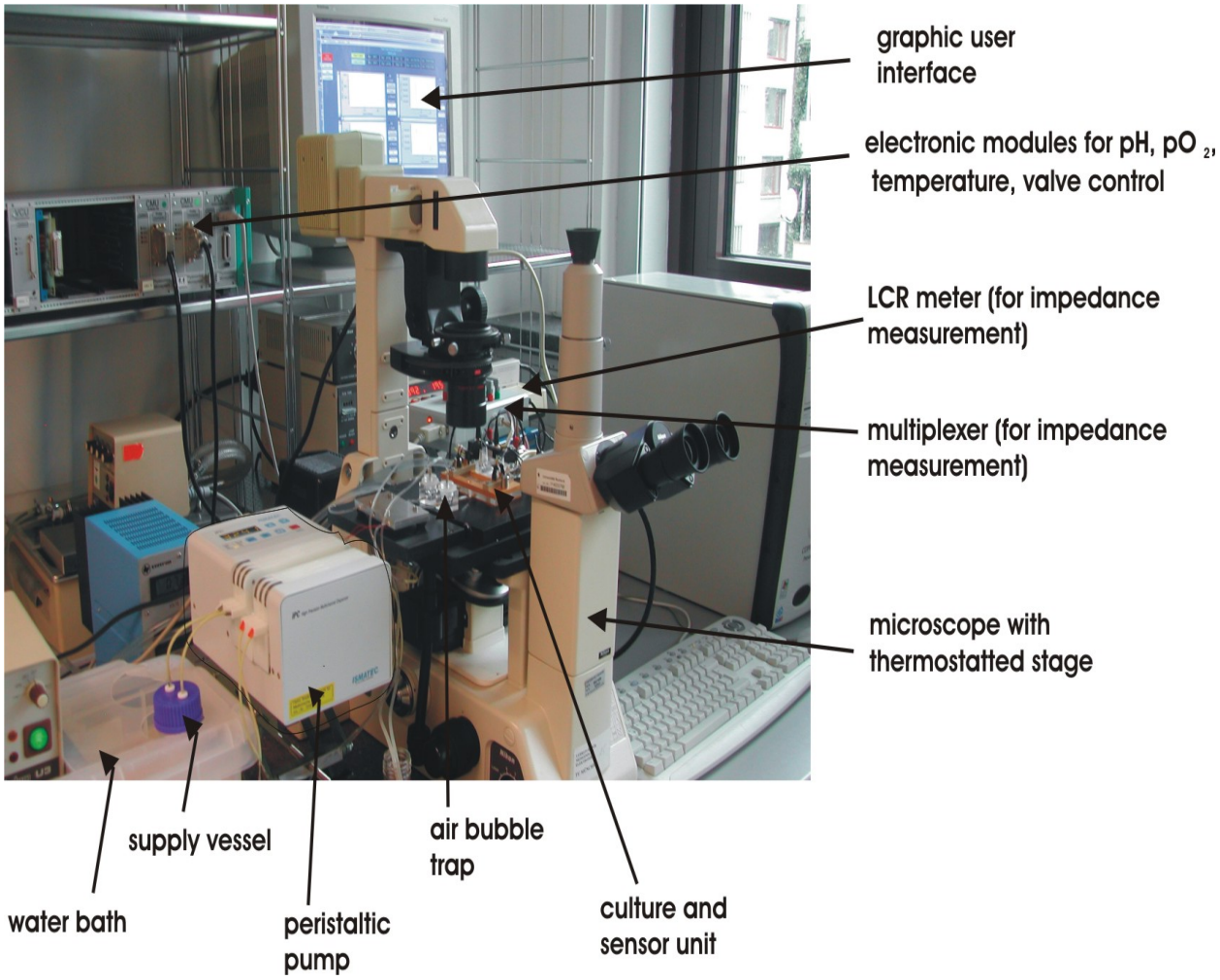


**Figure 2.9:** Cell monitoring system: experimental setup.

### 2.2.1 Culture and sensor unit

The culture and sensor units are made up of "double chambers", accommodating two glass sensor chips in parallel. The individual parts of this device are assembled into place in a *stainless steel housing* (Figure 2.10). On each of the chips, a small, disc shaped volume is

formed by a transparent, acrylic part. The chamber height can be adjusted in the range of 0.3 to 0.6 mm using spacers. It is important to adjust a small height of the chambers in order to maintain a high ratio of cell number to the volume of the surrounding cell culture medium, since this ratio is proportional to the sensitivity in detecting cell metabolic rates. Silicon rings are used to seal the chambers.

Adjustable needle contact sockets for planar sensors are fixed on the steel housing. Microsensors for pH and oxygen are placed in a separate acrylic housing behind the chambers.

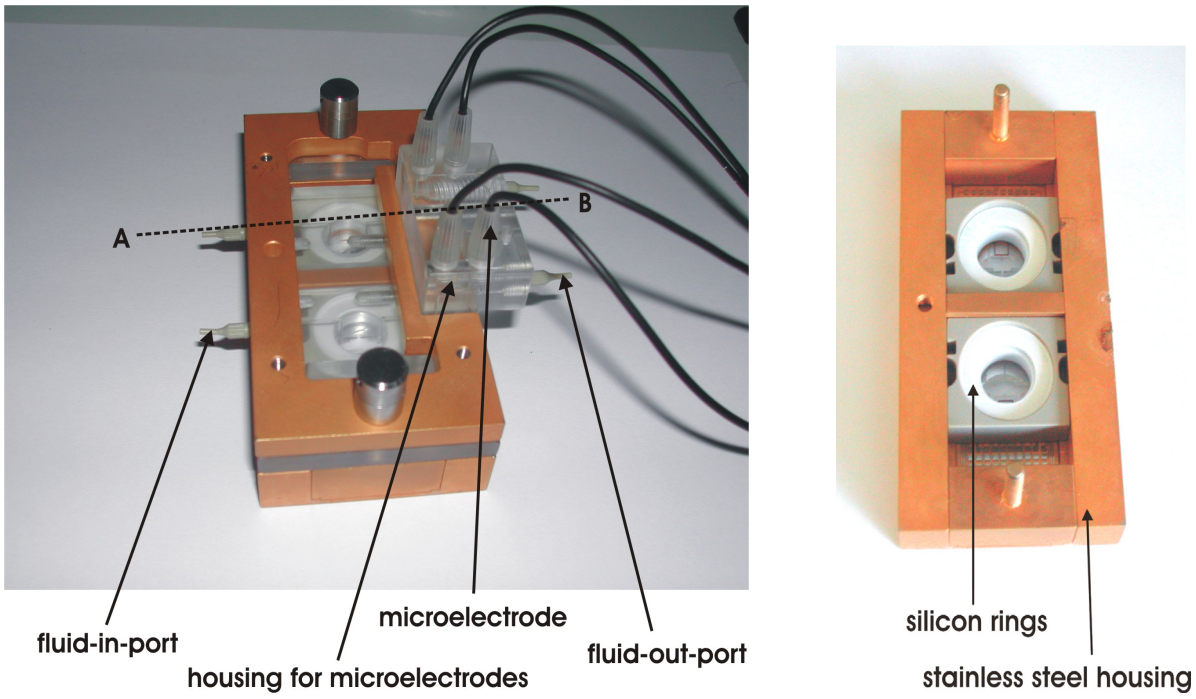


**Figure 2.10:** Photographs of the culture and sensor unit with the glass chips; cross-section A-B (see Figure 2.11).

During the experiments the double chamber is placed on a thermostatted stage (37 °C) of an inverse microscope (Diaphot 200, Nikon) allowing optical inspection of the cell cultures during the experiments. For a more detailed description of the microscope see part 2.1.1.1.

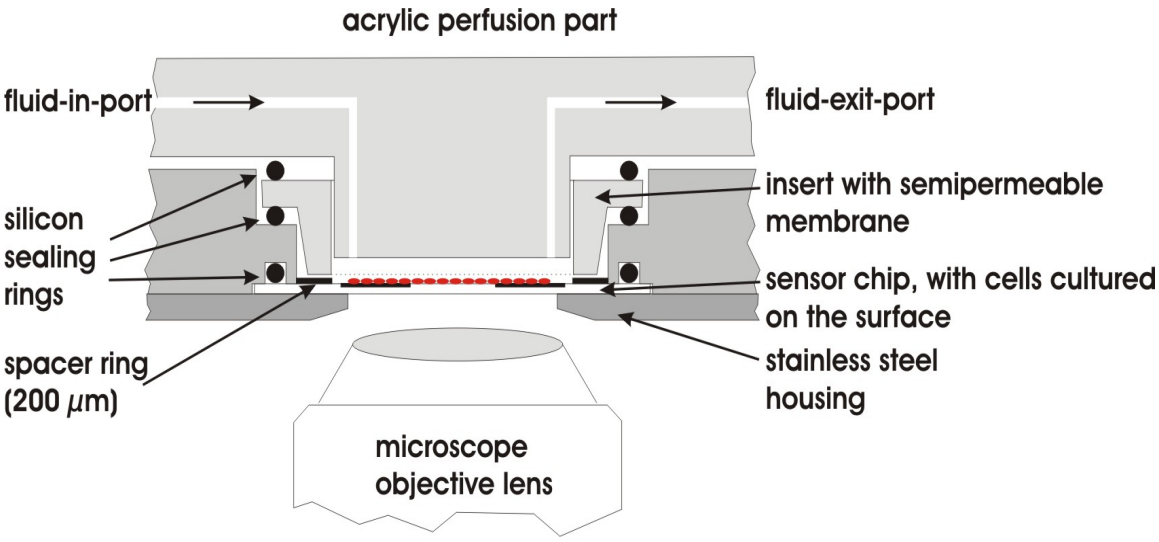


**Figure 2.11:**Cross-section, semi-schematic (A-B) of double chamber (see Fig. 2.10, left side).

### 2.2.1.1 Glass chips

The glass chips (Figure 2.12) have an outer dimension of 24.0 mm x 33.8 mm and a thickness of 0.5 mm. They were fabricated at the Technical University of Munich, Chair of Medical Electronics, using thin film technologies. Currently, the chip includes one Pt 100 temperature sensor, two amperometric three-electrode-structures and two interdigitated electrode structures. The metal structures are fabricated using a platinum lift-off process. Afterwards a single passivation layer is deposited ($Si_3N_4$, about 500 nm) to prevent electric shortcuts in liquids. Sensors for pH may be either integrated by a glass-silicon hybrid technology (insertion of ISFET-silicon chips into the glass chip) or by deposition of proton-sensitive layers of metal oxides such as $Al_2O_3$, $Ta_2O_5$ or $RuO_2$. However, since the work on planar pH- and oxygen sensors on glass chips is still in progress, these parameters (pH and dissolved oxygen) were measured in this study with non-planar sensors (microelectrodes) inserted into the double chamber setup.

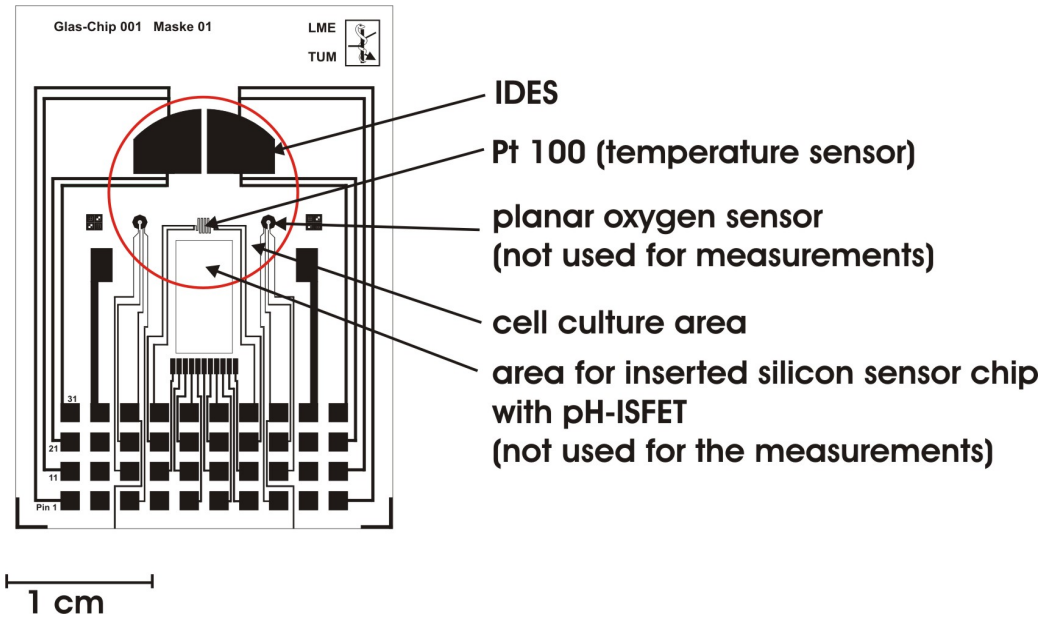


**Figure 2.12:** Diagram of a glass chip.

*Interdigitated electrode structures (IDES)* on glass chips were used for the measurement of electric impedance, yielding information about cell morphologic changes. Two IDES are structured on a chip. The material used for IDES on glass chips is platinum and the area of each sensor is about 20 mm². The width of the electrodes and the distance between the electrodes is 50 µm (Figure 2.13-A). The measurements were performed at a frequency of 10 kHz and a current density of about 20 µA/cm$^2$. At low frequencies the membranes of living cells are very poor conductors and therefore force electrical currents to bypass them (Figure 2.13-B). When the cells adhere to and grow on the sensor surface, the impedance value increase (Schwan, 1963; Wolf et al., 1998).

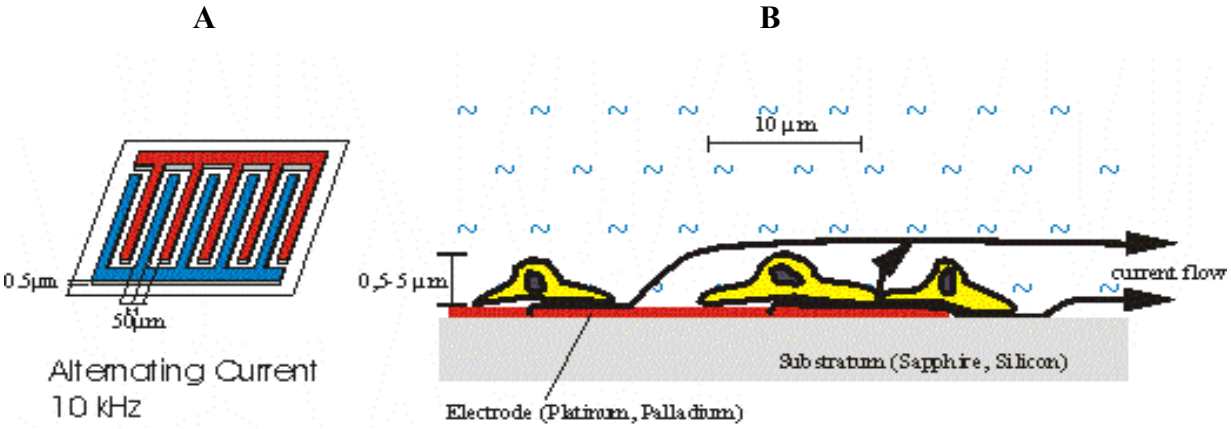


**Figure 2.13: (A)** Structure of IDES and **(B)** diagram of a cell culture modulating the resistance to an alternating current flow (Ehret, et al., 1998).

### 2.2.1.2 Ceramic chips

As a cost effective alternative to thin film technologies, even for small numbers of produced chips, thick film technology can be used to fabricate multisensor cell chips. In this case, glass is replaced by ceramic as a chip substrate (Figure 2.14). The technology used to fabricate these chips is based on screen printing. A paste which is a mixture of organic solutions, a component for maintaining a suitable viscosity, and a functional component (such as metal particles) is pushed through a steel mask on to a ceramic plate. In this case the structure resolution is limited to about 100 µm. During the hardening process, the paste is exposed to high temperatures (between 500 and 800 °C) and thus the organic solutions and metal particles are oxidized or reduced (Lambrechts & Sansen, 1992). These high temperatures and a bad adhesion of the paste currently prevent the use of glass as a thick film substrate. The final thickness of the film is about 10 µm.

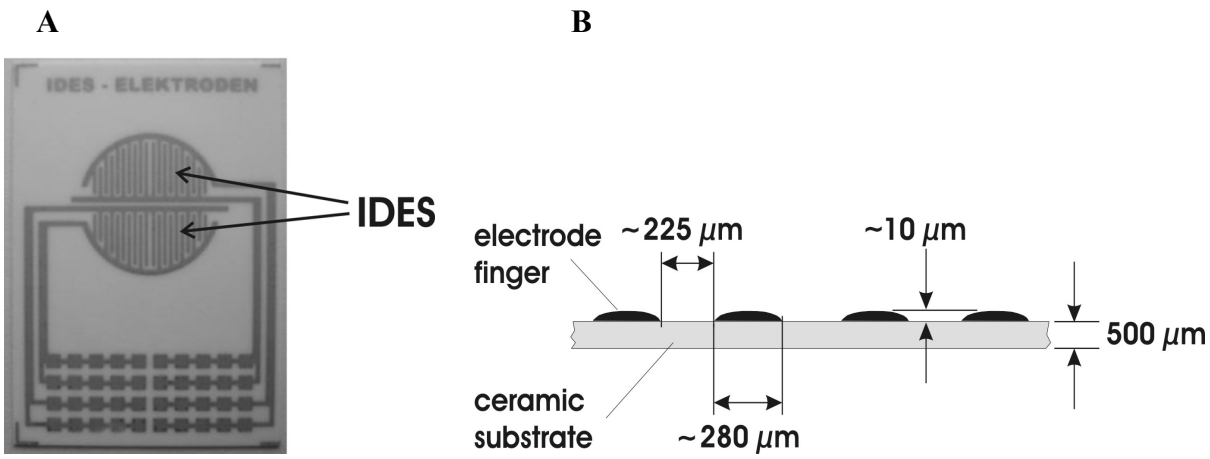


**Figure 2.14: (A)** Photograph of a ceramic chip and **(B)** diagram of IDES on a ceramic chip fabricated with thick film technologies in a cooperation project with the Kurt-Schwabe-Institut für Mess- und Sensortechnik e.V., Meinsberg (KSI).

## 2.2.2 Microelectrodes

The microelectrodes for measurement of pH and oxygen are positioned in a separate acrylic housing in the fluid out port of the double chamber.

### 2.2.2.1 Microelectrodes for measurement of oxygen

***A.*** *Miniaturized clark-type oxygen electrode*

Changes in extracellular concentrations of dissolved oxygen were measured with miniaturized Clark-type oxygen electrodes (Figure 2.15). These electrodes, specially adapted to the present measurement requirements, were obtained from KSI (Brischwein 1997). The sensor tip (diameter ~ 3.3 mm) has a slightly domed form in order to assure a stable membrane tension (Brischwein 1997). The basis of amperometric oxygen sensors is to place two electrodes in the test solution and to apply a potential sufficient to reduce dissolved oxygen at the working electrode (about -650 mV vs. Ag/AgCl reference electrode). The limiting current at this potential will be proportional to the partial pressure $pO_2$ of dissolved oxygen. According to the invention of L.C. Clark, patented in 1956, the electrodes are usually covered by a membrane permeable to dissolved gases (e.g. teflon, silicon), in order to increase signal stability and selectivity.

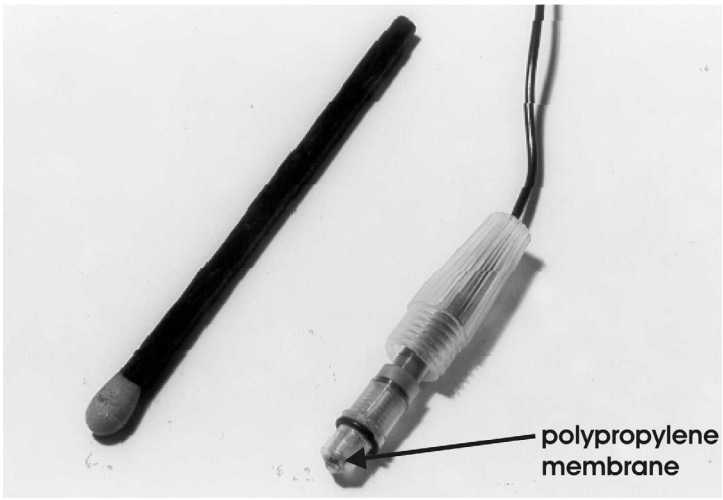


**Figure 2.15:** Photograph of the miniaturised $pO_2$-electrode (Brischwein 1997).

Particular requirements for the measurements presented in this thesis are: miniaturisation, stable function for at least one week and a low current flow. A platinum wire with a diameter

of 30 μm melted into a glass cylinder with a diameter of 1 mm was used as a working electrode. A polarisation voltage of -750 mV (working electrode vs. Ag/AgCl reference electrode) is used during operation. The sensor cable is bipolar, with the electric contact of the reference electrode used as a shield against electromagnetic interference. The characteristic values of the oxygen electrode are summarised in Table 2.1. A relatively large variation of the current flow is observed between the individual sensors in water saturated with air. This is caused by small differences in the diameter of the cathodes as well as mechanical fluctuations of the membrane tension. The temperature dependence of the measured signal is notably large (about 10% increase per degree of temperature increase), which is probably due to the relatively thick polypropylene membrane. Due to the low cathodic current (about 300 pA in air-saturated water) a small dependence of sensor sensitivity on the flow velocity in the solution is achieved.

| | |
|---|---|
| Current flow (in air saturated water, 25 $^{o}$C) | 300 - 600 pA |
| Electrolyte | 0.1 M KCl;<br>solution: 95% ethylene glycol, 5% water;<br>the volume of electrolyte: ca. 4.5 μl. |
| Membrane | polypropylene, 20 μm |
| Response time ($t_{90}$) | 25 - 30 s |
| Sensor lifetime, in air saturated water, (25 $^{o}$C) | ~350 - 700 h (appreciable variability) |
| Time stability (perfusion with air saturated water 25 $^{o}$C) | lower than 2% signal drift per hour |
| Noise level (of digital signal) | lower than 0.01 mg/L (0.5 pA) |
| Residual current | lower than 0.05 mg/L (2.5 pA) |
| Temperature dependence of the signal | ~10% increase per $^{o}$C of temperature increase |
| Dependence of output signal of perfusion flow velocity | increase of flow velocity from 0.3 mm/s to 0.6 mm/s results in ~1-2% signal increase. |

**Table 2.1:** Characteristics of the oxygen microelectrode.

**B.** *Optical oxygen sensor*

In addition to the Clark-type oxygen microelectrode, a fibre-optic oxygen minisensor (purchased from PreSens GmbH, Regensburg, Germany) was used for the measurement of cellular oxygen uptake. This fibre-optic oxygen sensor is constructed from a 2 mm polymer optical fibre (POF) which is polished and coated with a planar oxygen sensitive foil (Figure 2.16 -A). The oxygen sensor is connected to a fibox oxygen meter ("Fibox 2"), also purchased from PreSens GmbH (Figure 2.16-B).

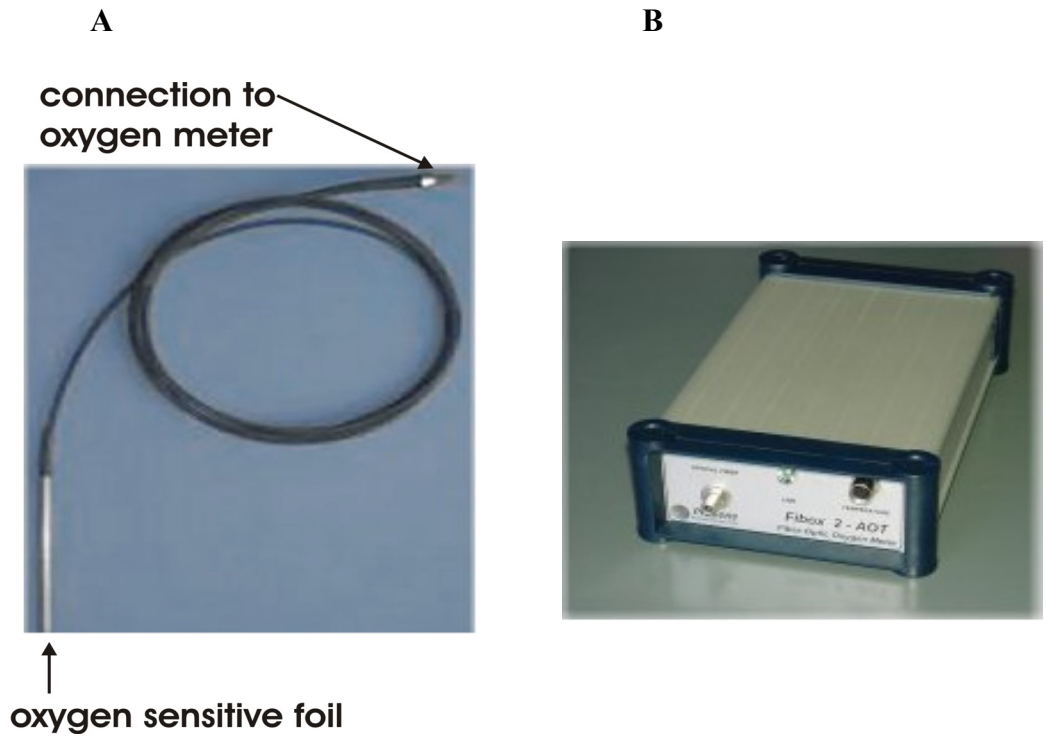


**Figure 2.16: (A)** Photograph of a 2mm-POF sensor and **(B)** photograph of the fibre optic oxygen meter, Fibox 2 (PreSens handbook).

The function of this sensor is based on fluorescence quenching as a result of collision between molecular oxygen and the fluorescent dye molecules in an excited state. A phase shift of the sinusoidal excitation light intensity vs. the fluorescent emission intensity is recorded instead of the fluorescence intensity itself, thereby eliminating the effect of a gradual photobleaching. In order to exclude ambient light, the fibre is coated with an optically isolating sensor material. A high grade steel tube is used at the end of the polymer optical fibre for protection of the sensor material and POF. The optical minisensor can be sterilised by EtOH or $H_2O_2$. The sensor does not consume oxygen, thus the sensor signal is independent of the flow velocity.

### 2.2.2.2 Microelectrodes for measurement of pH

Changes in extracellular pH values were detected using miniaturized glass electrodes (Figure 2.17), purchased from KSI. The spherical glass membrane at the top of the sensor has a diameter of ~ 1 mm and is protected by a screw cap. The external dimensions of the electrode are largely identical to those of the oxygen electrode.

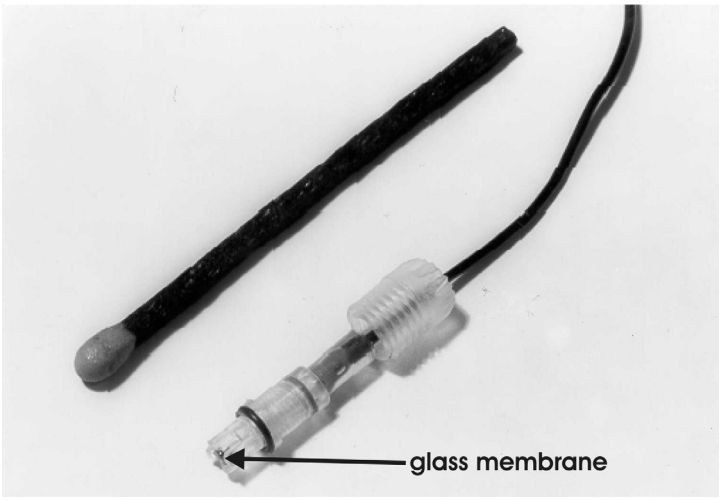


**Figure 2.17:** Photograph of a miniaturised pH-electrode (Brischwein 1997).

| | |
|---|---|
| Sensitivity | 55 – 59 mV per pH |
| pH of internal electrolyte | pH = 6.7 |
| Response time ($t_{90}$) | 20 s |
| Back ground noise level (digital signal) | ~ 0.0025 pH (0.15 mV) |
| Signal Drift | not detectable |

**Table 2.2:** Characteristics of the pH glass microelectrode.

A separate Ag/AgCl electrode (Type 8-702, flow-through type), obtained from Microelectrodes, Inc New Hampshire, USA, was used as a *reference electrode* for pH measurement (Figure 2.18).

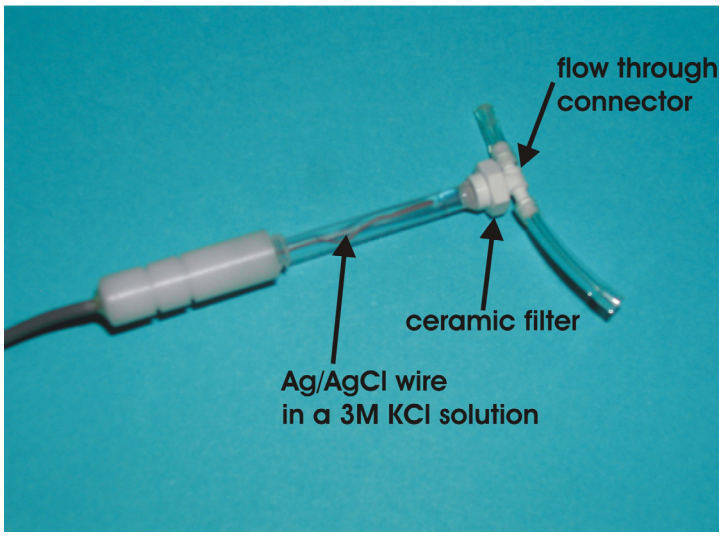


**Figure 2.18:** Photograph of the pH reference electrode with a flow through connector at the tip.

### 2.2.3 Impedance measurement

A LCR Meter (model "SR 715“ from Stanford Research Systems) was used to measure the impedance of IDES. The LCR meter produces a sinusoidal voltage u(t) at a fixed frequency of 10 kHz and measures the current i(t). From these values, it calculates the impedance Z(t). With the assumption of a capacitance and a resistance in parallel as an equivalent circuit, the values of $C_{par}$ and $R_{par}$ (capacitance in parallel and resistance in parallel) can be calculated from Z . $C_{par}$ and $R_{par}$ are usually calculated for an exact frequency (Schrüfer,1995).

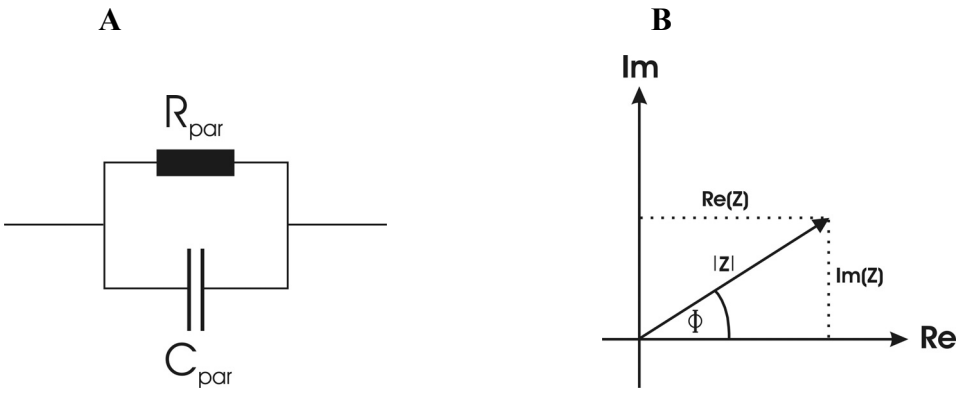


**Figure 2.19: (A)** Equivalent circuit with resistance and capacitance in parallel, used for the description of experimental results and **(B)** representation of the complex impedance $\underline{Z}$ .

According to Ohm`s law, the complex impedance $\underline{Z}$ is calculated from the following equations:

$$\underline{Z} = Z' + jZ'' = \mathrm{Re}\{\underline{Z}\} + j\,\mathrm{Im}\{\underline{Z}\}$$

$$|\underline{Z}| = \frac{U_{eff}}{I_{eff}} \qquad \text{for sinus signals.}$$

$$Z' = |\underline{Z}|\cos\varphi \;; \quad Z'' = |\underline{Z}|\sqrt{1-(\cos\phi)^2}$$

with $R_{par} = f_1(\mathrm{Re}, \mathrm{Im})$

$$C_{par} = f_2(\mathrm{Re}, \mathrm{Im}, f)$$

The analytical functions to calculate $R_{par}$ and $C_{par}$ from Z´ and Z´´ are:

$$R_{par} = \frac{Z'^2 + Z''^2}{Z'}; \qquad C_{par} = \frac{Z''}{2\pi f (Z'^2 + Z''^2)}$$

where:

$\underline{Z}$: complex impedance

Z´: real part of the impedance

Z´´: imaginary part of the impedance

j : imaginary number

Φ: phase angle

$U_{eff}$: RMS (root mean square) voltage

$I_{eff}$ : RMS (root mean square) current

$f$: frequency

Alternatively, the impedance Z may be represented by its absolute value and the phase angle (see Figure 2.19-B). It is important to note, that there is no theoretical concept that assigns these figures ($R_{par}$, $C_{par}$, absolute value of Z, phase angle) to any cell biological meaning. Impedance measurements presented in this thesis are used merely to demonstrate the presence of cell morphologic changes. In order to interpret the observed changes in impedance, additional information, e.g. obtained from light microscopy, is necessary.

The measurement of more than one IDES is controlled by a multiplexer, built at the TUM, Chair of Medical Electronics.

## 2.2.4 Electrical ground concept

A correct setup of the electrical ground is particularly important for parallel multisensor measurements with sensors not galvanically separated from each other. The term "galvanical separation" in this context means, that sensors are in electrochemical contact to each other via a common electrolyte solution. On the level of sensor electronics, the different circuits are separated, i.e. there is no common ground contact. An "electrical ground" means, that the common electrolyte solution (the culture medium) is contacted to a ground conductor of electronic circuitry by an electrode. For single sensor measurements, an electrical ground is not expected to make sense, since leakage currents to ground may occur. However, practical experience with parallel multisensor records have shown, that the connection of an electrical ground may have a positive influence on the stability of sensor signals (e.g. in potentiometric pH measurements with glass electrodes). However, current work is directed to circumvent the problem of possible mutual interferences between different sensors by a signal multiplexing protocol which assigns distinct time intervals for switching on the various sensors (i.e. potentiometric, amperometric and impedimetric sensors). This would allow to avoid an additional electric ground electrode (personal communication with M. Brischwein and J.Ressler).

## 2.2.5 Fluidic system:

*Pump and tubes:*

A 4-channel peristaltic pump (Ismatec, Glattbrueg, Switzerland) was used to drive the fluidic system. Cell culture media and various test substances are pumped from the medium supply vessels through the tubes to the cells with a nearly constant flow velocity. The material of the tubing is Pharmed and Tygon (Ismatec). The tubing between the supply vessel and the cell culture contains approximately 750 µl of medium. The medium volume between the cell culture and the position of the microelectrodes is approximately 10 µl. At a flow rate of 5 ml/h the time required for the fluid to pass this section is thus approximately 10 seconds. A water bath is used in order to maintain the supply vessels at a constant temperature (37 °C).

## 2.2.6 Elimination of air bubbles

Air bubbles in the culture medium may seriously disturb cell culture conditions as well as the microsensor measurements. In order to eliminate air bubbles from the culture medium, a degassing device is mounted at the inlet before the fluid-in-ports of the double chamber. Different models of degassers have been tested (see Brischwein, 1997). Since the results were not completely satisfactory, we have recently developed a bubble trap which is inserted into the fluid system instead of the degasser. The working principle of this bubble trap is shown in Figure 2.20. Emerging gas bubbles are eliminated from the flowing medium by applying a small negative pressure through an opening in the bubble trap, which is connected to the peristaltic pump.

In addition to the degasser the presence of air bubbles can be avoided by:

- heating to 37 °C and degassing the medium (without FCS) by applying a vacuum (about 1 mbar, 10 minutes) before starting the experiment,
- maintaining the temperature of the culture medium at 37 °C using a water bath during the experiment,
- using a tubing material with a low gas permeability such as tygon for transport of the medium from the medium supply to the chips with the cells.

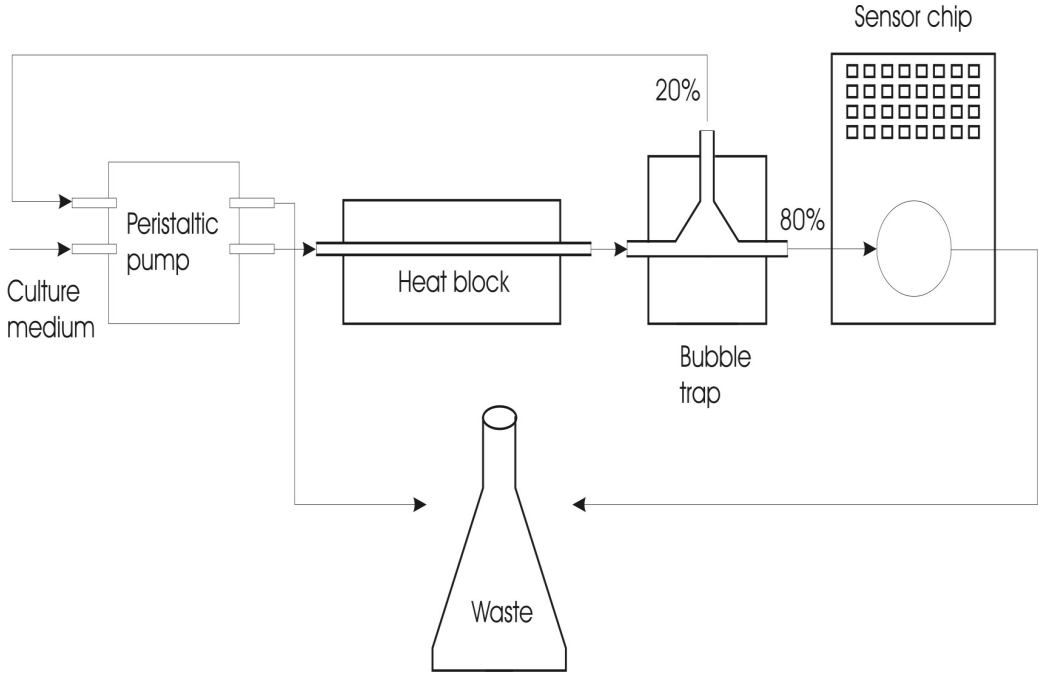


**Figure 2.20:** Positioning of the bubble trap in the cell monitoring system.

### 2.2.7 System handling

The glass chips are rinsed with water and ethanol, mounted in the stainless steel housing and sterilized by autoclaving. Afterwards, the cells are seeded on the sterile chips and incubated at 37 °C and 5 % $CO_2$ for 24 to 48 hours. Before starting the measurement the fluidic system is sterilized by perfusion with a 1% sodium hypochlorite solution (about 2 hours), followed by sterile water (about 2 hours) and then with culture medium for about 20 minutes. During sterilization, rinsing and priming of the fluidic system, the double chamber stainless steel housing with the chips is replaced by a "dummy" plexiglass unit. The experiment is started with the insertion of the mounted chips into the fluidic system. At the end of the experiments, the detergent Triton X-100 is added, destroying cell membranes, in order to obtain base line sensor signals.

### 2.2.8 Data evaluation

The Cell Monitoring System allows the adjustment of the ‘stop’ and ‘flow’ rate of the fluid perfusion system to the actual experimental conditions. Data from microsensors for pH and oxygen mounted in the fluid-exit-port of the double chamber are evaluated on the basis of the following consideration: when the pump is on, fresh medium is pumped into the double chamber to the chips and cells. This is represented in Figure 2.21 by the time period X1 to X3. The following ‘stop’ interval with stagnation of the medium over the cells is between X3 and X4. The time period X1 to X4 represents a complete measurement cycle. Due to cellular metabolism during the stop interval, the values of $pO_2$ and pH in the medium enclosed in the chambers change. In the following ‘flow-interval’, this medium is transported to the sensors, causing a decrease of pH and $pO_2$, with a minimum at X2. A short time delay occurs due to the small volume of about 10 µl between the chamber and the sensors. This decrease is followed by a recovery of the values (X3) which is incomplete due to continuous exchange between cells and medium (comparison between X3 and X4).

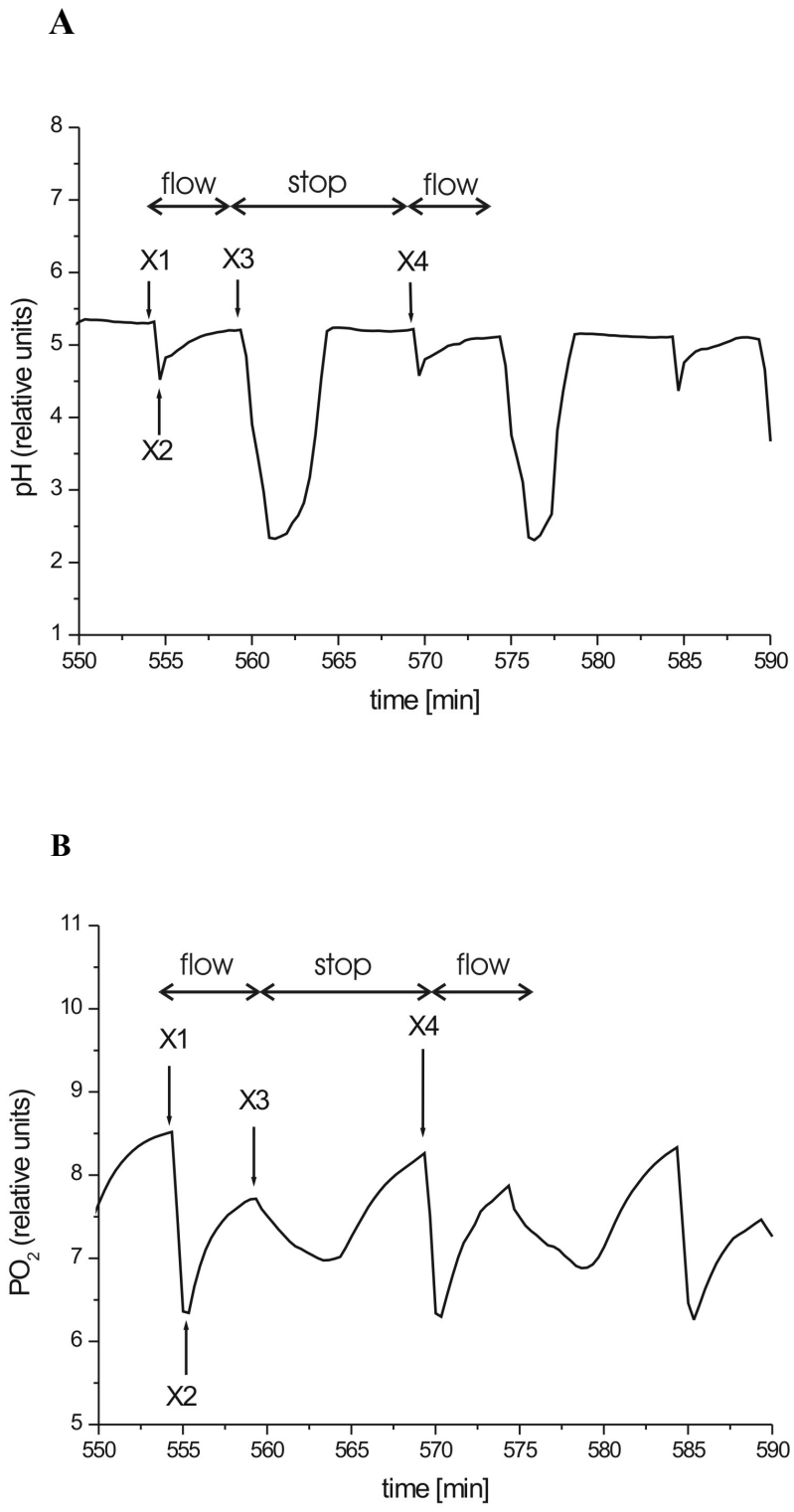


**Figure 2.21:** Characteristic measurement curve with 'stop-and-go' mode for **(A)** pH- and **(B)** $pO_2$-microelectrodes.

Added to these fluctuations caused by cell metabolic activity are regular fluctuations due to temperature variations at the sensors. To avoid such disturbances, a fluid mode was elaborated providing a constant flow at the sensors. The flow is alternatively switched

between the cell chambers and additional bypass channels by a valve. Cell chambers and bypass channels are kept at the same temperature. Thereby a considerable improvement of the signal curves can be achieved (Figure 2.22).

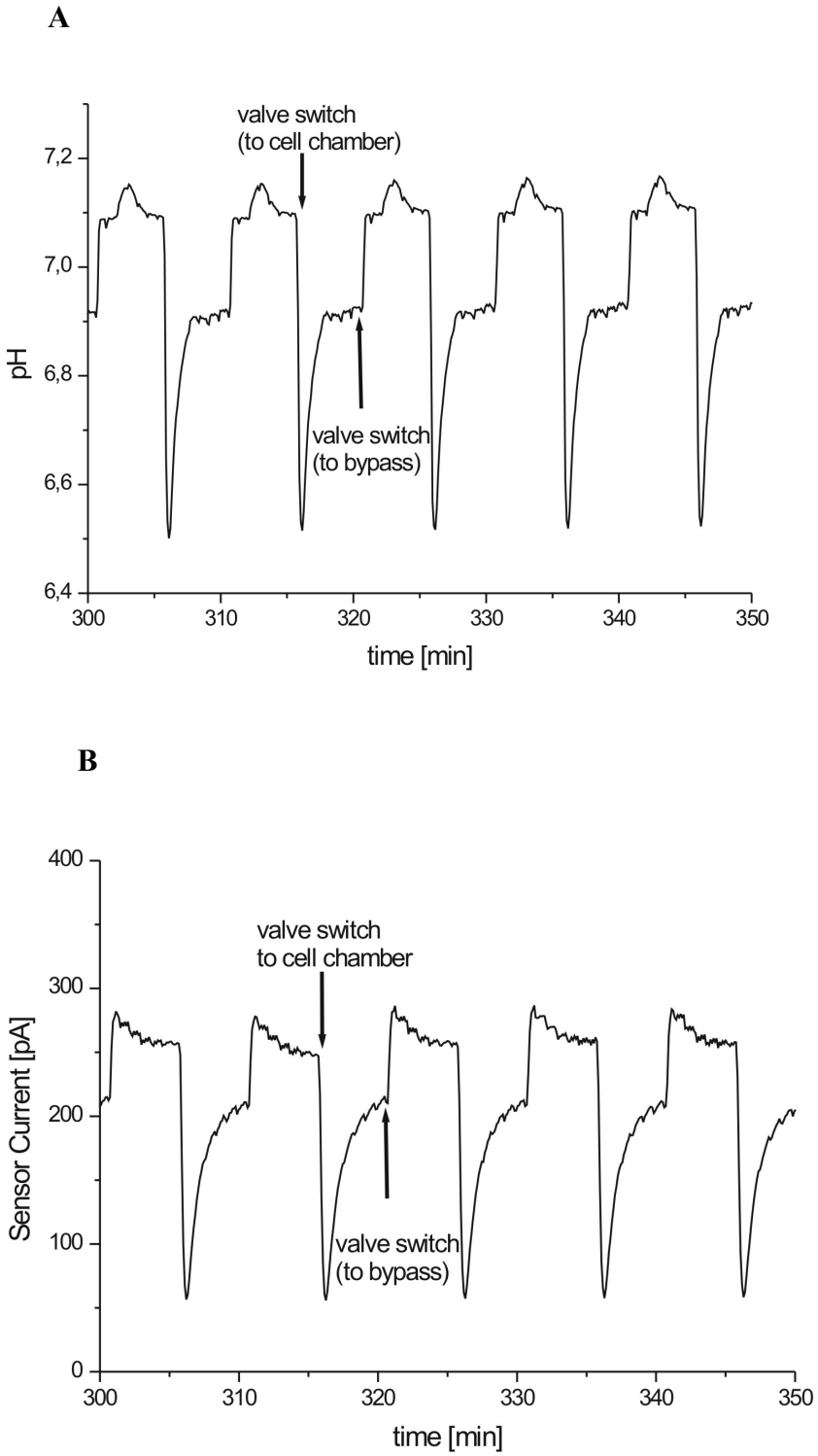


**Figure 2.22:** Characteristic measurement curve with 'stop-and-go' mode for **(A)** pH- and **(B)** $pO_2$-microelectrodes.

Generally, absolute values of pH and oxygen are not in the focus of interest. Instead, the calculation of cell metabolic rates is based on the determination of relative changes during short time intervals where long term signal drift is neglectable.

**Measurement without cells**

In order to observe which part of the signals are due to cellular activity and which are just artefacts of the system, measurements without cells were performed. A convenient way to control such effects is to solubilise the cells at the end of the experiment with Triton X-100. The signals obtained after Triton application (signals without living cells) are subtracted from the initial signals.

## 2.2.9 Software

A computer program which allows parallel measurements from all the sensors to be recorded simultaneously was written by Eléonore Cabala. The advantages of this new program in comparison with the old one are:

- It is possible to display the measured points graphically during the measurement, thus allowing better control during a running experiment (see Figure 2.23). Before this program was available, a Qbasic program was used.
- This program allows the measurements to be displayed as they are recorded by the IDES and the optical oxygen sensor; until now two different programs were used in order to display this information.
- It records and also automatically archives the measured data.
- It was programmed in C++ and Tcl/Tk and runs under different operating systems (Windows/Linux).
- The modular incorporation of data obtained from additional sensors (microelectrodes for pH and $pO_2$, planar sensors) is possible and under progress. This work goes along with a reorganisation of the electronic modules necessary for the different sensor types.

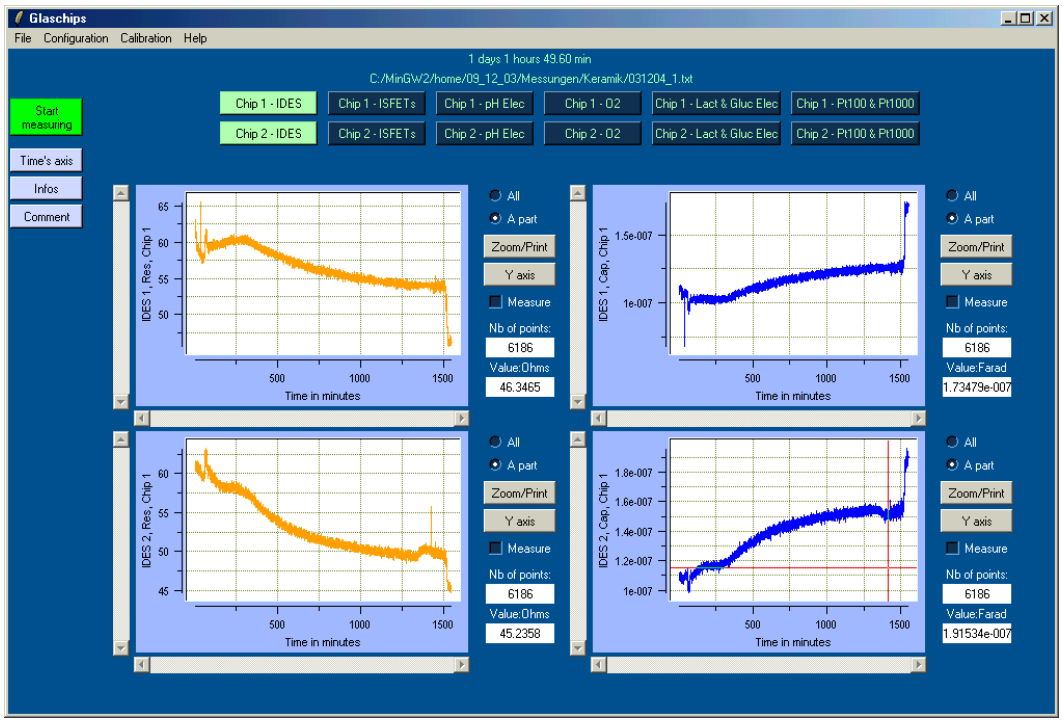


**Figure 2.23:** Example for an impedance measurement by IDES; curve displayed during the experiment.

## 2.3 Electronic cell counter

In order to count cells with a high throughput, an electronic cell counter (CASY 1, Schaerfe System, Reutlingen) was used (Figure 2.24).

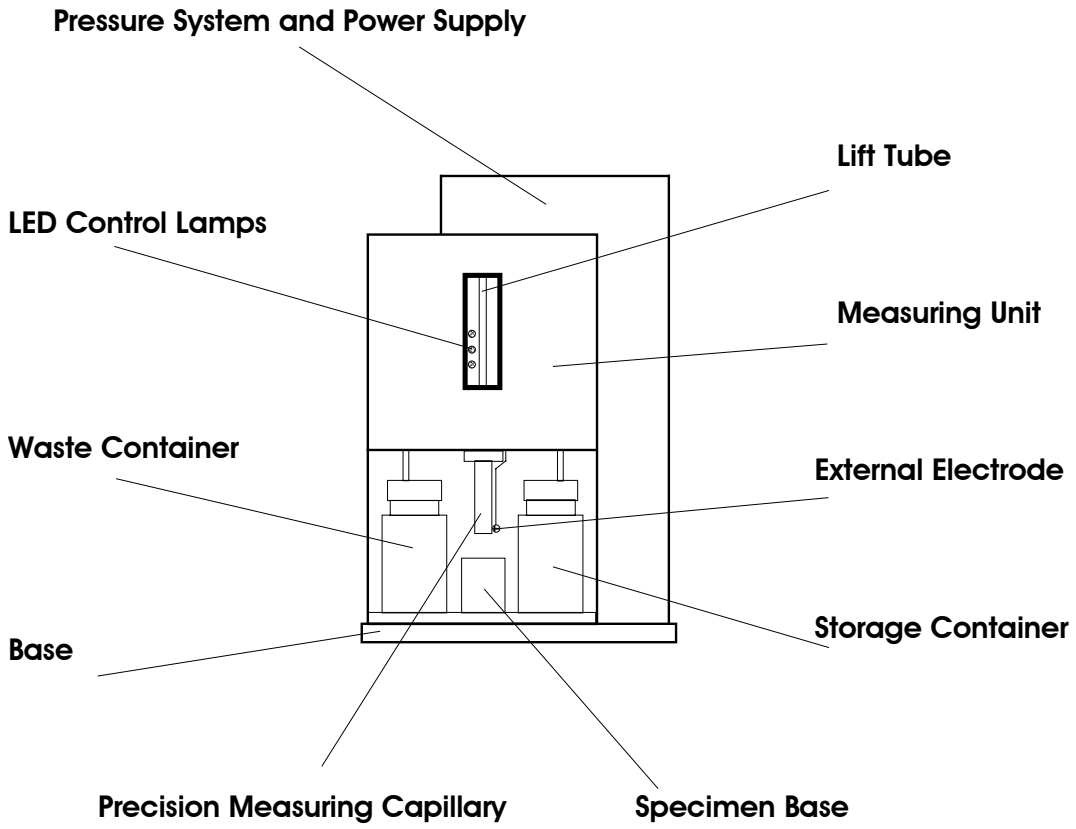


**Figure 2.24**: Casy 1, front view (Schaerfe Systems, handbook).

The cells are suspended in an electrolyte and are drawn through the capillary. During the measurement, a sinusoidal voltage is generated between two platinum electrodes and the electric impedance is measured. One of the electrodes is placed outside the capillary (external electrode), the other one is placed inside (not shown in Figure 2.24). The capillary used for cell counting has an aperture of 150 µm. As cells pass the electrodes in the capillary, the impedance increases. The time required for a cell to pass the capillary is typically $10^{-3}$ seconds. Due to a measurement frequency of about $10^{6}$ Hz, the shape of a cell can be analysed with a high precision. The recorded changes are related to the cell volume. Small particles (e.g. cell debris) can be identified by the small effective particle volume.

In the experiments presented in this thesis the cell nuclei were counted in order to avoid the problems associated with cell clumping. This was achieved by incubating the cells for 20

minutes with hypotonic buffer which leads to cell swelling. Subsequently, cell lysis solution was added and the cells were incubated for another 10 minutes. Finally the cells were resuspended in fresh buffer and the cell nuclei were counted.

## 2.4 Cell lines and media

- *Hela* is a human cervix carcinoma cell line, established from the epitheloid cervix of a 31 year old black woman (obtained from ATTC, CCL-2).
- *LS174T* is an adenocarcinoma colorectal cell line (obtained from ATCC, CL-188). This cell line is the trypsinised variant of LS180 colon adenocarcinoma cell line and offers the advantage of being more easily subcultivated than the parent line LS180.
- *MDA-MB 231* is a highly invasive breast cancer cell line, established from an effusion of a 48 year old woman with breast carcinoma in 1976 (obtained from DSMZ).

The cell lines LS174T and MDA-MB231 were maintained in Dulbecco`s Modified Eagle`s Medium with F12 (1:1), DMEM-F12 (from Sigma, Munich, Germany) supplemented with 2.5 mM L-glutamine and 10 % FCS (Seromed, Biochrom, Berlin, Germany). For the Hela line an RMPI culture medium supplemented with 10 % FCS was used (from Sigma). For analysis of cellular activity by the chip system the same medium was used as for the cell culture, but with 5 % FCS, 50 µg/ml gentamycin (Sigma) and only 0.2 g/l bicarbonate content to reduce the buffer capacity. Further details are described in Part 3 of this thesis.
PBS (phosphate buffered saline) and EBS (Earle`s balanced salts) were purchased from Sigma, Munich, Germany.
Hypotonic buffer (containing HEPES buffer, $MgCl_2 \cdot 6H_2O$, $CaCl_2 \cdot 2H_2O$ and $CaCl_2$) and cell lysis solution (containing 5% acetic acid in benzalkonium chloride) were freshly prepared.

## 2.5 Special biochemicals

*Fluorescence dyes:* The following fluorescence dyes were purchased from Molecular Probes: Fluo 4-AM AM “cell permeant” (Prod. Nr. F-14201) for analysis of the intracellular concentration of free calcium ions; JC-1, 5,5`,6,6`-tetrachloro-1,1`,3,3`-tetraethylbenzimid-azolylcarbocyanine iodide (Prod. Nr. T-3168) for staining mitochondria; 2`,7`-

dichlorodihydro fluorescein diacetate, $H_2$DCFDA (Prod. Nr. D-399) as an indicator for intracellular reactive oxygen species.

*ATP (adenosine triphosphate) determination kit* (ATPLite $^{TM}$ –M, Prod. Nr. 6016941) was obtained from Perkin Elmer Life Sciences, Rodgau-Jügesheim, Germany.

*Growth Factor Reduced Matrigel Matrix* (Prod. Nr. 356230) was obtained from Becton Dickinson Bioscience, Heidelberg, Germany.

*Chloroacetaldehyde, cytochalasin B and histamine* (2-[4-imidazolyl]ethylamine) were purchased from Sigma, Munich, Germany. Stock solutions of chloroacetaldehyde in water (5 mM), cytochalasin B in DMSO (5 mg/ml) and histamine in water (25 mM) were prepared.

# 3. Description of the Experiments and Results

## 3.1. Experiments to validate data from sensor chips with results from biochemical assays

The central question of this study was how the different sensor data are related to the results of independent analytical methods. To investigate this relation, two model experiments were chosen: (1) the analysis of the effects of histamine stimulation on the cervix carcinoma cell line Hela and (2) the action of two different drugs, (i.e. the alkylating substance chloroacetaldehyde (CAA) and the mold alkaloid cytochalasin B (CB)) on the colon cancer cell line LS174T. Moreover, new information about the mechanism of action of these substances was obtained from these studies.

### 3.1.1 Assays to investigate the effect of histamine on Hela cells

Histamine is a hormone activating the so called inositol phospholipid pathway and thus liberating calcium ions from vesicles in the cytoplasm. The intracellular concentration of calcium ions plays an important role in cellular activity, acting as a "second messenger" for many processes by transmitting information from receptors to intracellular target segments.
Two methods were used to study the response of Hela cells to stimulation with histamine: (1) the sensor based detection of cell metabolic and cell morphologic responses and (2) the detection of changes in intracellular calcium levels using a fluorescence dye.

#### 3.1.1.1 Histamine stimulation on glass chips

The effect of histamine on Hela cells was analysed with the glass chip based cell monitoring system: Hela cells were seeded on glass chips ($10^5$ cells per chip) and incubated for 24 hours at 37 °C and 5% $CO_2$. After 24 hours, the chips with the cells were mounted into the cell monitoring system and the measurement was started. Upon addition of 25 µM histamine, the $C_{par}$ component of the electric impedance changed immediately, reflecting a morphological response of the cells. During the experiment the cells were stimulated twice. The changes were clearly more pronounced after the first stimulation in comparison to the second stimulation, suggesting an adaptation of the involved signalling chain (Figure 3.1). Moreover, for the first stimulation a biphasic response of cells could be detected (initial increase of $C_{par}$

values for about five minutes**,** followed by a marked decrease). At the end of the experiment the detergent Triton X-100 was added.

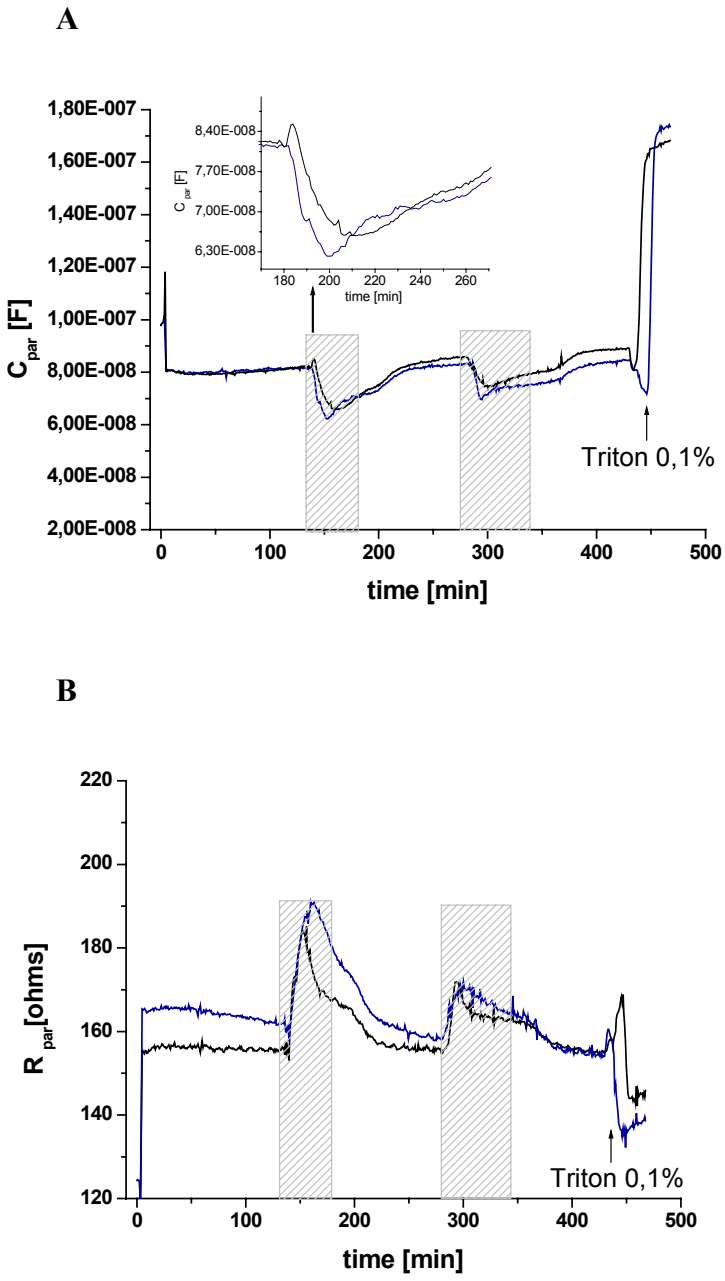


**Figure 3.1:** Impedance graphs for Hela cells treated with histamine; histamine (25 µM) during the time periods indicated by the shaded areas; the two graphs represent two impedance sensors on a single glass chip; **(A)** $C_{par}$ component, **(B)** $R_{par}$ component.

While changes in impedance values indicate an increase in cell-cell and cell-substratum adhesion, no effect of histamine on Hela cell metabolism could be found as revealed by sensor measurements of oxygen consumption and extracellular acidification (Figure 3.2).

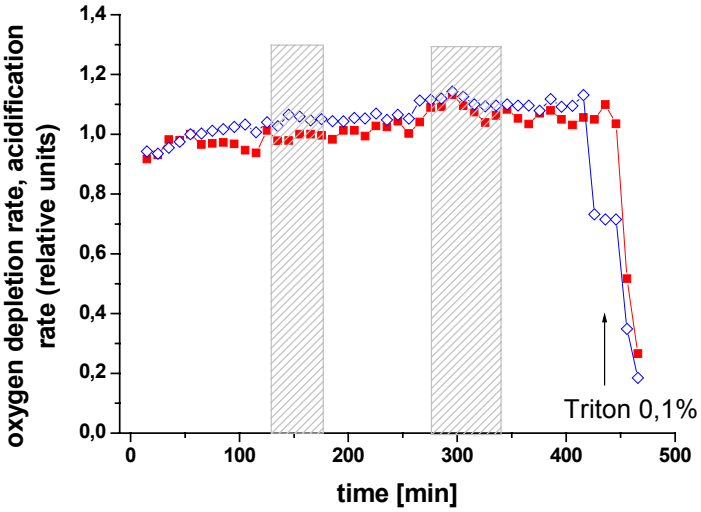


**Figure 3.2:** Metabolic activity of Hela cells cultured on glass chips and stimulated with histamine; histamine was present during the time periods indicated by the shaded areas; red line: the rate of extracellular acidification; blue line: the rate of oxygen consumption.

### 3.1.1.2 Histamine stimulation as detected with a fluorescent assay

In order to test whether the observed impedance changes correlate with an intracellular calcium signal, the effect of histamine on Hela cells was further analysed using the fluorescence dye Fluo 4-AM, which binds free $Ca^{2+}$ ions. For both methods, cell monitoring with IDES and the photometric analysis of cell population, signals integrated over an adherently growing cell population were obtained. Fluo 4-AM (Molecular Probes, Figure 3.3) is a cell permeant acetoxymethyl ester which passively enters the cell interior and emits fluorescence only when bound to calcium ions. Once inside the cell, the ester is cleaved by cytosolic esterases, resulting in the formation of formaldehyde, acetate and the acidic form of the dye which then acts as an indicator for intracellular calcium ions. Fluo 4-AM is excited at 485 nm and emits light at 520 nm.

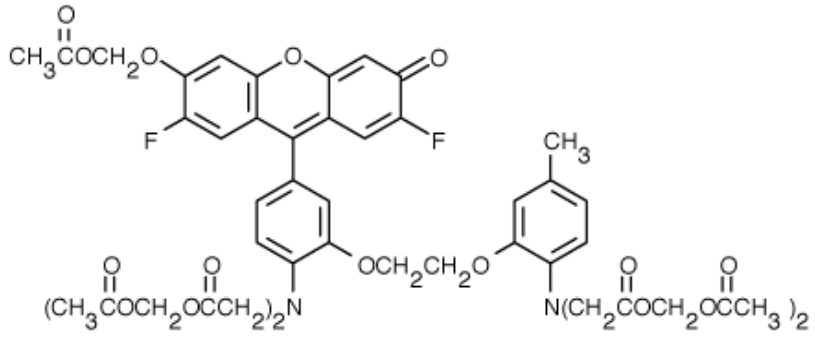

**Figure 3.3:** The chemical structure of Fluo 4-AM (www.probes.com).

Hela cells were seeded on a black 96 multi-well plate with a clear bottom in a concentration of 3 x $10^4$ cells per well and incubated for 24 hours at 37 °C and 5 % $CO_2$. After 24 hours the culture medium was replaced and the cells were rinsed once with 100 µl EBS. This was followed by an incubation for 30 minutes at room temperature with 50 µl of Fluo 4-AM at a concentration of 0.25 µM. After 30 minutes the dye was replaced and the cells were rinsed twice with EBS. Prior to the measurement the cells were incubated in EBS (95 µl/well) allowing de-esterification of the dye by action of intracellular esterases. The measurement was started in the well mode and after 35 seconds histamine was added at a final concentration of 25 µM via automatic injection. Intracellular calcium ions are liberated from vesicles when histamine is added, as indicated by an increase in fluorescence intensity (Figure 3.4).

As a control, an identical volume of EBS buffer was added to the cells stained with Fluo 4-AM in the same plate. Addition of histamine induced rapid changes in the fluorescence intensity over 20 seconds. A maximum of intensity was observed after approximately 10 seconds. Thereafter, the fluorescence intensity decreased gradually to baseline values. No biphasic signal could be observed. However, the time resolution of the plate reader system with its injection fluid system is considerably higher than that of the sensor based cell monitoring system. The time resolution of the latter one is limited by the perfusion system. On the other hand, dynamic recording of intracellular $Ca^{2+}$ ions for more than a few minutes is hardly possible with the plate reader system. It results, that a direct comparison of the signal kinetics is not possible. The plate reader detects integral changes (no single cell measurements) of the cytoplasmic free $Ca^{2+}$ concentration. In this respect it is similar to cell monitoring on impedance sensors detecting integral cell morphologic changes of cell populations.

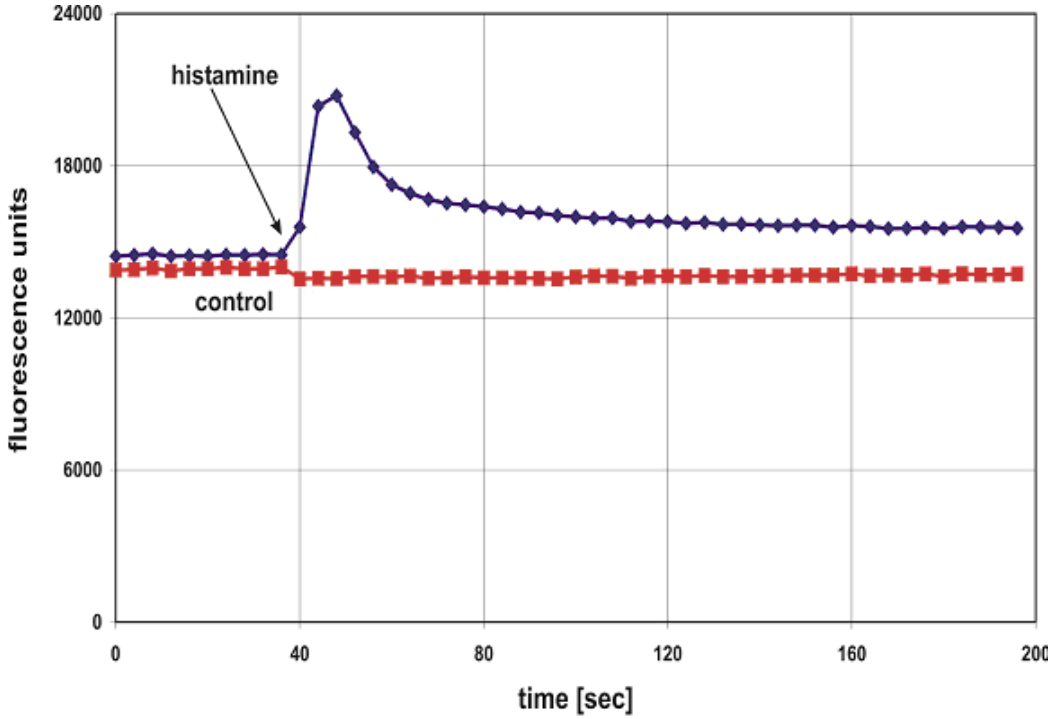


**Figure 3.4:** Analysis of free $Ca^{2+}$ ions on Hela cells stained with Fluo 4-AM and stimulated with 25 µM histamine (blue line); as a control, EBS was added alone to Hela cells (red line); a fluorescence plate reader (Fluostar) was used for the measurements.

### 3.1.2 Assays to investigate the mechanism of action of chloroacetaldehyde and cytochalasin B on colon cancer cells

Tumor metabolism not only affects the activity of different drugs (Gerweck et al., 1999) but the reverse is also true, i.e. the action of different drugs also influences tumor metabolism and microenvironment. In order to investigate the changes in tumor metabolism caused by two selected drugs (CAA and CB), metabolic parameters (rates of oxygen consumption and extracellular acidification) and changes in cell morphology/cell adhesion were analysed with microsensor techniques. For the interpretation of these sensor data, assays for mitochondrial membrane potential, cellular ATP content, production of reactive oxygen species (ROS), and for cell number were applied. Some aspects of the effect of CAA and CB on tumor metabolism have been described in previous work from the group (Ehret, et al., 2001; Henning, et al., 2002).

Oxygen consumption, extracellular acidification, cell-cell and cell-substratum adhesion were analysed in parallel using multiparametric silicon sensor chips. The different sensors integrated in a silicon chip are: pH-ISFETs (ion sensitive field effect transistors) for

monitoring the extracellular acidification, planar amperometric electrodes for monitoring the oxygen consumption in the cell culture medium and interdigital electrode structures (IDES) for detection of changes in membrane properties, cell number and cell morphology/cell adhesion. A detailed description of the silicon sensor chip system has been published by Brischwein et al., 2003. The LS174T human colon carcinoma cell line was chosen as a model since it has been well characterised in our group (Brischwein, et al., 1996; Otto, et al., 2003). It is known that CAA is a reactive metabolite of the anticancer drugs ifosfamide and cyclophosphamide. Even though ifosfamide and cyclophosphamide were introduced for the treatment of cancer about 40 years ago, many aspects of the mechanism of action of these drugs are still not well understood. CAA induces interstrand DNA cross-links, inhibits DNA synthesis and has nephrotoxic and neurotoxic effects (Huang, et al., 1999; Sood, et al., 1993). CB is known to inhibit glucose transport into the cells, to cause the depolymerisation of actin filaments (Mizel & Wilson, et al., 1972). The substance induces changes in all three parameters measured with sensor chips (Ehret, et al., 2001). CB is not used in clinical oncology as a chemotherapeutic drug although there are experimental studies suggesting an anti-metastatic effect in tumor bearing mice (Bousquet et al., 2003).

#### 3.1.2.1 Analysis of changes in oxygen consumption, extracellular acidification, cell-cell and cell-substratum adhesion with microsensors

The silicon chip system was used for the parallel online analysis of six cell culture samples over a time period of 24-72 hours. First of all the cells were added to the chips ($1.5 \times 10^5$ cells per chip) and subsequently incubated for 48 hours at 37 °C under a 5 % $CO_2$ atmosphere in an incubator. After 48 hours the cells formed a monolayer and the measurement was started. It has to be mentioned that for the experiments performed with sensor chips only relative changes are evaluated. Absolute values of pH, oxygen and impedance are not in the focus of interest. Instead, the calculation of cell metabolic rates is based on the determination of relative changes during short time intervals where long term signal drift is neglectable. Similarly, only changes of impedance ocurring upon cell stimulation are interpreted. Absolute values of impedance depend on the chip batch and the exact conditions of cell culture.

##### 3.1.2.1.1 Effects of chloroacetaldehyde

In order to determine a metabolic profile of the LS174T colon cancer cells on the basis of extracellular acidification and oxygen consumption, the cells were cultivated on the sensor

chips. Figure 3.5-A shows a dynamic online monitoring of oxygen consumption and of extracellular acidification; Figure 3.5-B shows an impedance measurement.

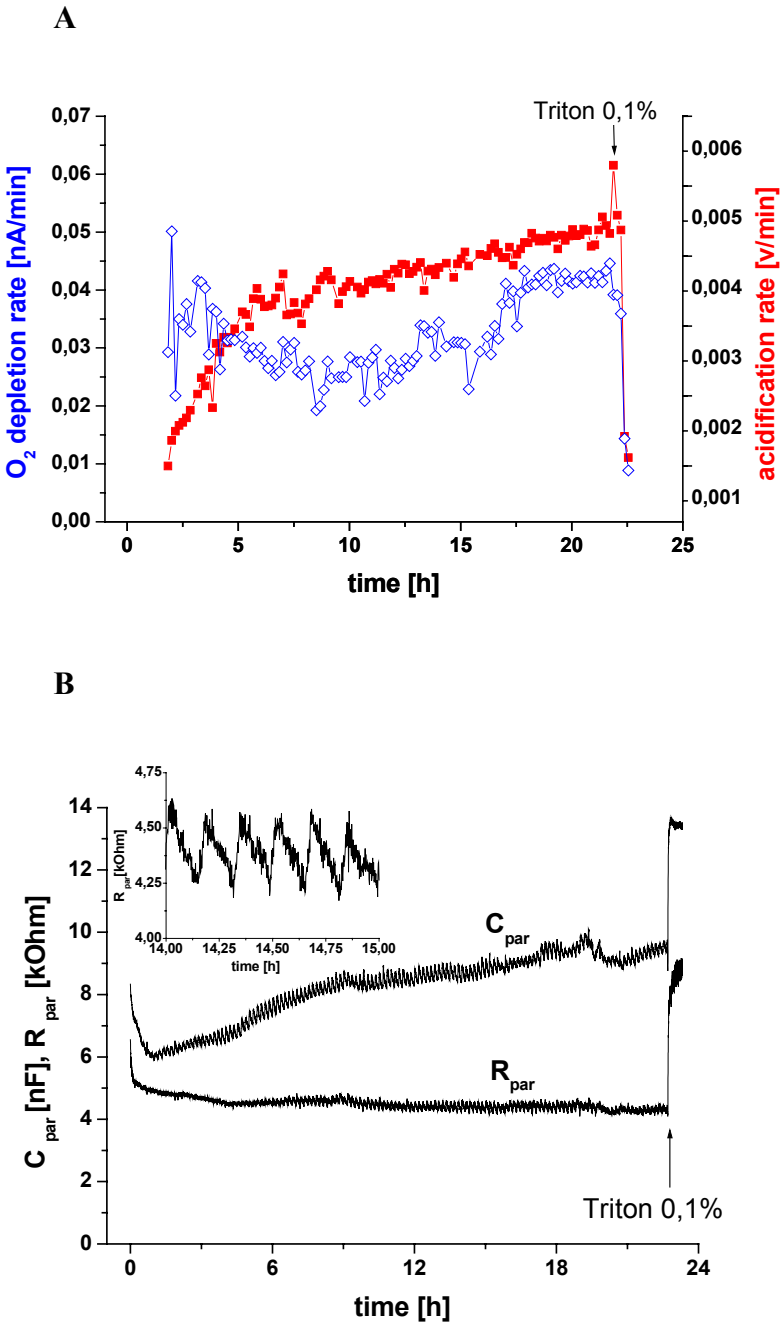


**Figure 3.5**: LS174T, untreated control cultures on silicon sensor chips; **(A)** monitoring of the rate of $O_2$ consumption (blue line) and extracellular acidification (red line); **(B)** impedance; during the experiment with no substance added.

A frequently observed phenomenon in impedance measurements with cell cultures on growing on impedance sensors is the oscillation of measured impedance values (here: $R_{par}$

component) which is correlated with the periodic mode of the fluidic system. $R_{par}$ values increase when the flow interval begins and decrease again during the stop intervals. Although there is no definite explanation for this phenomenon, it is assumed that pH variations ocurring regularly during the fluid cycles influence cell morphology and thereby the detected electric impedance. This assumption is supported by experimental studies showing the effect of pH-changes on the electric impedance of sensors grown with Hela cell monolayers (unpublished results, data not shown).

The impedance graph represents directly the sensor raw data while a linear regression algorithm was used for the calculation of acidification and oxygen consumption rates from the raw data of oxygen and pH sensors. A characteristic feature of the raw data plots is the periodic oscillation of pH and $pO_2$ correlating with the stop and flow mode of the fluidic system. Values of pH and oxygen partial pressure decrease during the stop intervals due to cell metabolic activity, which is measured as increasing ISFET voltage (Figure 3.6-A) and decreasing the values of the absolute current (Figure 3.6-B). During the flow intervals, the medium is exchanged and pH and oxygen values return to the initial levels. In the case of raw data of pH sensors, the slope of the graph (voltage vs. time) during the flow-off interval was calculated using this algorithm and the resulting acidification rate is called "Δ U/Δ t". For data presenting the rate of oxygen consumption only the first three minutes of the flow-off interval are calculated using the linear regression and the resulting slope is corrected by sensor sensitivity, which is likely to change during long measurements. The sensor sensitivity is estimated from the current values during the flow intervals. The resulting respiration rate is named "Δ I/Δ dt". Since only relative changes during the course of an experiment are relevant, the values of ΔU/Δdt and ΔI/Δt are normalized in the following diagrams, i.e. the initial values are set equal to unity. The raw data showing the rate of extracellular acidification and rate of oxygen consumption on LS174T cells cultured on silicon chips and evaluated without using the linear regression are shown in Figure 3.6.

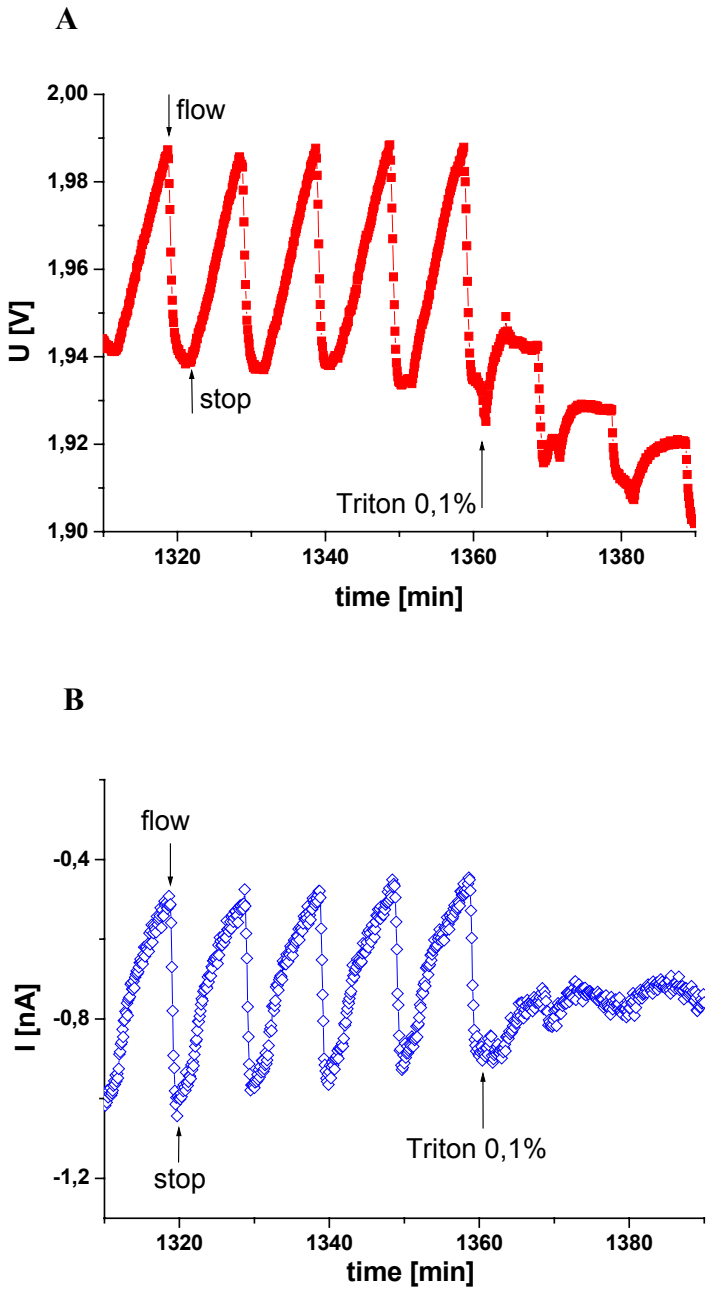


**Figure 3.6:** Sensor raw data for **(A)** monitoring of the rate of extracellular acidification (red line) and **(B)** $O_2$ consumption (blue line) in LS174T cells cultured on silicon chips; during the experiment no substance was added (Brischwein, et al, 2003).

When CAA was added at a concentration of 10 µM, the rate of oxygen consumption slightly decreased, while no difference to the control was observed in the rate of acidification (Figure 3.7-A). No effect on the impedance signals ($C_{par}$) was evident (Figure 3.7-B), since in control plots (Figure 3.5-B) a slight increase of $C_{par}$ values during the first 15 hours was also observed.

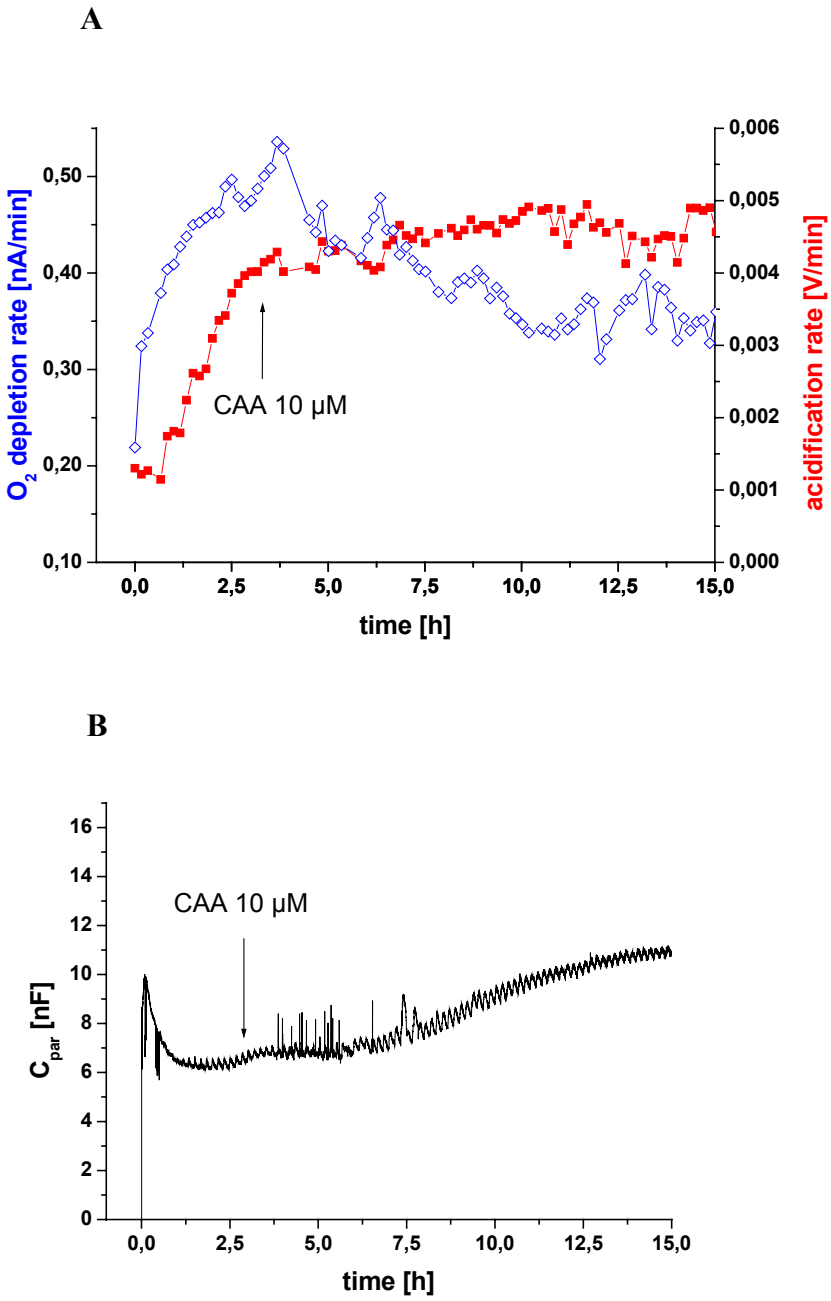


**Figure 3.7:** Effect of 10 µM chloroacetaldehyde on LS174T cells on silicon sensor chips; **(A)** monitoring of changes in the rate of $O_2$ consumption (blue line) and extracellular acidification (red line); **(B)** changes in the capacitance component of impedance; chloroacetaldehyde was added at the time indicated by the arrow.

When the cells were incubated with CAA at a higher concentration (50 µM), changes in the rate of oxygen consumption were more pronounced. The decrease of extracellular acidification rate proceeded slower than oxygen consumption rate (Figure 3.8-A).

Changes in impedance indicate cell rounding (see Figure 3.14) and loss of cell-substratum adhesion (Figure 3.8-B)

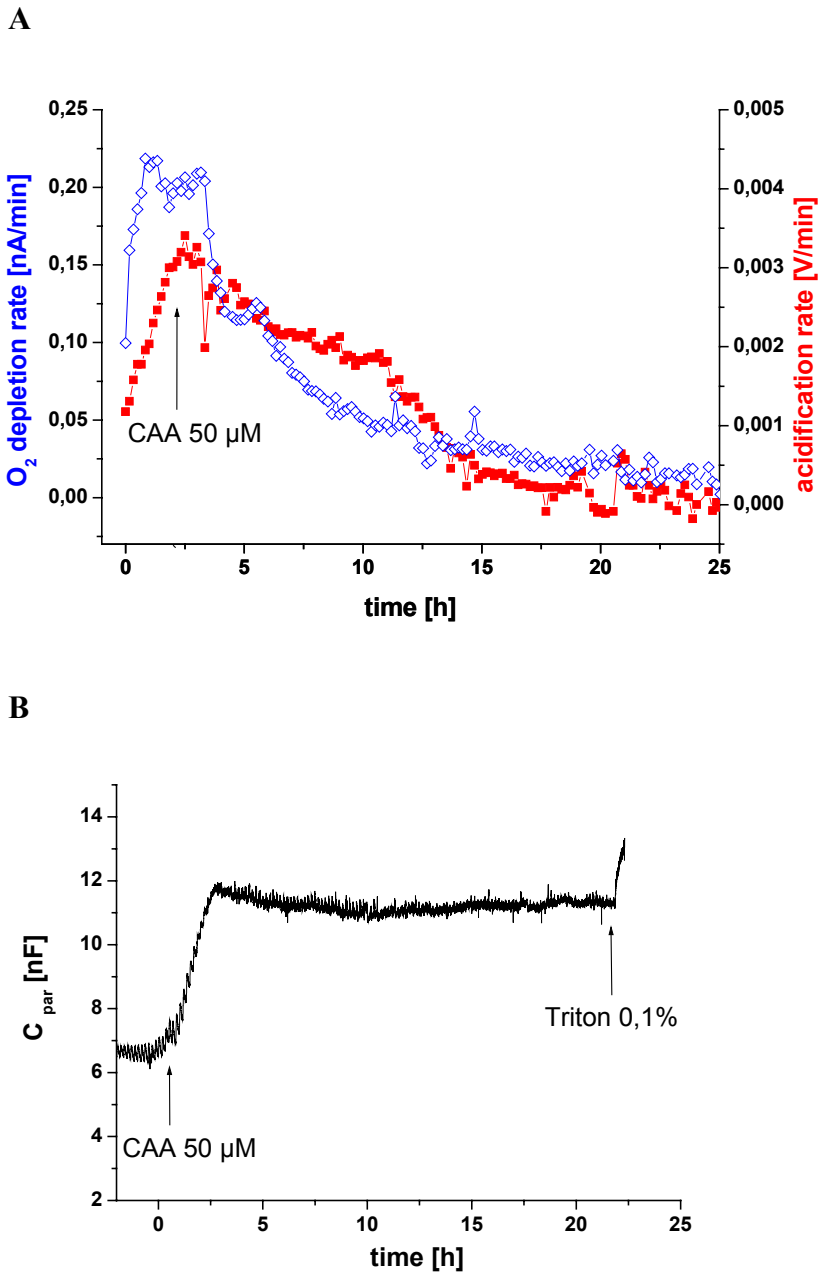


**Figure 3.8:** Effect of 50 µM chloroacetaldehyde on LS174T cells on silicon sensor chips**; (A)** monitoring of changes in the rate of $O_2$ consumption (blue line) and extracellular acidification (red line); **(B)** capacitance component of impedance; chloroacetaldehyde was added at the time indicated by the arrow; (Brischwein, et al., 2003).

### 3.1.2.1.2 Effects of cytochalasin B

Cytochalasin B (CB) was applied to the cell culture for 2 hours. 2 µM of CB caused a rapid increase in the rate of oxygen consumption, concomitant with a decrease in the rate of extracellular acidification (Figure 3.9-A). At the same time, a sharp increase in $C_{par}$ values of

the impedance sensor occurred, reflecting the inhibition of the actin cytoskeleton and the resulting cell morphological alteration (Figure 3.9-B). The removal of the drug revealed that the effect of CB on the LS174T cells is reversible (Figure 3.9).

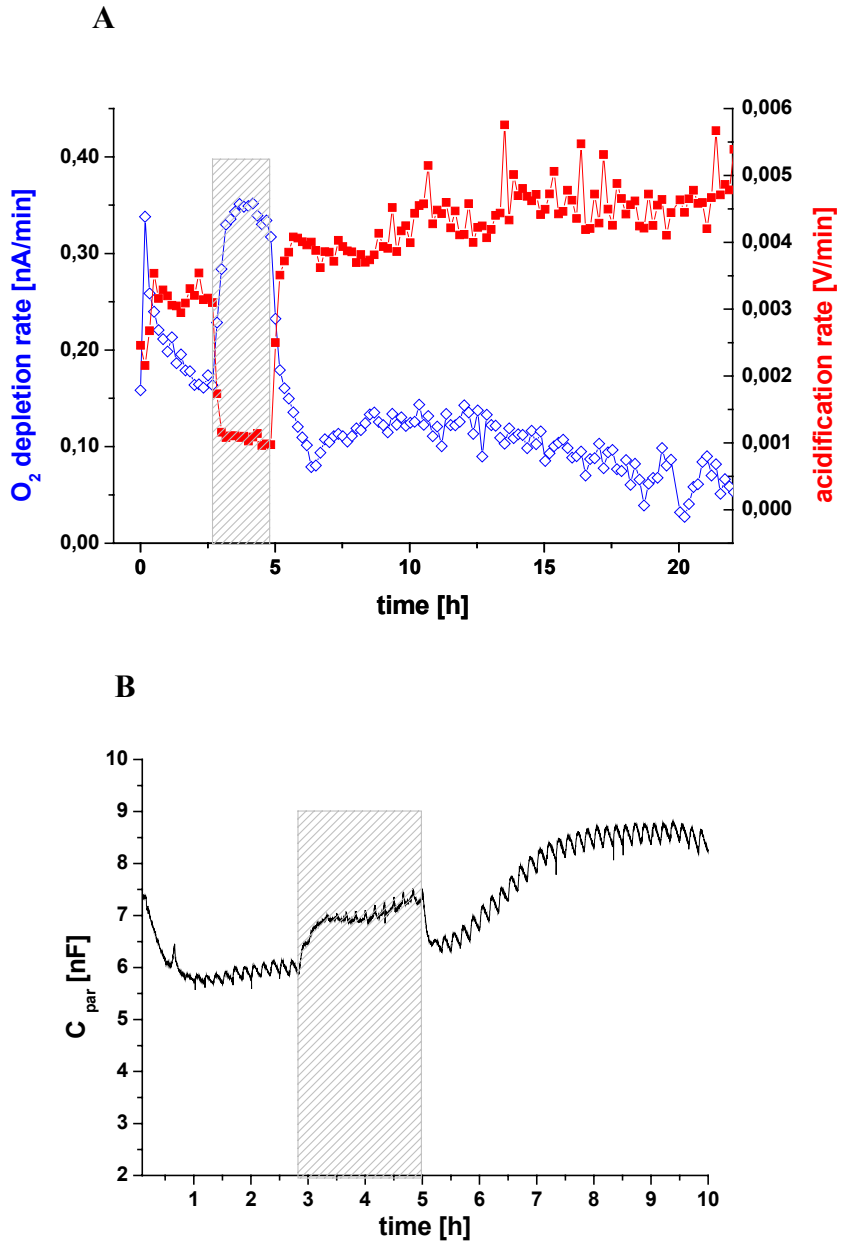


**Figure 3.9:** Effect of 2 µM cytochalasin B on LS174T cells on silicon sensor chips; **(A)** monitoring of changes in the rate of $O_2$ consumption (blue line) and extracellular acidification (red line); **(B)** changes in the $C_{par}$ component of impedance. CB was present during the time period indicated by the shaded area (Ehret, et al., 2001).

Glucose is not the only possible nutrient that can be used as a source of cellular energy. The question arises, whether the obvious metabolic switch to oxidative pathways upon inhibition of glucose import by CB also occurs, when alternative energy sources are withdrawn. The

amino acid glutamine is known to be catabolised in many tumor cells by oxidative pathways (Dang, et al., 1999; Petch, et al., 1994). In order to investigate whether glutamine oxidation is responsible for the marked increase in oxygen consumption rates observed, the normal culture medium was replaced by a medium without glutamine in an experiment on silicon sensor chips. It resulted that the changes in the rate of oxygen consumption and in the rate of extracellular acidification persisted when CB was added even if glutamine was absent (Figure 3.10).

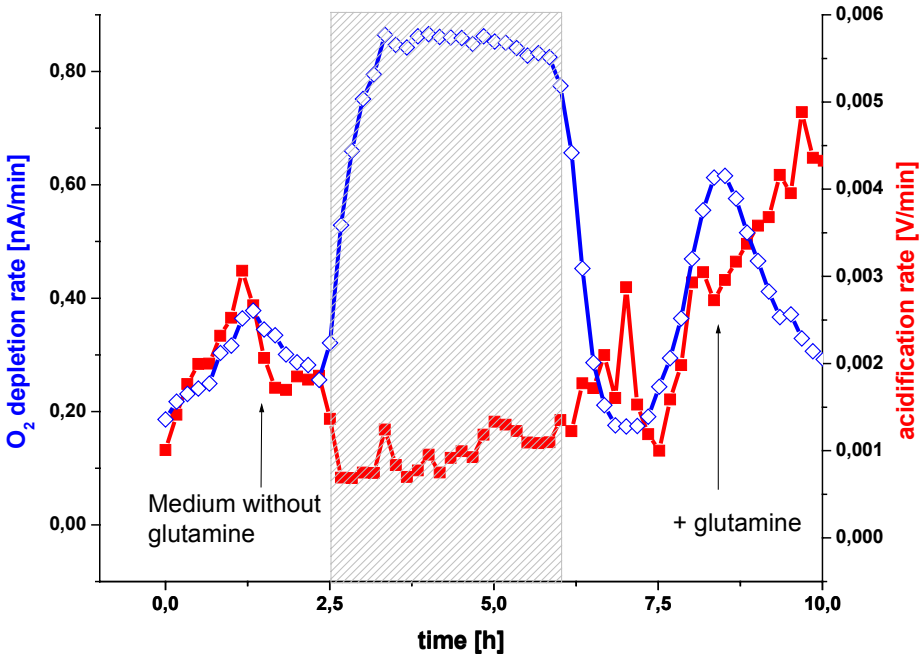


**Figure 3.10:** Effect of 2 µM cytochalasin B on LS174T cells on silicon sensor chips, culture medium without glutamine; monitoring of changes in the rate of $O_2$ consumption (blue line) and extracellular acidification (red line); the measurement started with normal medium, glutamine was withdrawn after 1.5 h as indicated by the arrow. CB was present during the time period indicated by the shaded area. The observed effects are discussed in detail in part 4.1.2.

In Figure 3.11 a similar experiment as in Fig. 3.9 is shown (LS174T cells are treated with 2 µM CB). However, CB was added twice and the experiment was performed in the glass chip system with planar impedance sensors and non-planar microelectrodes for pH and $pO_2$.

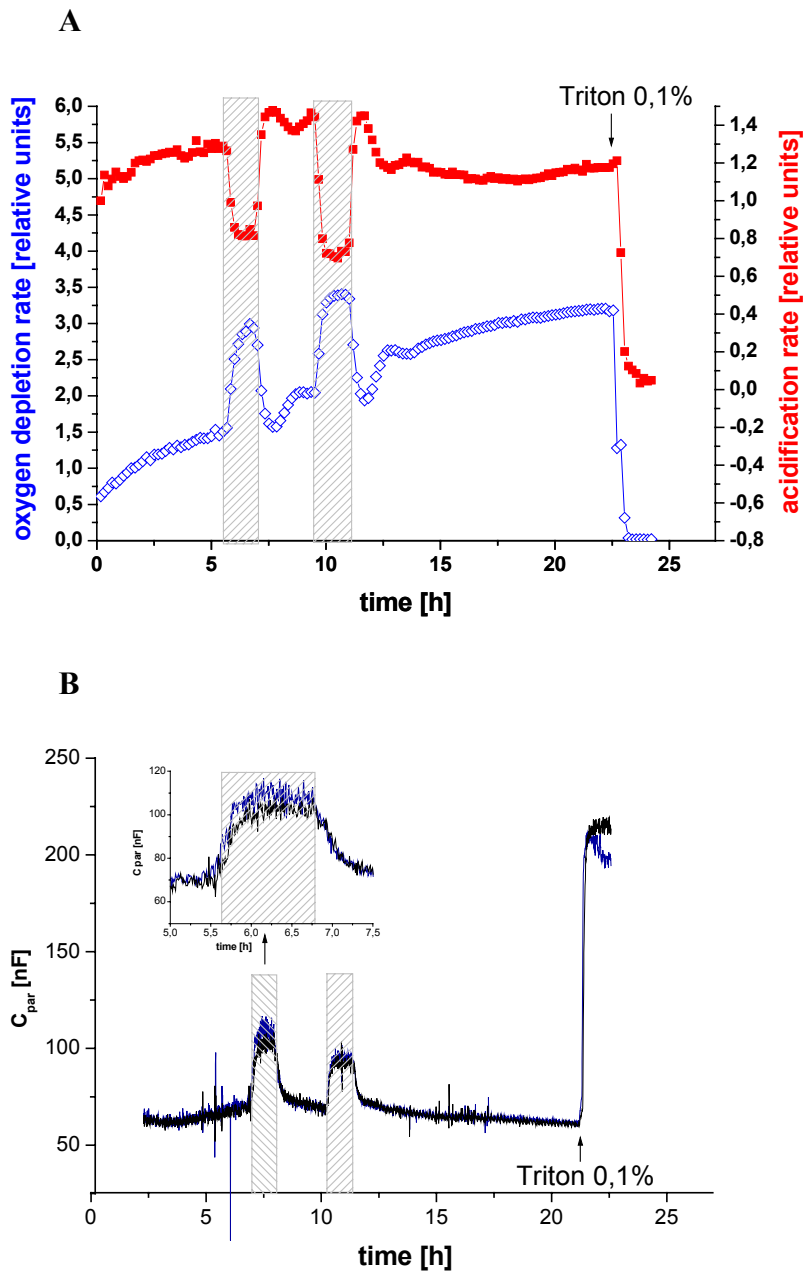


**Figure 3.11:** Effect of 2 µM cytochalasin B on LS174T cells on glass sensor chips; **(A)** monitoring of changes in the rate of $O_2$ consumption (blue line) and extracellular acidification (red line); **(B)** changes in capacitance component of impedance. Cytochalasin B was present during the time periods indicated by the shaded areas.

The results obtained with both systems are qualitatively the same. Notably, relative changes in $C_{par}$ induced by CB are more pronounced when detected on glass chips (~ 42 % increase) in comparison to silicon chips (~ 17 % increase, Figure 3.9).

### 3.1.2.2 Analysis of cellular ATP levels

Since oxidative metabolism is particularly efficient in producing ATP, the correlation between cellular ATP levels and oxygen consumption was analysed. Intracellular ATP levels were determined with an ATP bioluminescence assay kit. The cells (5 x $10^3$ pro well) were seeded into a 96 well plate and incubated for 48 hours at 37 °C and 5 % $CO_2$. This was followed by incubation in CAA- and CB-containing media for different time periods. Subsequently, the cells were lysed, luciferase-luciferin solution was added as a substrate according to the kit instructions and the luminescence was measured with the Lumistar plate reader. The results show that changes in ATP content do not correlate with those of oxygen consumption for cells incubated with either CAA nor CB. It is most remarkable that CAA causes a transient increase in ATP levels, with a maximum about 2 hours after CAA addition (Figure 3.12-A). In contrast, in cells treated with CB it appears that cellular ATP content decreases transiently with a minimum after 2 h, which was followed by a recovery to almost normal values (Figure 3.12-B).

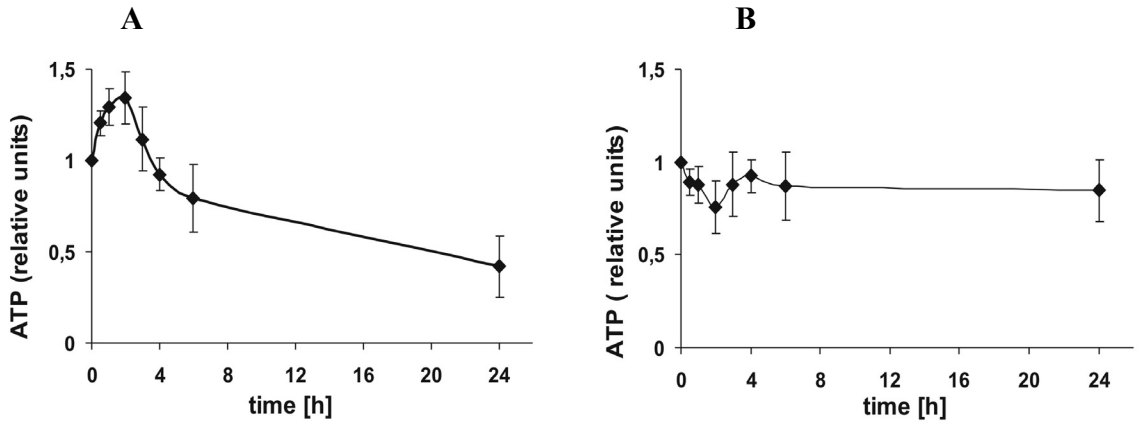


**Figure 3.12:** ATP content in LS174T cells incubated with (A) 50 µM chloroacetaldehyde and (B) 2 µM cytochalasin B for different time periods; the standard deviation has been calculated from 10 experiments. Correlations between the ATP levels and sensor results are presented in part 4.1.2.

### 3.1.2.3 Analysis of reactive oxygen species (ROS)

Oxygen is known to be involved in the generation of ROS (Esposti, et al., 2002). In order to investigate whether there is a correlation between ROS production and oxygen consumption, cellular ROS content was analysed by fluorescence microscopy. ROS production was

assessed using 2`7`-dichlorodihydrofluorescein diacetate ($H_2$DCFDA). $H_2$DCFDA is a non-fluorescent compound which is de-esterified in cells by endogenous esterases and can be oxidized by hydroperoxides originating from intracellular sources to the fluorescent product 2`7`-dichlorofluorescein (DCF). The cells were seeded on coverslips in Petri dishes and incubated for 48 hours at 37 °C and 5 % $CO_2$. Thereafter the cells were incubated in CAA- or CB-containing media for different time periods in parallel cultures. After each time period the drug containing medium was replaced by a 1µM $H_2$DCFDA solution (in EBS) and the cells were incubated for 15 min. The cells were then rinsed with EBS and the fluorescence intensity per cell was analysed with a fluorescence microscope (Zeiss, Axiovert S100) with an attached CCD camera. The measurements of fluorescence intensity in cells incubated for different time periods showed that ROS production is increased about 10-fold by 50 µM CAA. The maximum ROS production could be detected after about 6 hours of incubation. After 24 hours of incubation it appears that the level of ROS production decreases (Figure 3.13-A).

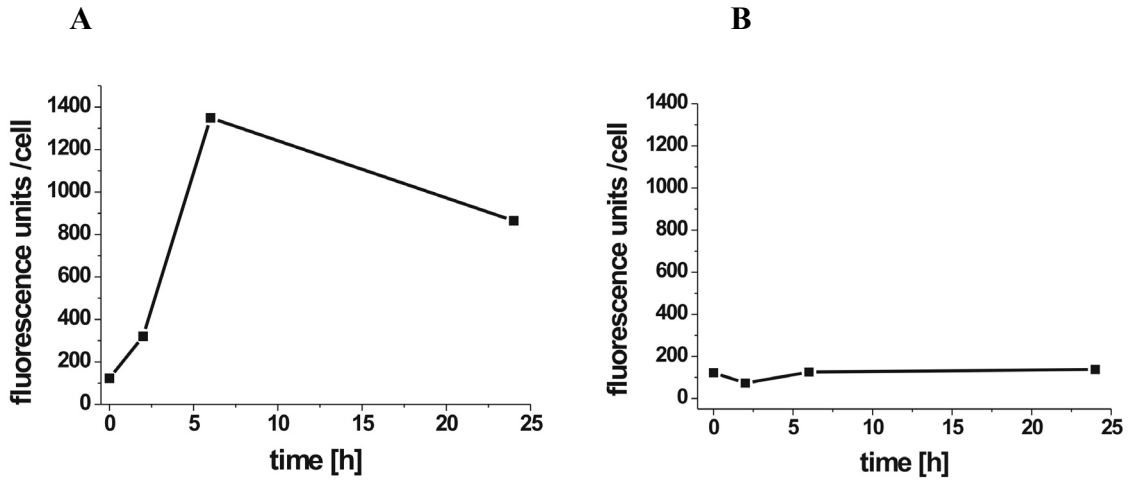


**Figure 3.13:** ROS production in LS174T cells incubated with **(A)** 50 µM chloroacetaldehyde and **(B)** 2µM cytochalasin B for different time periods; these graphs are representative of 4 experiments. Correlations between ROS production and the results obtained using sensor chips are presented in part 4.1.2.

Cell morphology is also clearly affected by chloroacetaldehyde. The cells increasingly acquire a round morphology and there is a tendency to detach from the solid substrate (Figure 3.14). In the cell populations on the cover slides, a considerable heterogeneity in ROS concentration could be observed, reflecting different cellular activities.

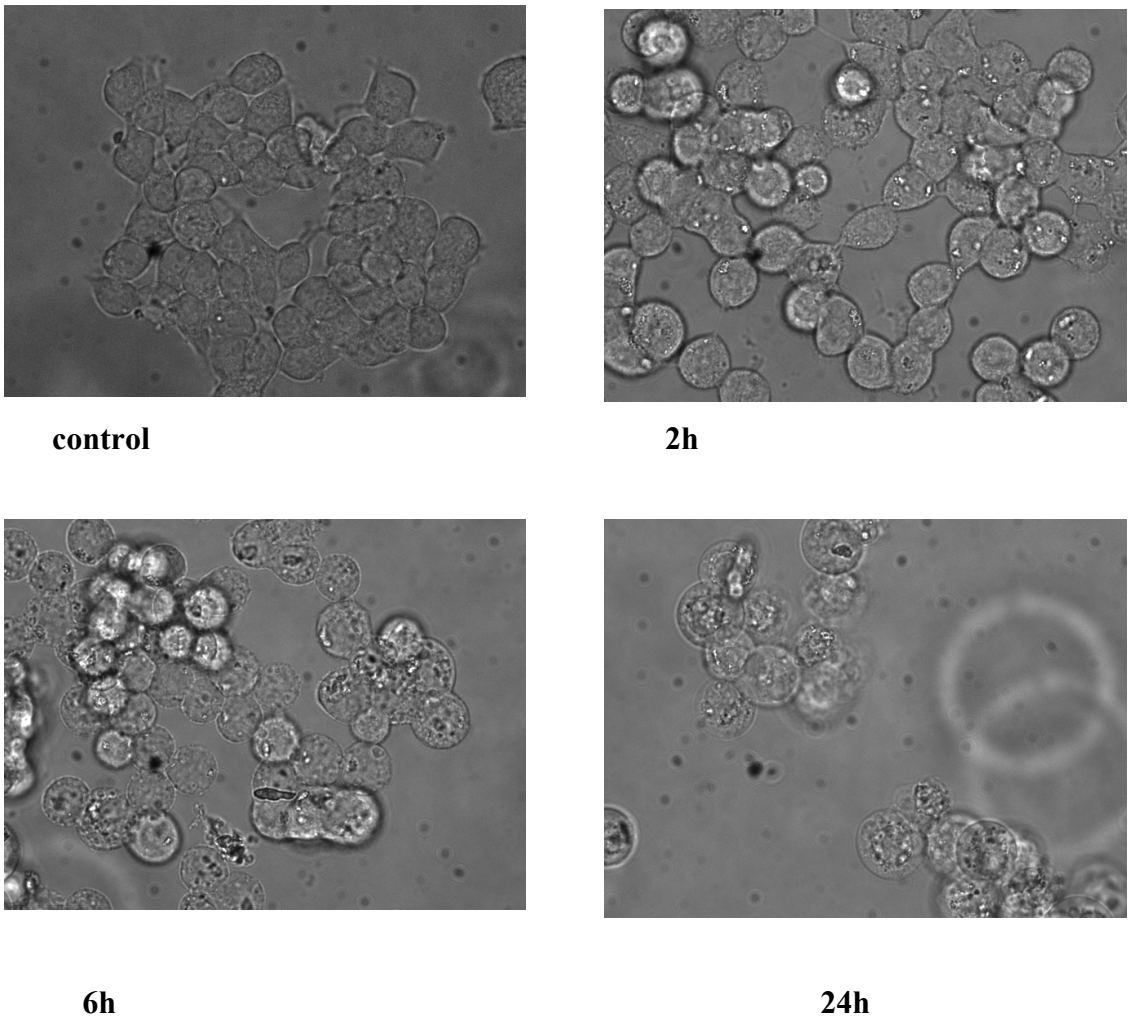


**Figure 3.14:** Phase contrast microscope images of LS174T cells incubated with 50 µM chloroacetaldehyde for different time periods and then stained with $H_2$DCFDA. The effect of CAA on cell morphology is clearly visible. The correspondent fluorescence images are not shown, the results of fluorescence imaging are evaluated quantitatively in Figure 3.13-A.

No clear correlation between ROS production and CB incubation could be found (Figure 3.13-B). The impact of CB on actin filaments is accompanied by a change of cell morphology, which is detected by impedance measurements. In phase contrast microscopy, these changes are manifested by a tendency to acquire a round morphology and to retract cytoplasmic protrusions (Figure 3.15).

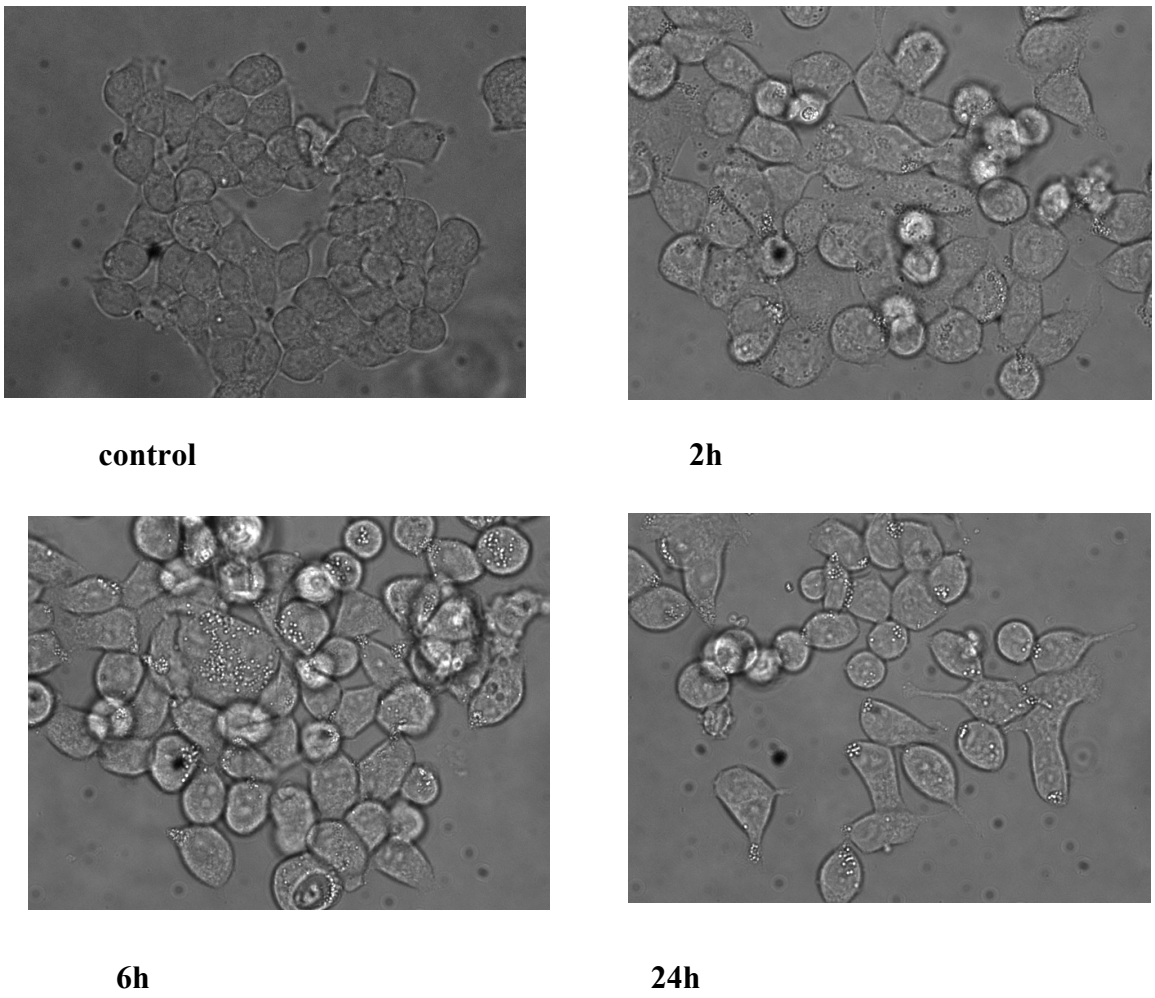


**Figure 3.15:** Phase contrast microscope images of LS174T cells incubated with 2 µM cytochalasin B for different time periods and then stained with $H_2$DCFDA. The correspondent fluorescence images are not shown, the results of fluorescence imaging are evaluated quantitatively in Figure 3.13-B.

### 3.1.2.4 Analysis of mitochondrial membrane potential

In order to relate the observed effects of cellular oxygen consumption rates with the mitochondrial membrane potential, the cells were stained with the fluorescence dye 5,5`,6,6`-tetrachloro-1,1`,3,3`-tetraethylbenzimidazolylcarbocianine iodide (JC-1). JC-1, a positively charged dye, can exist in an aggregated form at high mitochondrial transmembrane potential due to its high accumulation in the mitochondrial matrix (emission maximum of dye aggregates at 590 nm), or in the monomer form which prevails at low mitochondrial transmembrane potential (emission maximum of dye monomers at 527 nm). The ratio between fluorescence emission at 590 nm and 527 nm is taken as a measure of the

mitochondrial transmembrane potential (Hirsch, et al., 1998; Mancini, et al., 1998). LS174T cells were seeded on coverslips in Petri dishes and incubated for 48 hours at 37 °C and 5 % $CO_2$. The cells were then incubated for different time periods in a medium containing CAA or CB. These drug containing media were aspirated and the cells were incubated for 30 minutes with JC-1 dye at a 1 µM final concentration in EBS before starting the measurement. After 30 minutes the cells were rinsed with EBS and the fluorescence intensity was measured using a fluorescence microscope (Nikon, TE-2000). It was observed that CAA leads to a rapid decrease in the mitochondrial membrane potential (Figure 3.16-A), while CB induces an increase with a maximum at about one hour after the begin of incubation (Figure 3.16-B; Figure 3.17).

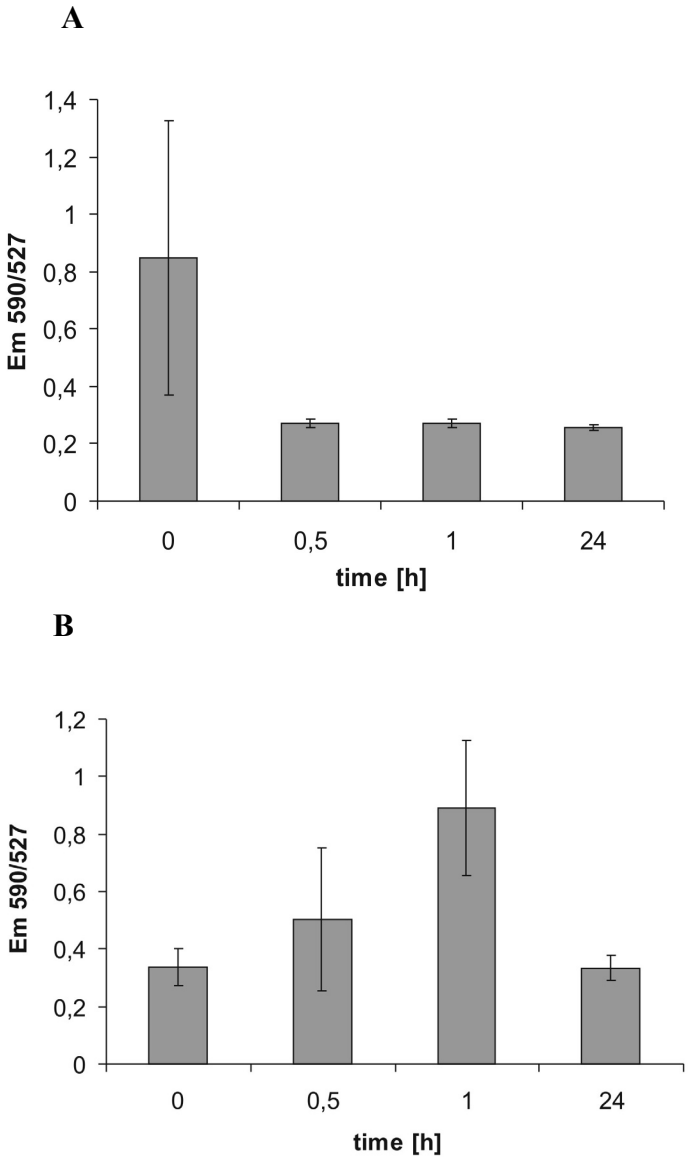


**Figure 3.16:** Mitochondrial activity in LS174T cells incubated with **(A)** 50 µM chloroacetaldehyde and **(B)** 2 µM cytochalasin B for different time periods and then stained with JC-1 (Data from A.M. Otto).

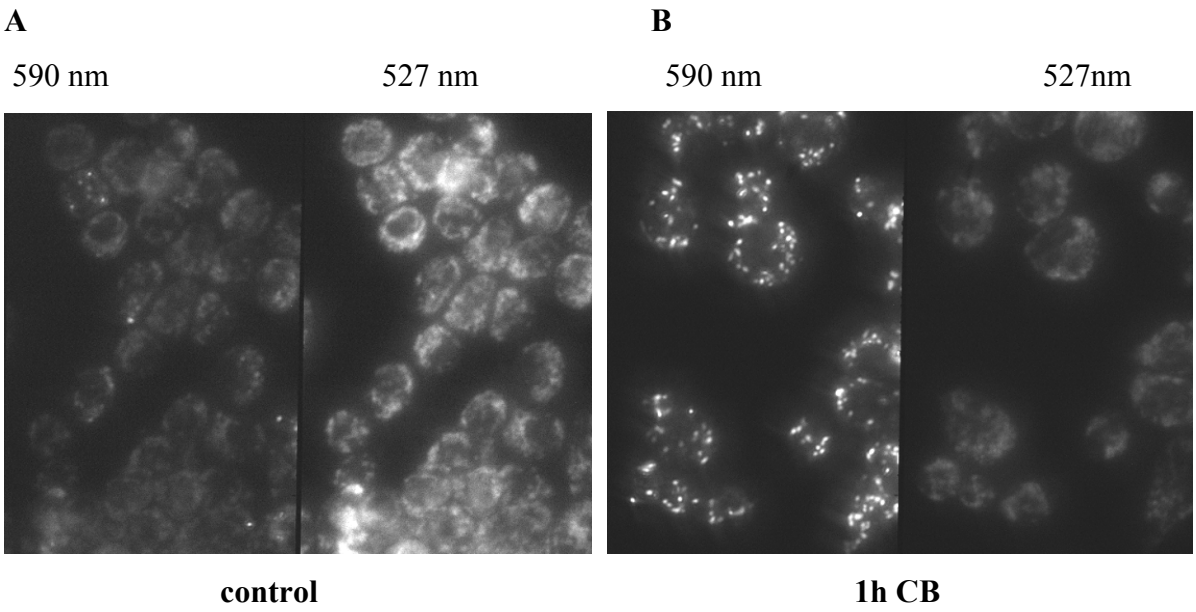


**Figure 3.17:** Fluorescence microscope images of LS174T cells **(A)** control and **(B)** incubated with 2 µM cytochalasin B for 1 hour; the cells were stained with JC-1, indicator of mitochondrial membrane potential (Data from A.M. Otto).

### 3.1.2.5 Analysis of cell number

To determine the effect of CAA and CB on cell number, the cells were seeded at a density of $10^5$ cells/well, cultivated in a 24 well plate and incubated for 24 hours at 37 °C and 5 % $CO_2$ in a medium containing different concentrations of CAA or CB. After 24 hours the media were aspirated and the cells were incubated for 20 minutes in hypotonic buffer. In order to release cell nuclei, the cells were subsequently incubated with cell lysis solution for another 10 minutes. This was followed by a re-suspension in fresh buffer and the number of cell nuclei was counted using an electronic cell counter. CAA at a concentration of 50 µM induces a drastic reduction of the cell number (Figure 3.18-A) while it remains relatively constant at a concentration of 2µM cytochalasin B (Figure 3.18-B). The slightly lower cell number observed in Figure 3.18-B can be explained by inhibition of mitosis.

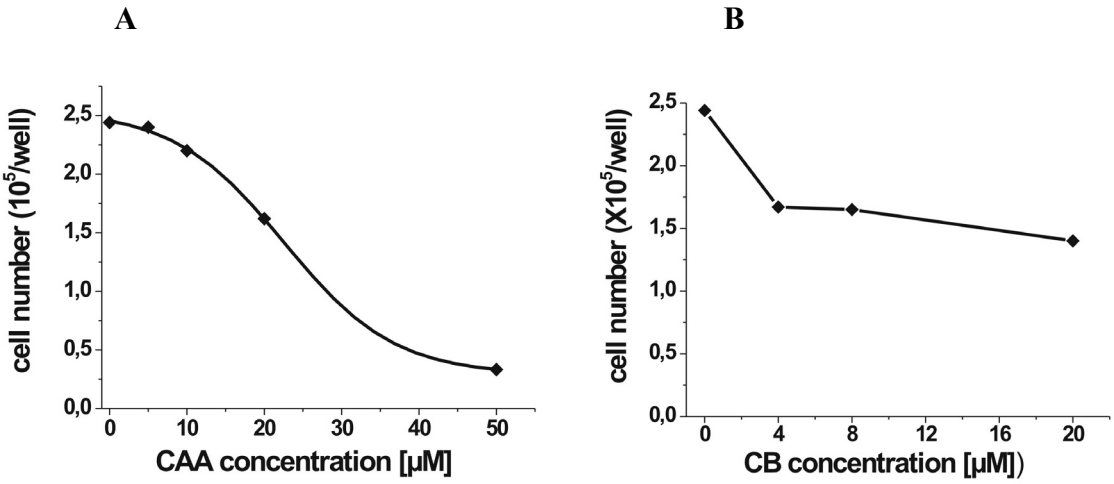


**Figure 3.18:** Number of LS174T cells incubated for 24 hours with different concentrations of **(A)** chloroacetaldehyde and **(B)** cytochalasin B; the initial cell density was $10^5$ cells/well (Data from A.M. Otto).

## 3.2 Invasion assay

An important step in the metastatic process of tumor cells is invasion through an extracellular matrix. The extracellular pH value is an important parameter for the invasion process. It is known that cathepsin enzymes, which play an important role in matrix degradation, have an optimum of activity at low pH values (Briozzo, et al., 1988). In order to monitor directly the invasive behaviour of cancer cells *in vitro* and in a dynamic mode, glass sensor chips with interdigitated electrodes structures (IDES) were used. The cells have to pass through a matrigel layer in order to come into contact with the electrode structures. Subsequent attachment and spreading of cells on IDES is detectable as changes in impedance and is taken as a measure of invasion.

The MDA-MB 231 breast cancer cell line was used in this experiment due to its highly invasive properties. The cells were maintained in culture in Dulbecco`s Modified Eagle's Medium DMEM-F12 supplemented with 10 % FCS and 2.5 mM L-glutamine. For measurements with glass chips the same medium was used with the exception of a 5 % FCS supplementation, a lower bicarbonate content (0.2 g/l), gentamycin (50 µg/ml) and HEPES (25 mM). The pH values of the measurement medium were adjusted to pH 7.3 and pH 6.4 with 1 N HCl.

Matrigel (extract of Engelberth-Holm-Swarm Mouse tumor), gelling at room temperature was used as a model substance for the extacellular matrix. The cell culture area on the glass chips, which is approximately 180 mm², was coated with a 0.5 mm matrigel layer (Figure 3.19).

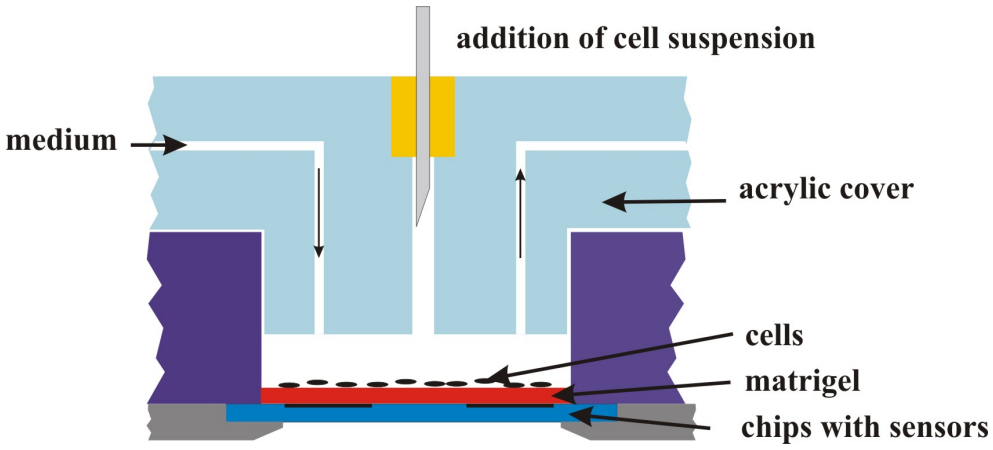


**Figure 3.19:** Cross-section of the measurement setup.

During coating the chips and matrigel were kept cold on ice. The coated chips were incubated for 3 hours in an incubator at 37 °C to allow the matrigel to gel. After 3 hours the chips were mounted into the double chamber setup and connected to the perfusion system.
To be able to compare the changes in the impedance signal caused by matrigel alone, only one chip of the double chamber was coated with matrigel. Impedance monitoring and perfusion with the measurement medium (pH 7.3) was started. After 3 hours the cells were added (2.5 x $10^5$ cells per chip). At the end of the experiment the cell membranes were destroyed with Triton X-100 (Figure 3.20).

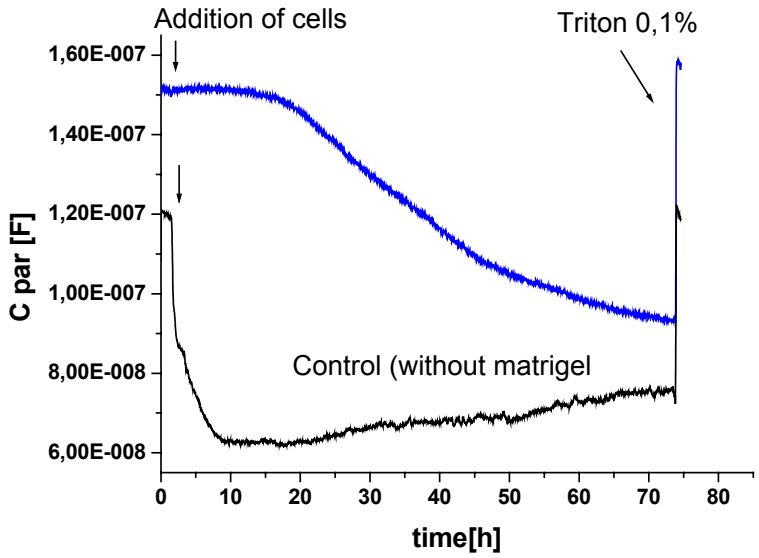


**Figure 3.20:** Comparison of the $C_{par}$ component of impedance signals from 2.5 x $10^5$ cells cultured on sensor chips with matrigel (blue line) and without matrigel (black line). The black graph shows a rapid cell adhesion and spreading on the uncoated sensor chip. The barrier formed by matrigel delays both processes (and even inhibits them for cells without invasive potential).

The influence of pH values on the invasion process was analysed in another experiment in which both glass chips were coated with matrigel. Cells on the chip were first incubated in a culture medium with a pH value of 7.3. After 14 hours this medium was replaced for one chip by a medium with a pH value of 6.4 and the experiment was continued over the next 4 days (Figure 3.21). The graphs shown in Figure 3.21 suggest that cells perfused with a medium at pH 6.4 are able to migrate faster through the matrigel layer than cells perfused with a medium at pH 7.3.

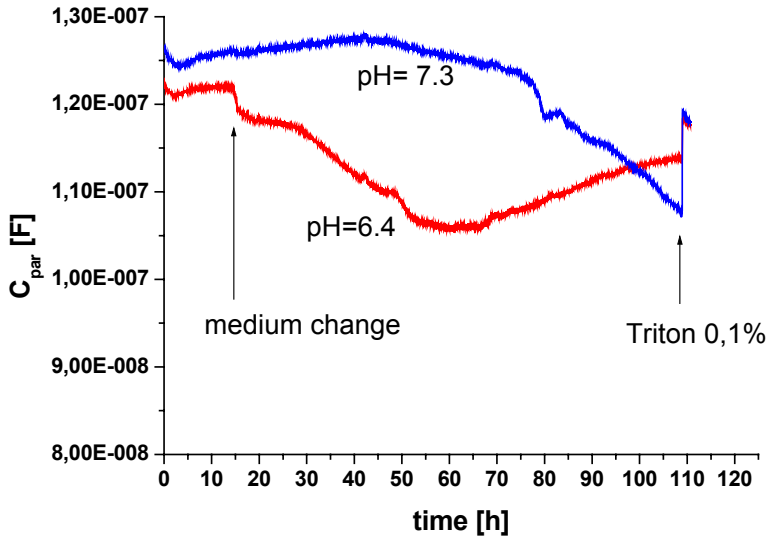


**Figure 3.21:** Effect of pH on the $C_{par}$ component of impedance signals from 2.5 x $10^5$ cells cultured on sensor chips coated with matrigel; perfusion with medium at pH 7.3 (blue line); perfusion with a medium at a pH that was changed from pH 7.3 to pH 6.4 (red line).

In order to analyse the influence of pH on matrigel alone, a control experiment without cells was started. A matrigel coated chip was perfused with a low pH medium (pH 6.4) and another one with a normal pH medium (pH 7.3) (Figure 3.22).

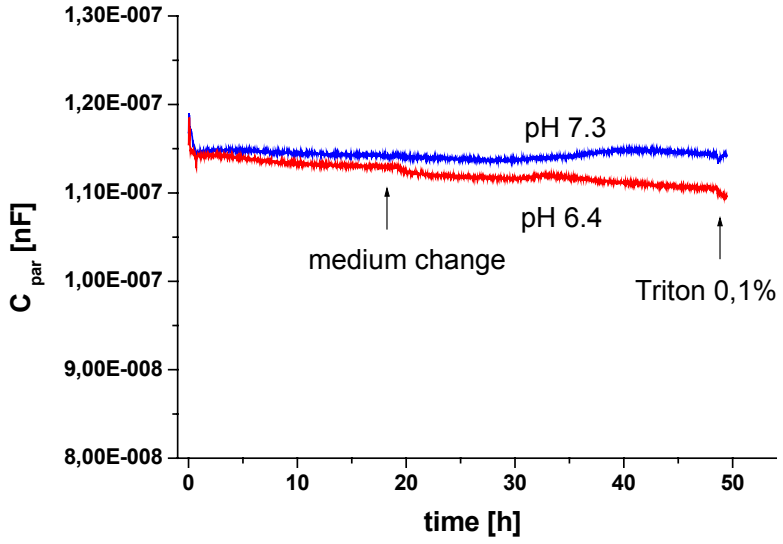


**Figure 3.22:** Effect of pH on the $C_{par}$ component of impedance signals from sensor chips coated with matrigel but without cells; perfusion with medium at pH 7.3 (blue line); the pH of the perfusion medium was switched to 6.4 at the time indicated (red line).

The results show that changes in the impedance signal caused by the pH on matrigel alone can be neglected in a first approach, in comparison with the cell-related effects shown in Figure 3.21.

In addition to monitoring the impedance signal, the glass chips allow an optical control during an experiment. In all experiments it was observed that invading cells change their morphology over a period of several days. At the beginning of the experiment, a round cell shape prevails. This morphology is maintained as long as the cells are invading through the matrigel layer. Upon contact with the solid chip substrate, the cells spread and form adherent cell colonies with a flattened cell shape (Figure 3.23).

**A** **B**

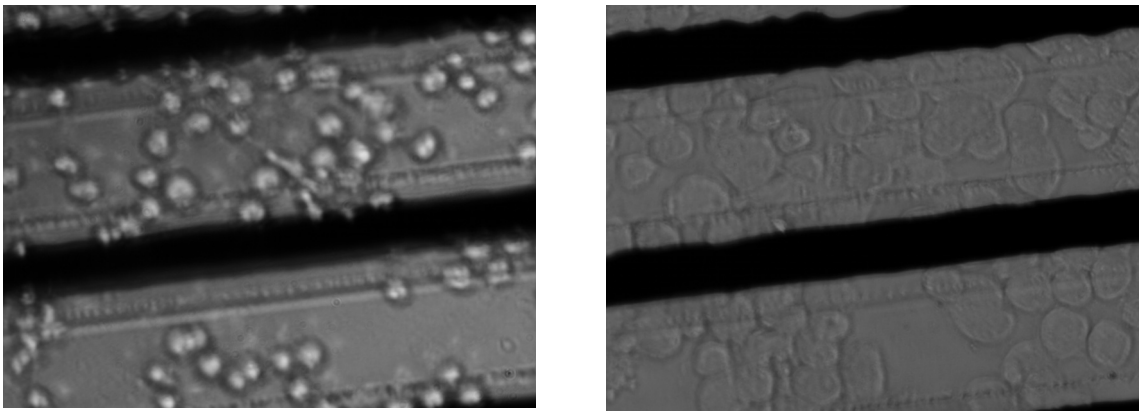

**Figure 3.23:** MDA-MB 231 cells on the matrigel coated chips; **(A)** cells have a round shape at the beginning of the experiment and **(B)** cell colonies have a flattened shape after 42 hours; the black bars represent the IDES.

## 3.3 Characterisation of sensor chips

### 3.3.1 Reproducibility of the experiments

A most important parameter for the reliability of any cell based assay is the reproducibility of the experimental results. The experiment chosen to test reproducibility of sensor based cell assays was the analysis of the effect of CAA on LS174T cells. Both experimental setups were used, i.e. cell monitoring systems based on silicon (Figure 3.24) and on glass sensor chips (Figure 3.25). Unfortunately due to failures of the impedance measurement setup, no test for the reproducibility of impedance could be completed for the silicon chip system.

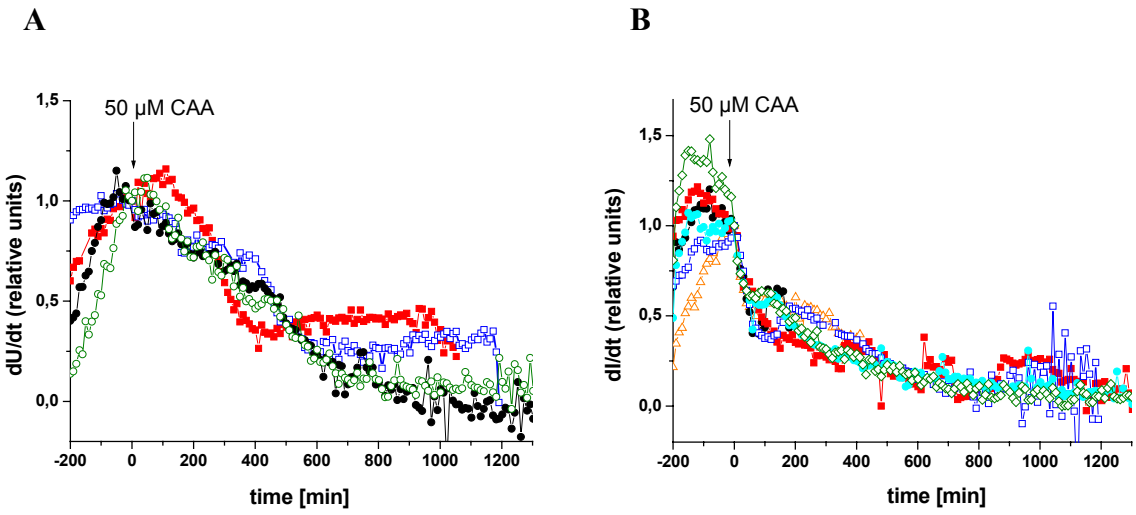


**Figure 3.24:** Effect of 50 µM chloroacetaldehyde on LS174T cells as recorded by the silicon chip based cell monitoring system; **(A)** changes in the rate of oxygen consumption; six graphs from different experiments are plotted in a single diagram; **(B)** changes in the rate of extracellular acidification; four graphs from different experiments are plotted in the same diagram; the absolute values of $\Delta I/\Delta t$ and $\Delta U/\Delta t$ have been normalized (Brischwein, et al., 2003).

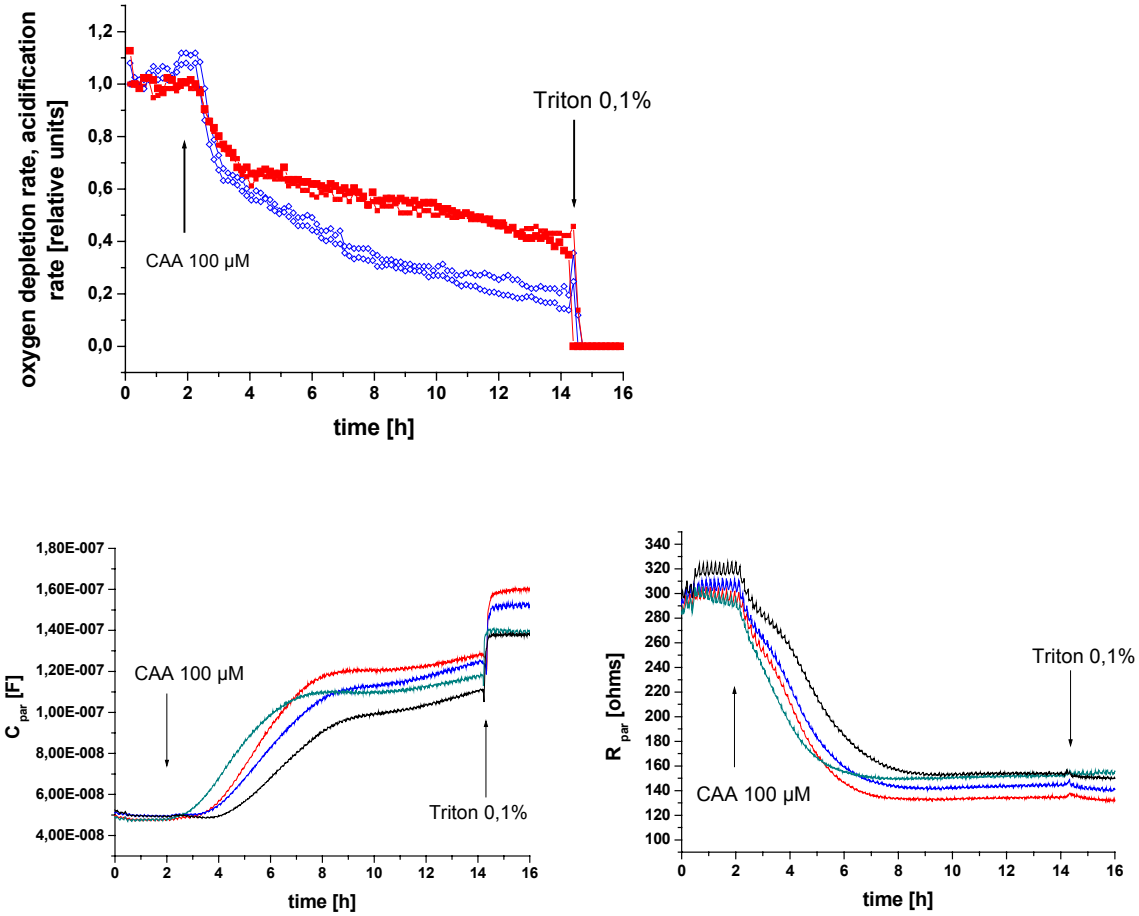


**Figure 3.25:** Effect of 100 µM chloroacetaldehyde on LS 174 T cells as recorded by the glass chip based cell monitoring system; **(A)** changes in the rate of oxygen consumption (blue graphs) and extracellular acidification (red graphs); two experiments running in parallel in the double chamber are plotted in a single diagram; **(B)** changes in electric impedance; four graphs from two experiments running in parallel (each experiment with two IDES); left side: changes of $C_{par}$; right side: changes of $R_{par}$.

### 3.3.2 Comparison of the impedance sensors on different chip types

#### 3.3.2.1 Glass chips

The measurements presented in part 3.1.1.1 were performed on glass chips with the layout shown in Figure 2.12. The surface area of a single IDES on these chips is about 12 mm², the electrode width and distances are 50 µm. While the surface area should have an impact on the absolute values of the measured parameters ($C_{par}$, $R_{par}$), the magnitude of relative changes is not expected to vary given that the sensors are covered with homogeneous cell monolayers. The influence of electrode width and spacing however, is less predictable. A computer

simulation currently in progress should allow to estimate the distribution of the electric field on top of the sensors with varying geometric parameters. In order to test this factor experimentally, histamine stimulation of Hela cell layers was performed with other types of glass chip impedance sensors with an electrode width and spacing of about 250 µm and a surface of about 50 $mm^2$ (Figure 3.26).

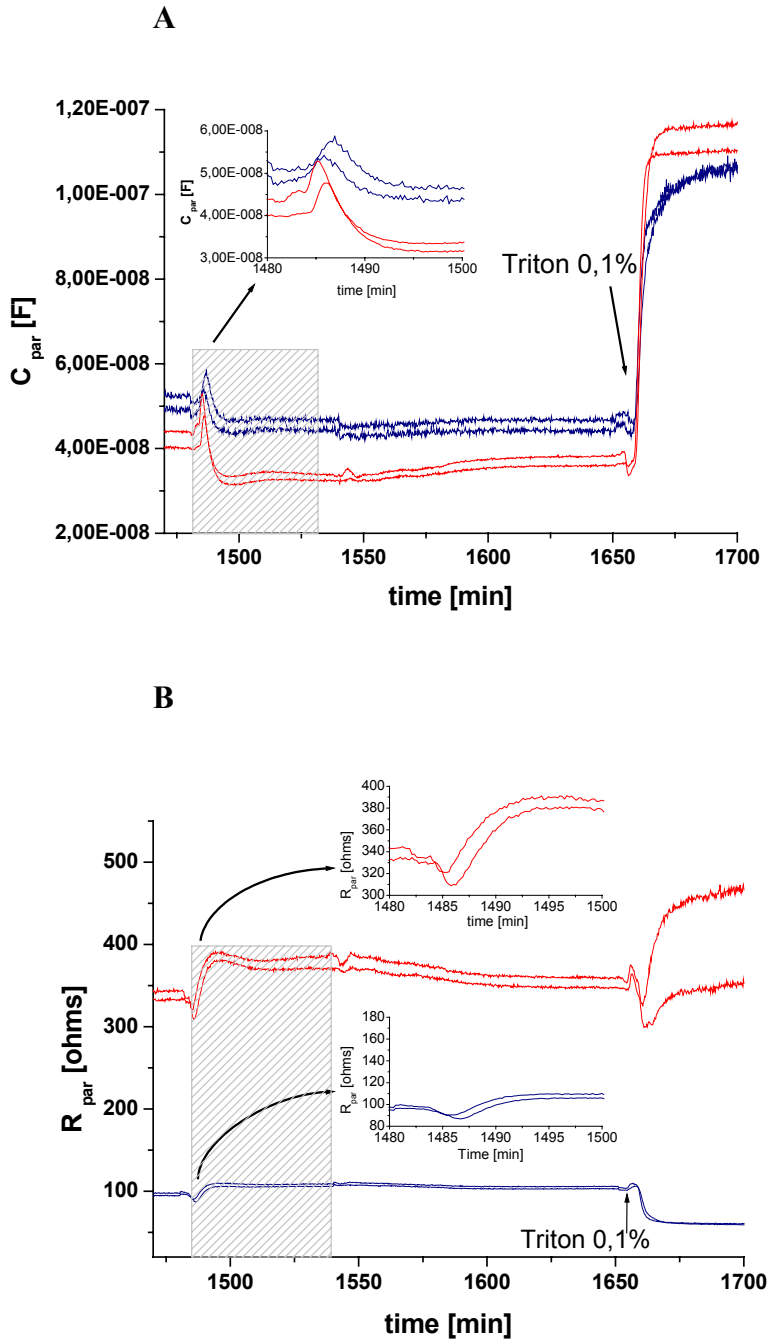


**Figure 3.26:** Comparison of changes in impedance signals upon stimulation of Hela cells with histamine; histamine was present during the time period indicated by the shaded area; glass chips with 50 µm IDES geometry (red line) and with 250 µm IDES geometry (blue line); **(A)** $C_{par}$ component, **(B)** $R_{par}$ component.

Both sensors were covered with homogeneous cell monolayers (as controlled by phase contrast light microscopy, images not shown). The results indicate that the amplitude of relative changes of the electric impedance is higher for sensors with a 50 µm geometry than for sensors with a 250 µm geometry (decrease in $C_{par}$ upon histamine administration of about 22% with 50 µm structures vs. about 10% with 250 µm structures). This is valid for both histamine stimulation and application of Triton X-100. Upon addition of Triton X-100, $R_{par}$ values are expected to decrease since the isolating cell membranes are solubilised. This response was consistently observed with sensors with a 250 µm geometry. With sensors with a 50 µm geometry however, no consistent reaction of $R_{par}$ values upon the destruction of cell membranes was found.

#### 3.3.2.2 Ceramic chips

Changes in impedance signals induced by histamine were recorded (1) with ceramic sensor chips fabricated by thick film technology and (2) with glass sensor chips fabricated by thin film technology. In part 3.3.2.1 a comparison of impedance signals between sensors with a 50 µm geometry and 250 µm geometry, both on glass chips, was presented. This was done in order to differentiate between the influence of electrode width/spacing from the influence of chip substrate and fabrication technology. This is necessary for the interpretation of signals obtained with ceramic chips, since the lateral resolution of thick film technology currently does not only allow the fabrication of electrode structures with a 50 µm geometry.

The surface area of IDES on both chip types (glass and ceramic) considered in this section was about 50 mm², the electrode width/spacing about 250 µm (see Figure 2.14). Hela cells were cultivated in parallel in the double chamber system under the same conditions on a glass and ceramic chip and stimulated with 25 µM histamine. The amplitude of changes in $C_{par}$ and $R_{par}$ values were higher with glass chips (transient increase of $C_{par}$ by about 18 %) than with ceramic chips (transient increase of $C_{par}$ by about 12 %). A similar difference is observed upon application of Triton X-100: the increase of $C_{par}$ values was about 120 % on glass chips and about 60 % on ceramic chips (Figure 3.27). A further result of this study was the observation that the transient increase in $C_{par}$ values upon histamine stimulation was much more pronounced than in previous studies (see Figure 3.1). Triton X-100 application on both chips resulted in the expected decrease of $R_{par}$ values.

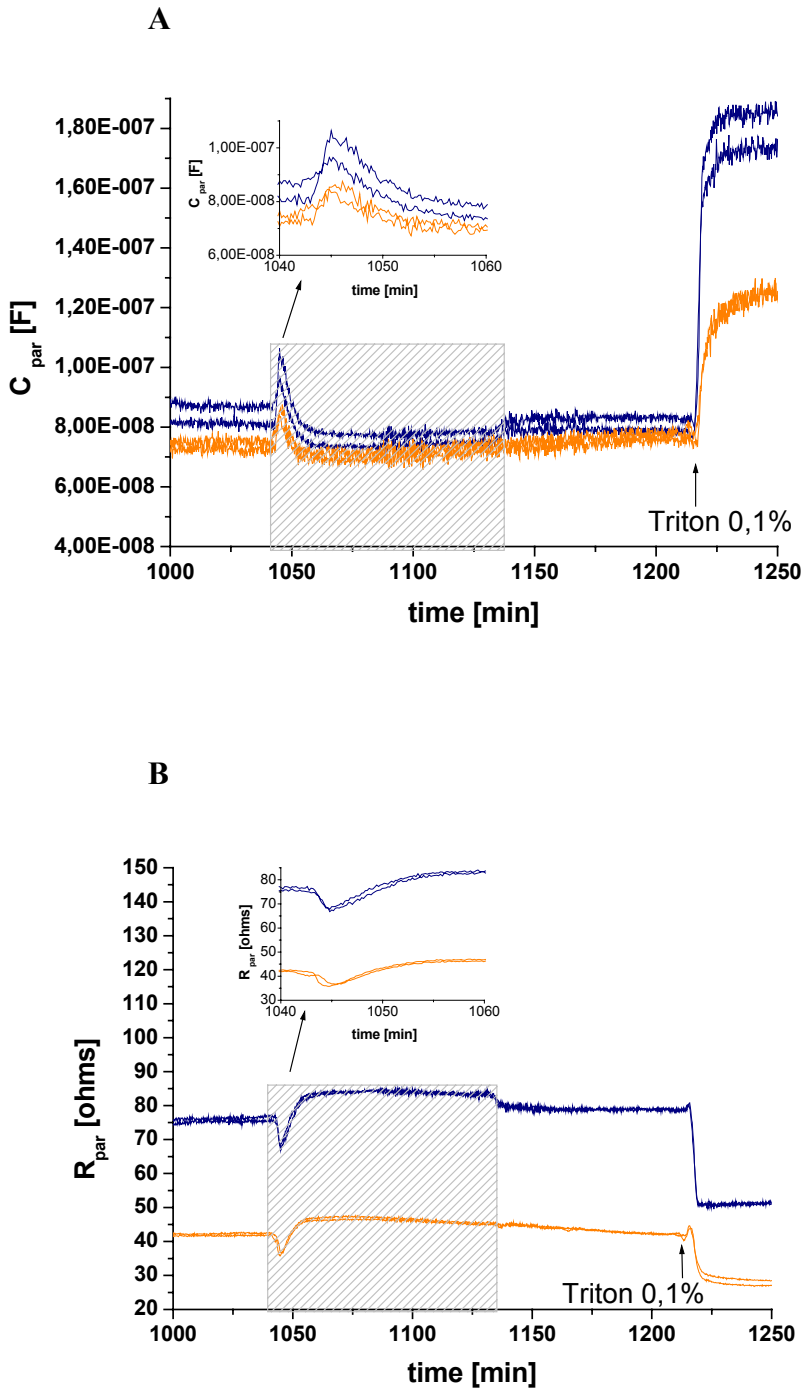


**Figure 3.27:** Comparison of glass and ceramic chips covered with Hela cells. Histamine stimulation of Hela cells on glass chips fabricated with thin film technology (blue line) and ceramic chips fabricated with thick film technology (orange line). On both chips were two IDES. Histamine was present during the time period indicated by the shaded area; **(A)** $C_{par}$ component, **(B)** $R_{par}$ component.

To summarise, the presented results suggest that (1) the geometrical configuration of IDES and (2) the chip substrate and technology of fabrication influence the sensitivity of assays on cell morphological changes. Glass chips (thin film electrode structures with 250 µm electrode width and electrode distance) seem to be superior to ceramic chips with thick film electrode structures. Moreover, a higher sensitivity can be achieved with a finer sensor geometry (50 µm vs. 250 µm). Data from impedance sensors on silicon sensor chips (sensor area: 2 $mm^2$, 50 µm geometry) are shown in section 3.1.2.1.

# 4. Discussion

## 4.1 Comparison between data obtained from sensor chips with data obtained from biochemical assays

The aim of this part of the work was to validate and to interpret the results obtained with the sensor chip systems by comparison with the results obtained from other assays. Two model cell lines were chosen: (1) a human cervix carcinoma cell line (Hela) which was stimulated with histamine and (2) a human colon carcinoma cell line (LS174T) which was stimulated with two drugs, i.e. chloroacetaldehyde (CAA) and cytochalasin B (CB). For both model systems different aspects of the cellular response were to be studied.

### 4.1.1 Hormone stimulation of cancer cells: histamine and Hela cells

The "output" signals induced by histamine in the human cervix carcinoma cell line (Hela) were analysed with glass sensor chips and a fluorescence assay. Histamine induces an increase in the concentration of intracellular free $Ca^{2+}$ ions in Hela cells by activating the H1 receptor on the cell membrane, which transmits the information via G-proteins to the enzyme phospholipase C. This enzyme cleaves the membrane constituent phosphatidylinositol 4,5-biphosphate to inositol 1,4,5-triphosphate ($InsP_3$) and diacylglycerol (DG). $InsP_3$ diffuses into the cytoplasm, stimulates the opening of $Ca^{2+}$ channels in the endoplasmic reticulum and thus causes the release of $Ca^{2+}$ ions into the cytosol (Montero, et al., 2003; Sauve, et al., 1991). In Hela cells stained with the calcium sensitive fluorophore Fluo 4-AM, addition of histamine leads to an increase in fluorescence intensity, which correlates with an increase in $Ca^{2+}$ ions in the cytoplasm (Figure 3.4). Metabolic changes, namely in the rate of oxygen consumption and the rate of extracellular acidification of Hela cells stimulated with histamine were monitored with the glass sensor chip system. Histamine did not cause detectable changes in the rates of oxygen consumption and extracellular acidification (Figure 3.2). A histamine-mediated stimulation of extracellular acidification was measured, however, in LS174T cells (data not shown).

In contrast, a change in the electric impedance was observed (Figure 3.1). The capacitance increases sharply after histamine administration within the first five minutes which is followed by a slower decrease to a level lower than the initial value over approximately 20 minutes. Subsequently the capacitance value is observed to increase slowly even with the continued presence of histamine. The resistance behaves approximately inversely to the

capacitance. The biphasic changes in the impedance signals observed above, correlate with the biphasic release of $Ca^{2+}$ from intracellular vesicles described in the literature (Parys, et al., 2000). From the kinetic point of view, the decrease in capacitance (and the correspondent increase in resistance) could be correlated to the transient increase of intracellular $Ca^{2+}$ which has been shown to enhance integrin mediated cell adhesion (Sjaastad, et al., 1994). Moreover, histamine also induces adherence of equine eosinophils to serum and fibronectin coated plastic (Foster & Cunningham, 1998). However, in human umbilical endothelial cells (HUVEC) cultivated on electrode structures, histamine has been shown to decrease transendothelial resistance by affecting the cell-cell contacts (Moy, et al., 2000).

These contradictory effects of histamine on different cell types can be explained in the context of different signalling pathways. There is a connection between intracellular calcium oscillations and the phosphorylation of protein kinase C (PKC) (Violin, et al., 2003). PKC is known to be involved in the modulation of cell-cell and cell-substratum adhesion, which differs depending on the cell type (Cowell, et al., 1999). The fact that the same drug may induce opposite responses in two different cell types is illustrated in an example shown in Figure 4.1. In this experiment, the PKC activating drug phorbol 12-myristate 13 acetate (PMA) was applied to L929 cells (mouse fibroblast cells) and to J82 cells (human bladder carcinoma). While for L929 cells the measured impedance data indicate an increased cell adhesion, the opposite is observed for J82 cells.

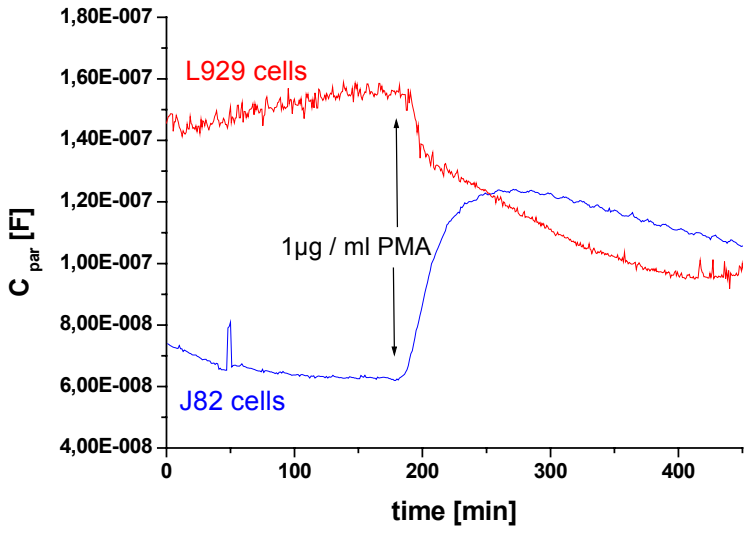


**Figure 4.1:** Comparison between changes in the signal of the capacitance component of electric impedance induced by phorbol 12-myristate 13 acetate (PMA) in J82 cells (bladder carcinoma , blue line) and L929 cells (mouse fibroblasts, red line).

Consecutive addition of histamine leads to biphasic changes in the impedance signal which were weaker after the second addition than after the first. This is explained by an adaptation of the involved signalling chain with receptor-desensitisation as a regulatory response of the cells.

In contrast to the changes in the impedance signal, changes in fluorescence intensity using Fluo 4-AM were not biphasic. However it should be noted, that the addition of histamine to cells cultured on multiwell plates was more rapid in comparison to the addition with the perfusion system used for cells cultured on sensor chips. A prolonged acquisition of fluorescence data for several hours on living cells and thus a complete comparison of impedance and fluorescence data was not possible.

### 4.1.2 Mechanism of action of chloroacetaldehyde and cytochalasin B on cancer cells

Metabolic changes induced by CAA and CB on the colon cancer cell line LS174T were analysed with a silicon sensor chip system as well as with assays for intracellular ATP levels, cellular ROS production, mitochondrial membrane potential and cell number.

Some aspects of the effects of CAA and CB on the rates of respiration and extracellular acidification in cancer cells have been described in previous work from our group (Wolf et al., 1998; Ehret et al., 2001; Henning, et al., 2002). In contrast to the microsensor system used in previous studies, which employed non-planar microelectrodes for pH and oxygen partial pressure for the determination of cell metabolic rates, the silicon based sensor chip system used for the results presented in this thesis included only planar sensors. A detailed description of this system is given in Brischwein, et al., 2003.

In this work, new aspects of the mechanism of action of CAA and CB on the colon cancer cell line LS174T were investigated. The measurements presented in part 3.1.2 of this thesis demonstrate that cellular metabolism reacts almost immediately upon drug addition. CAA leads to a rapid decrease in the rate of oxygen consumption, while CB causes a marked and instantaneous increase. It was observed that both substances decrease the rate of extracellular acidification.

Glucose, the main source of cellular energy, is metabolised in tumor cells predominantly to lactate, even in the presence of oxygen, which results in a high rate of extracellular acidification. The glycolytic pathway contributes significantly to ATP production. Oxidative ATP generation in mitochondria however, takes place in parallel. The quantitative relation between glycolysis and oxidative metabolism of glucose is not exactly known. It depends on the cell type considered and on the exact conditions of cell culture. The stoichiometric release

of acid per generated ATP is 1.0 mol $H^+$/mol ATP in the glycolytic pathway and 0.167 mol $H^+$/ATP with glucose respiration (Owicki & Parce, 1992).

About 90 % of cellular oxygen consumption is due to mitochondrial respiration (Balaban, 1990) which proceeds via oxidative phosphorylation. Therefore, a reduction of oxygen consumption implies impaired mitochondrial activity and thus a reduction in ATP synthesis. Surprisingly, analysis of ATP levels showed that incubation with CAA (50 µM) caused a transient increase of cellular ATP content by about 45 %, with the peak concentration at about 2 hours (Figure 3.12-A). Thereafter, the ATP content decreased continuously. This means that oxygen consumption does not correlate with ATP content. A transient increase of ATP concentration in tumor cells after drug incubation was also observed by other groups (Walenta, et al., 2001). Besides, addition of the tumor necrosis factor (TNF) to metabolically inhibited L292 mouse sarcoma cells leads to transient increases in ATP content (Sanchez-Alcazar et al., 1997). The question arises, how do the cells manage to increase their ATP levels under conditions of impaired mitochondrial activity? Since glycolytic ATP generation appears not to be augmented (considering slightly decreasing extracellular acidification rates after CAA administration), the conclusion is that energy consuming pathways in the cell are down-regulated. In a recent investigation it was shown that the treatment of human tumor cells with adriamycin caused a decrease in mitochondrial membrane potential before energy metabolism declines (Serafino et al., 2000). This could explain the discrepancy between the transient increase in ATP level and the decrease in oxygen consumption. When apoptosis is induced, ATP consumption for anabolic processes is reduced in order to ensure sufficient ATP for the energy dependent processes involved in apoptosis. This correlates with the results presented above, and with the experimental evidence which showed that sufficient ATP is a prerequisite for the induction of apoptosis (Richter et al., 1996; Eguchi et al., 1997).

It would also be interesting to analyse how the different ionic gradients across the cell membrane react upon drug administration. It has been estimated by two different groups that the $Na^+/K^+$ pump system contributes to the metabolic energy consumption for Ehrlich ascites cells with about 30 % (Balaban & Bader, 1984) and about 50 % (Skog, et al., 1982). The dynamic behaviour of the cell membrane potential and the distribution of ions such as $H^+$ across the cell membrane should be analysed in future, e.g. by fluorescence imaging methods.

Cells treated with CB remain viable during the whole experiment (Figure 3.9). CB is known to inhibit glucose uptake by non-covalent binding to the GLUT1 glucose transporter protein. Since the dissociation constant Kd of CB and GLUT1 as determined by fluorescence

spectroscopy is 0.14 µM (Walmsey, et al., 1994), the adjusted CB concentration of 2 µM would still allow about 10 % of GLUT1 to remain in the active state. This means that the glucose uptake is not totally inhibited. A rapid increase in the rate of oxygen consumption is observed, which again does not correlate with cellular ATP levels. Instead of an expected increase, the cellular ATP level appears to transiently decrease up to 2 h, followed by a recovery to the initial values (Figure 3.12-B). This can be explained by an increase of cellular oxygen consumption (and oxidative phosphorylation) while glycolysis is reduced due to impaired glucose uptake. Generally, glycolysis is a major source of ATP in tumor cells (Warburg, 1930). In drug resistant tumor cells it has been observed that glucose deprivation caused a decrease in the ATP level of approximately 25 % within an hour (Lee et al., 1997). Since ATP would have to be produced by oxidative processes under glucose deficient conditions, a higher rate of oxygen consumption would be expected. This is indeed supported by the experiments (Fig. 3.9-A) and by others (Casciari et al., 1992). A low remaining level of glucose would direct glycolysis to produce acetyl-CoA instead of lactate and ultimately lead to ATP production via oxidative phosphorylation in mitochondria. Switching from glycolysis to oxidative phosphorylation would result in an increased efficiency of glucose metabolism, i.e. the molar relation between generated ATP and consumed glucose would increase markedly. The transient decrease in the ATP level observed upon partial glucose deprivation may reflect such a regulatory transition phase.

Under glucose deficit conditions, other nutrient substrates could be used as a source of energy. Glutamine is believed to be another main source of cellular energy (Dang & Semenza, 1999; Petch, et al.,1994). It was observed however, that when cells were cultivated in a glutamine depleted medium, addition of CB induced the same increase in the rate of oxygen consumption and reduced extracellular acidification (Figure 3.10). This implies, that oxidative glutamine metabolism is not responsible for the increased oxygen uptake after CB administration in these cells.

Another parameter analysed with respect to $O_2$ consumption was the generation of reactive oxygen species (ROS) within cells. CAA induced an increase in ROS production in LS174T cells still 6 hours after the begin of drug incubation, followed by a gradual decrease (Figure 3.13-A). One possible explanation for the increase in the ROS content is that CAA reacts with glutathione leading to the irreversible formation of conjugates (Sood & O'Brien, 1993). The reduced form of glutathione plays an important role in removing free radicals in cells (Murphy, et al., 1990; Pereira & Oliveira, 2000). Moreover, glutathione depleted cells were shown to be more susceptible to CAA toxicity (Sood & O'Brien, 1993). For cells incubated

with CB no correlation between oxygen consumption and ROS production could be found (Figure 3.13-B). ROS generation remained at the control level.

Since neither cellular ATP nor ROS levels correlate with oxygen consumption, mitochondrial membrane potential was analysed. A rapid decrease in mitochondrial membrane potential was observed for cells incubated with CAA (Figure 3.16-A). This correlates with changes in the rate of oxygen consumption and the rate of extracellular acidification.

CB causes a transient increase in the mitochondrial membrane potential with a peak at about one hour after drug addition (Figure 3.16-B). This correlates with the oxygen consumption rate, which increases immediately after addition of CB. However, for LS174T cells stimulated with cytochalasin B the increase in the oxygen consumption monitored by sensor chips is more rapid than the increase in the mitochondrial membrane potential. At the moment no explanation for this difference can be given.

In addition to metabolic changes, morphologic changes induced by CAA and CB on LS174 T cells were analysed. A reduction of cell number (Figure 3.18-A) and changes in the cell morphology (increasing tendency to round up and to detach from the solid substrate, Figure 3.14) were observed upon CAA incubation. These changes are also detected by impedance measurement. The capacitance component of the electric impedance, which is taken as a measure of cell adhesion to the sensor electrodes, begins to increase without detectable delay upon addition of CAA (Figure 3.8-B). The morphologic effect of CB on cells is the disruption of microfilaments, which results in cell rounding. These changes are also evident by an increase in the capacity component of impedance (Figure 3.9-B). Cell viability was not affected and thus there was no significant reduction of cell number by CB (Figure 3.18-B). The slightly lower cell number can be explained by inhibition of mitosis, this being a consequence of the disruption of actin filaments which leads to the inhibition of cell division. This is supported by the observation that nuclei of increased size have been found in the cells incubated with CB (data not shown).

When 50 µM CAA was added twice for an hour during an experiment (Henning, et al., 2002), two phenomena could be observed: (1) the effect on cellular oxygen consumption and cell morphology were reversible, while the effect on extracellular acidification appeared to persist; (2) the decline in the rate of oxygen consumption was less prominent after the second addition than after the first addition. A possible explanation for the second phenomenon is that cell metabolism has been regulated to deal with oxidative stress by synthesizing more glutathione. The first phenomenon demonstrates that the reversibility of drug effects can be well analysed with dynamic sensor techniques. Early effects detected with sensors are not due to cell death

or a reduction of cell number (both necrotic and apoptotic cell death is a process usually requiring several hours), but to reversible changes in cell physiology.
The baseline for impedance measurements is usually obtained by killing the adherent cell layer on the sensor with a membrane solubilising detergent such as Triton X-100 (0.1%). The resulting impedance values are equivalent to the values without cells. The difference between values with intact cells and after Triton application is a measure of the insulating properties of the cell sheet at the measurement frequency used (10 kHz), i.e. a measure of the cell-cell and the cell-substrate sealing impedance. The value of the resistive component of electric impedance ($R_{par}$) is expected to decrease upon Triton addition. This decrease was observed with impedance sensors on glass and ceramic substrate while unexpectedly, with impedance sensors on silicon chips the values of $R_{par}$ were observed to increase. At the moment, a conclusive explanation for this behaviour cannot be given.

In the experiments discussed in chapter 4.1. it is shown that the sensor chip systems allow the detection of morphologic changes with electric impedance sensors. Moreover, it can be used to describe a dynamic metabolic profile of tumor cells by a parallel monitoring of the rate of oxygen consumption and the rate of extracellular acidification. Information obtained with the sensor chips systems are correlated with data obtained by other biochemical assays. These correlations help to elucidate the mechanism of drug action.

## 4.2 Sensor chips as a tool for analysis of tumor invasion

The sensor chip system was used to analyse a process of tumor cell invasion *in vitro*. As described in part 3.2, the highly invasive breast cancer cell line MDA-MB 231 was used as a model. It was shown that sensor chips allow a continuous online monitoring of the invasive behaviour of cancer cells over several days. As expected, cells cultivated on matrigel-coated chips require a considerably longer time than cells on uncoated chips to come into contact with IDES and to cause a detectable signal change (Figure 3.20). This time period (about 42 hours) is necessary for the cell passage through the matrigel layer (which is about 0.5 mm thick) i.e. for the enzymatic degradation of the matrigel. MDA-MB 231 cells are known to extrude a considerably higher amount of metabolic acid into the extracellular space than the less invasive breast cancer cell line MCF-7 (Montcourrier, et al., 1997). A low pH activates catepsins, which are enzymes responsible for degradation of the extracellular matrix (Briozzo, et al., 1988). This is the foundation of the hypothesis that a low pH stimulates the process of

tumor cell invasion through extracellular matrix. A comparison between breast cancer cells cultivated on matrigel coated chips and perfused with media of two different pH values (one with pH 7.3 and the other one with pH 6.4) showed that at a low pH value cell invasion through matrigel is indeed stimulated (Figure 3.21).

Up to date, only end point determination assays have been described for the analysis of tumor invasion. In these assays the cells are cultivated on matrigel-coated polycarbonate membranes and incubated at 37 °C for different time intervals. In order to count the cells which had migrated through the matrigel layer, the matrigel and cells from the top of the membrane are removed with a cotton swab. The cells remaining on the bottom part of the membrane are then stained and counted under a microscope (Both, et al., 1999; Thompson, et al., 1992). This method is not suitable for routine clinical applications due to the complicated handling and difficulty in reproducing the results. Another possibility to analyse cell invasion is to load cells with fluorescent dyes and then to seed them on black polyethylene terephthalate membranes coated with matrigel. These black membranes block light transmission between 490 and 700 nm and thus allow the identification and quantification of the fluorescent cells from below (bottom optic configuration) or above (top optic configuration) the insert with a fluorescence photometer. The problem with the latter type of assay is that the dye may affect cell viability and the invasive capacity of cells during the incubation period.

In contrast to the last two assays described, the sensor chip-based system offers the following potential advantages: a dynamic online analysis of the invasion process for several days and a perfusion system which imitates conditions similar to those *in vivo* without affecting the cellular viability during the experiment. However, it was found to be difficult to coat the surface of the chip uniformly with matrigel in a reproducible way in different experiments.

## 4.3 Characterisation of the sensor chip systems

An essential criterion for the reliability of sensor chip system is the reproducibility of the results. As shown in part 3.3.1, experimental results have been reproduced well with both sensor chip systems (silicon chips and glass chips). The term "reproducibility" takes into account the normal standard deviation inherent to all biological experiments and means a qualitative reproduction of results within a given limit of variation. Although the experimental setup and conditions are slightly different in the glass chip and silicon chip systems, results obtained with one system can be reproduced with the other one. As mentioned in part 3.1.2.1, absolute values of pH, oxygen and impedance are not evaluated. Instead, the calculation of

cell metabolic rates is exclusively based on the determination of relative changes within short time intervals. Similarly, only relative changes of impedance occurring upon cell stimulation are interpreted.

The chip systems described offer the possibility of long term experiments (four to five days) and allow continuous and parallel monitoring of changes in the three parameters: extracellular acidification, oxygen consumption, and electric impedance. However, the chip technology is still relatively expensive. In order to decrease the 'cost per chip', either the chip fabrication numbers have to be increased, or the fixed costs of the employed technology have to be reduced. A possibility to reduce these fixed costs is to use thick film technology, which does not require expensive masks for photolithographic process steps as in thin film technologies presently used. A disadvantage of thick film technology is the difficulty in patterning structures smaller than about 100-150 µm. Thick film or screen printing technologies are usually performed on ceramic chip substrates. The high temperatures necessary during thick film processing and the difficulty to achieve a stable adhesion of thick film pastes on glass currently prevent the use of a normal glass as substrate. In cooperation with the Kurt Schwabe Institut e.V.(Meinsberg) ceramic chips with sensors for pH, oxygen and electric impedance are being fabricated and tested.

A comparative study on a cellular system with different impedance sensors has been performed. One type of sensor was on a ceramic substrate and fabricated with thick film technology, the other one was fabricated on a glass substrate (thin film technology). The results show, that the amplitude of changes in $C_{par}$ and $R_{par}$ values and thus the sensitivity in detecting subtle cell morphological changes were higher with glass chips than with ceramic chips.

Another problem is the strict requirement for sterility of the system. It was repeatedly observed that contaminations (with bacteria or Saccharomyces-like molds) become evident about 48-56 hours after starting an experiment. A particular problem is sterilisation of microelectrodes (for pH and oxygen), which are still used in the glass chip system. These microelectrodes, which do not tolerate autoclaving, have to be sterilized by treatment with 70 % ethanol or hypochlorite solutions. It is a common problem, that perfusion systems are prone to the formation of highly resistant biofilm layers. Apart from the aspects of cost reduction and improvement of handling, the problem of sterilisation is a particularly important motivation to avoid discrete microelectrodes in the system and to develop sterilizable and fully biocompatible chip systems combining all sensors on a single planar substrate. This requirement includes a planar and reference electrode system for both

potentiometric and amperometric sensor types. Nowadays, apart from the electrical methods, optical methods offer a large variety of analyses of cellular activity. Methods using fluorescence dyes able to stain specifically cellular components have been strongly improved in the recent years. A disadvantage of many optical methods is, however, that the sensitivity (i.e. the ratio of signal to background) often is not satisfactory. For example, the experiments concerning mitochondrial membrane potential as described in part 3.1.2.4 failed when performed with the fluorescence plate reader. The reason for this failure was found to be a high and inconsistent background level (fluorescence intensity in cell-free wells with buffer only) which approached the values of wells with cell cultures. Besides, fluorescent dyes have more or less cytotoxic and phototoxic side effects which are difficult to control. For example, the use of $Ca^{2+}$ complexing dyes in the cytoplasm necessarily interferes with the native concentrations of unbound $Ca^{2+}$ ions. A simultaneous analysis of cellular activity using electrical and (fluorescence-) optical methods would offer a more complex and complete picture of different cellular aspects.

In this thesis it has been shown that the sensor chips can be successfully used to monitor the cellular "output" signals. Evaluation of data obtained using other biochemical assays not only support and confirm the sensor results but also provide new information which helps to understand different aspects of cellular activity. The sensor chip systems give relevant information for various type of application such as chemosensitivity and invasion assays.

# 5. Outlook and Abstract

## 5.1 Outlook

The results presented in this thesis prove that electric sensors on glass and silicon chips are valuable tools for functional monitoring of living cells. This work demonstrates not only the applicability of such systems for cell based assays, but has also initiated current work which is directed to the further improvement and implementation of devices allowing a higher experimental throughput. This improvement is focussed on the following items:

- Firstly, non planar microelectrodes inserted into the glass chip system for the measurement of cell respiration and extracellular acidification rates are replaced by planar microsensors (Figure 5.1). This is expected to facilitate system handling and to increase the information content of sensor based assays such as invasion assays, which are so far based only on impedance sensors.

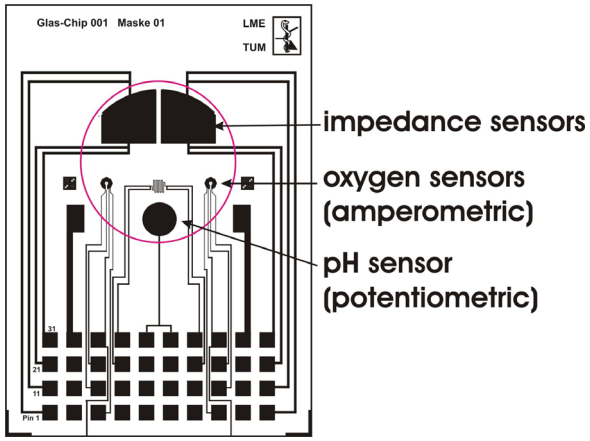


**Figure 5.1:** Diagram of a glass chip with planar electric microsensors for oxygen-, pH- and impedance. The red circle marks the sensor and culture area on the chip.

- Several mechanical features of the culture/sensor unit have been recently changed in order to facilitate the procedures of sterilisation, cleaning, pre-cultivation of cells, assembling and electrical contacting of the device.

● The development of a 24-well array has been recently initiated, combining electric microsensors on bottom glass chips with analytical optical tools directed to the cell cultures, particularly fluorescence microscope imaging (Figure 5.2). This system requires a complete re-design of the automation and liquid handling concept which will now rely on a pipetting robot system. The device is installed in a sterile climate box. An increased array density of sensor based cell monitoring systems is urgently necessary for statistical validation of experimental results.

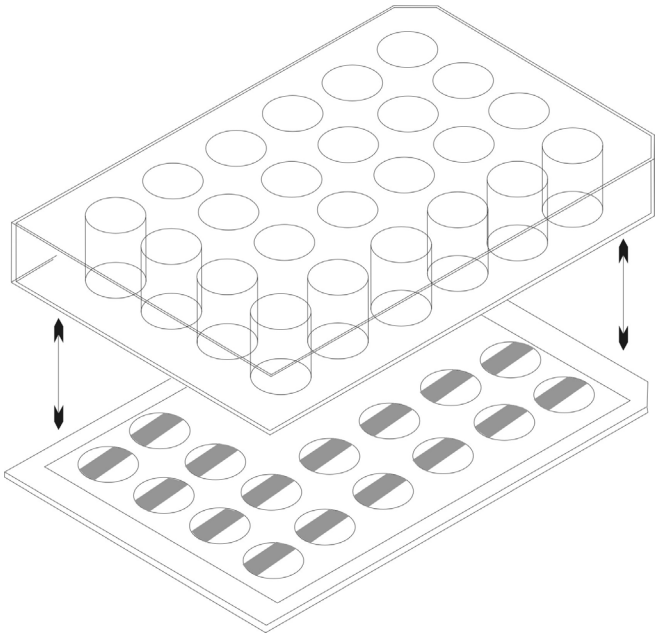

**Figure 5.2:** Scheme of a 24-well plate with bottom glass chips. Ongoing project at Heinz-Nixdorf Chair of Medical Electronics, TU Munich.

These technological advances are considered to be the basis for various further applications in biomedicine, such as:

- Comparison of cell metabolism and cell morphological alterations in tumor cell lines with different grades of malignancy.
- Studying cell metabolism and cell morphological changes in tumor cell lines under different, experimentally controlled conditions of the microenvironment, i.e. hypxia and different levels of pH.

- Short term culturing of tumor tissue slices derived from patients in order to obtain predictive in vitro information about tumor malignancy and/or cellular susceptibility to therapeutical measures.

## 5.2 Abstract

Multifunctional bioelectronic sensor chips allow dynamically changes in cellular metabolism (rate of oxygen consumption and extracellular acidification) as well as changes in cell morphology (cell-cell and cell-substratum adhesion) to be monitored online. In this work, data obtained from microsensor chips have been compared with results from standard biochemical assays in order to improve the cell biological interpretation of this new kind of cell based assay. Two experimental models were chosen:

(1) Receptor-mediated effects of histamine on a human cervix carcinoma cell line (Hela) were investigated. Histamine was shown to induce changes in cell-cell and cell-substratum adhesion on a time scale of about five minutes after drug application. An increase of intracellular free $Ca^{2+}$ ions was observed about ten seconds after histamine addition using a fluorescence assay. This increase was then followed by a gradual decline to a constant level above the original baseline. Stimulation of Hela cells with histamine was further used as a model experiment to test the sensitivity of different interdigital impedance sensors in detecting cell morphological changes. Sensors with varying electrode width/distance and with different underlying fabrication technologies have been used (i.e. thin film technology on glass substrate and thick film technology on ceramic substrate). Although results show, that the amplitude of changes in the impedance signals are higher with glass chips than with ceramic chips, thick film sensors could be a cost effective alternative to sensors fabricated with thin film technology.

(2) The mechanism of action of two substances with different spectra of effects, namely chloroacetaldehyde (CAA) and cytochalasin B (CB), on a human colon carcinoma cell line (LS174T) was analysed. The results obtained with sensor chips were correlated with the results obtained from several biochemical assays for analysis of the ATP level, mitochondrial membrane potential and reactive oxygen species (ROS). The comparative analysis of several cell based assays is a prerequisite (1) to improve the understanding of the information content of sensor based cell monitoring and (2) to elucidate the mechanism of action of the applied drug substances.

(3) The feasibility of an invasion assay using glass sensor chips coated with matrigel (a model substance for extracellular matrix) was tested. As a model system, a human breast cancer cell line with invasive character (MDA-MB 231) was chosen. Changes in electric impedance values monitored during the passage of invading tumor cells through the matrigel layer demonstrate that planar microsensors could provide the basis for a dynamic invasion assay.

Data obtained with this type of assay suggest that the invasive process is stimulated at low extracellular pH values, which is characteristic for the microenvironment found in many solid tumors. The sensor chips can be used in order to perform an online dynamic analysis of the invasion process over several days.

# 6. Reference List

Acker, T. and Plate, K.H. (2002). A role for hypoxia-inducible transcription factors in tumor physiology. Journal of Molecular Medicine, 80, 562-575.

Adam, G., Läuger, P. and Stark, G. (1988). Physikalische Chemie und Biophysik. Springer publishing company.

Alberts, B., Johnson, A., Lewis, J., Raff, M., Roberts, K. and Walter, P. (1994). Molecular Biology of the Cell. Garland Science.

Alberts, B., Johnson, A., Lewis, J., Raff, M., Roberts, K. and Walter, P. (2002). Molecular Biology of the Cell. Garland Science.

Balaban, R.S. and Bader, J.P. (1984). Studies on the relationship between glycolysis and ($Na^+$ + $K^+$)-ATPase in cultured cells. Biochimica et Biophysica Acta, 804, 419-426.

Balaban, R.S. (1990). Regulation of oxidative phosphorylation in the mammalian cell. The American Journal of Physiology, 258, C377-C389.

Berridge, M.V, Tan, A.S, McCoy, K.D. and Wang, R. (1996). The biochemical and cellular basis of cell proliferation assays that use tetrazolium salts. Biochemica, 4, 14-19.

Bingeli, R. and Weinstein, R.C. (1986). Membrane potentials and sodium channels: Hypotheses for growth regulation and cancer formation based on changes in sodium channels and gap junctions. Journal of Theoretical Biology, 123, 377-401.

Blancher, C., Moore, J.W., Talks, K.L., Houlbrook, S. and Harris, A.L. (2000). Relationship of hypoxia-inducible factor (HIF)-1{{alpha}} and HIF-2{{alpha}} expression to vascular endothelial growth factor induction and hypoxia survival in human breast cancer cell lines. Cancer Research, 60, 7106-7113.

Both, N.J., Vermey, M., Dinjens, W.N. and Bosman, F.T. (1999). A comparative evaluation of various invasion assays testing colon carcinoma cell lines. British Journal of Cancer, 81, 934-941.

Bousquet, P.F., Paulsen, L.A., Fondy, C., Lipski, K.M., Loucy, K.J. and Fondy, T.P. (2003). Effects of cytochalasin B in culture and in vivo on murine madison 109 lung carcinoma and on B16 melanoma. Cancer Research, 50, 1431-1439.

Briozzo, P., Morisset, M., Capony, F., Rougeot, C. and Rochefort, H. (1988). In vitro degradation of extracellular matrix with Mr 52,000 cathepsin D secreted by breast cancer cells. Cancer Research, 48, 3688-3692.

Brischwein, M., Baumann, W., Ehret, R., Schwinde, A., Kraus, M. and Wolf, B. (1996). Microsensory systems in cell biology basic research and medical diagnostics. Die Naturwissenschaften, 83, 193-200.

Brischwein, M., (1997). Entwicklung und Charakterisierung von Biosensor-Systemen mit immobilisierten Zellen und Geweben. Doctoral thesis at the Faculty for Biology, Albert-Ludwigs-University, Freiburg i Br., Germany.

Brischwein, M., Motrescu, E.R., Cabala, E., Otto, A.M., Grothe, H. and Wolf, B. (2003). Functional cellular assays with multiparametric silicon sensor chips. Lab on a chip, 3, 234-240.

Brown, J.M. and Wouters, B.G. (1999). Apoptosis, p53, and tumor cell sensitivity to anticancer agents. Cancer Research, 59, 1391-1399.

Burgman, P., O`Donoghue, J.,A., Humm, J.,L. and Ling, C.,C. (2001). Hypoxia-induced increase in FDG uptake in MCF7 cells. Journal of Nuclear Medicine, 42, 170-175.

Casciari, J.J., Sotirchos, S.V. and Sutherland, R.M. (1992). Variations in tumor cell growth rates and metabolism with oxygen concentration, glucose concentration, and extracellular pH. Journal of Cellular Physiology, 151, 386-394.

Chiesa, A., Rapizzi, E., Tosello, V., Pinton, P., de Virgilio, M., Fogarty, KE, and Rizzuto, R. (2001). Recombinant aeqorin and green fluorescent protein as valuable tools in the study of cell signalling. The Biochemical Journal, 355, 1-12.

Cortopassi, G.A. and Wong, A. (1999). Mitochondria in organismal aging and degeneration. Biochemica et Biophysica Acta, 1410, 183-193.

Cowel, H.E. and Garrod, D.R. (1999). Activation of protein kinase C modulated cell-cell and cell-substratum adhesion of a human colorectal carcinoma cell line and restores "norma" epithelial morphology. International Journal of Cancer, 80, 455-464.

Cuvier, C., Jang, A. and Hill, R.P. (1997). Exposure to hypoxia, glucose starvation and acidosis: effect on invasive capacity of murine tumor cells and correlation with cathepsin (L + B) secretion. Clinical and Experimental Metastasis, 15, 19-25.

Dang, V.C. and Semenza, L.G. (1999). Oncogenic alterations of metabolism. Trends in Biochemical Sciences, 24, 68-72.

Denekamp, J., Dasu, A. and Waites, A. (1998). Vasculature and microenvironmental gradients: The missing links in novel approaches to cancer therapy. Advanced Enzyme Regulation, 38, 281-299.

Dumont, J.E., Pecasse, F. and Maenhaut, C. (2001). Crosstalk and specificity in signalling. Are we crosstalking ourselves into general confusion ? Cellular Signalling, 13, 457-463.

Eguchi, Y., Shimizu, S. and Tsujimoto, Y. (1997). Intracellular ATP levels determine cell death fate by apoptosis or necrosis. Cancer Research, *57*, 1835-1840.

Ehret, R., Baumann, W., Brischwein, M., Schwinde, A., Stegbauer, K. and Wolf, B. (1997). Monitoring of cellular behaviour by impedance measurements on interdigitated electrode structures. Biosensors and Bioelectronics, 12, 29-41.

Ehret, R., Baumann, W., Brischwein, M., Schwinde and Wolf, B. (1998). On-line control of cellular adhesion with impedance measurements using interdigitated elecrode structures. Medical & Biological Engineering & Computing, 36, 365-370.

Ehret, R., Baumann, W., Brischwein, M., Lehmann, M., Henning, T., Freund, I., Drechsler, S., Friedrich, U., Hubert, L., Motrescu, E., Kob, A., Palzer, H., Grothe, H. and Bernhard, W. (2001). Mutiparametric microsensor chips for screening applications. Fresenius Journal of Analytical Chemistry, 369, 30-35.

Esposti, M.D. (2002). Measuring mitochondrial reactive oxygen species. Methods, 26, 335-340.

Fertig, N., Blick, R.H. and Behrends, J.C. (2002). Whole cell patch clamp recording performed on a planar glass chip. Biophysical Journal 82, 3056-62.

Foster, A.P. and Cunningham, F.M. (1998). Histamine-induced adherence and migration of equine eosinophils. American Journal of Veterinary Research, 59, 1153-1159.

Gerweck, L.E., Kozin, S.V. and Stocks, S.J. (1999). The pH partition theory predicts the accumulation and toxicity of doxorubicin in normal and low-pH-adapted cells. British Journal of Cancer, 79, 838-842.

Ghosh, R.N., Chen, Y.T., DeBiasio, R., DeBiasio, R.L., Conway, B.R., Minor, L.K. and Demarest, K.T. (2000). Cell-based, high-content screen for receptor internalization, recycling and intracellular trafficking. BioTechniques, 29, 170-75.

Gillies, R.J., Raghunand, N., Karczmar, G.S. and Bhujwalla, Z.M. (2002). MRI of the tumor microenvironment. Journal of Magnetic Resonance Imaging, 16, 430-450.

Glaser, R.(2001). Biophysics. Springer publishing company.

Griffiths, J.R., McSheehy, P.M., Robinson, S.P., Troy, H., Chung, Y.L., Leek, R.D., Williams, K.J., Stratford, I.J., Harris, A.L. and Stubbs, M. (2002). Metabolic changes detected by in vivo magnetic resonance studies of HEPA-1 wild-type tumors and tumors deficient in hypoxia-inducible factor-1beta (HIF-1beta): Evidence of an anabolic role for the HIF-1 pathway. Cancer Research, 62, 688-695.

Gross, G.W. and Schwalm, F.U. (1994). A closed flow chamber for long-term multichannel recording and optical monitoring. Journal of Neuroscience Methods, 52, 73-85.

Halkar, G., Sayin-Özveri, E., Yüksel, M., Aktan, A.Ö. and Yalcin,S. (2001). Different kinds of oxygen and nitrogen were detected in colon and breast tumors. Cancer Letters, 165, 219-224.

Hamill, O.P., Marty, A., Neher, E., Sakmann, B. and Sigworth, F.J. (1981). Improved patch-clamp techniques for high-resolution current recording from cells and cell-free membrane patches. Pflügers Archiv: European Journal of Physiology, 381, 85-100.

Harguindey, S., Pedraz, J.L., Canero, R.G., Perez de Diego, J. and Cragoe, E.J. (1995) Hydrogen ion-dependent oncogenesis and parallel new avenues to cancer prevention and treatment using a $H^+$-mediated unifying approach: pH-related and pH-unrelated mechanisms. Critical Reviews in Oncogenesis, 6, 1-33.

Henning, T., Brischwein, M., Baumann, W., Ehret, R., Freund, I., Kammerer, R., Lehmann, M., Schwinde, A. and Bernhard,W. (2002). Approach to a multiparametric sensor-chip-based tumor chemosensitivity assay. Anticancer Drugs, 12, 21-32.

Hirsch, T., Marzo, S.I., Marchetti, P., Zamzami, N. and Kroemer,G. (1998). Mitochondrial permeability transition in apoptosis and necrosis. Cell Biology and Toxicology, 14, 141-145.

Huang, Z. and Waxman, D.J. (1999). High-performance liquid chromatographic-fluorescent method to determine chloroacetaldehyde, a neurotoxic metabolite of the anticancer drug ifosfamide, in plasma and in liver microsomal incubations. Analytical Biochemistry, 273, 117-125.

Ivanov, S., Liao, S.Y., Ivanova, A., Danilkovitch-Miagkova, A., Tarasova, N., Weirich, G., Merrill, M.J., Proescholdt, M.A., Oldfield, E.H., Lee, J., Zavada, J., Waheed, A., Sly, W., Lerman, M. and Stanbridge,E.J. (2001). Expression of hypoxia-inducible cell-surface transmembrane carbonic anhydrases in human cancer. American Journal of Pathology, 158, 905-919.

Kraus, M. and Wolf, B. (1995). Structured biological modelling. A new approach to biophysical cell biology. Boca Raton, Florida: CRC Press, Inc.

Kraus, M. and Wolf, B. (1996). Implications of acidic tumor microenvironment for neoplastic growth and cancer treatment: a computer analysis. Tumour Biology, 17, 133-154.

Lambrechts, M. and Sansen, W. (1992). Biosensors: microelectrochemical devices. Institute of Physics Publishing Bristol, Philadelphia and New York.

Laris, P.C. and Henius, G.V. (1982). Influence of glucose on Ehrlich cell volume, ion transport, and membrane potential. The American Journal of Physiology 242, C326-C332.

Lee, I., Bender, E., Arnold, S. and Kadenbach B. (2001). New control of mitochondrial membrane potential and ROS formation - A hypothesis. Biological Chemistry., 382, 1629-1636.

Lee, Y.J., Galoforo, S.S., Berns, C.M., Tong, W.P., Kim, H.R. and Corry, P.M. (1997). Glucose deprivation-induced cytotoxicity in drug resistant human breast carcinoma MCF-7/ADR cells: role of c-myc and bcl-2 in apoptotic cell death. Journal of Cellular Science, 110, 681-686.

Lin, K., Sadée W. and Quillan, J.M. (1999). Rapid measurements of intracellular calcium using a fluorescence plate reader. BioTechniques, 26, 318-26.

Lodish, H., Baltimore, D., Berk, A., Zipurski, L., Matsuidaira, P. and Darnell, P. (1996). Scientific American Books.

Lottspeich, F. and Zorbas, H. (1998). Bioanalytik. Spektrum publishing company

Mancini, M., Sedghinasab, M., Knowlton, K., Tam, A., Hockenbery, D. and Anderson, B.O. (1998). Flow cytometric measurement of mitochondrial mass and function: A novel method for assessing chemoresistance. Annals of Surgical Oncology, 5, 287-295.

Manfredi,G., Yang,L., Gajewski,C.D., Mattiazzi,M. (2002). Measurements of ATP in mammalian cells. Methods 26, 317-326.

Manning, T.M. and Sontheimer, H. (1999). Dynamic recording of intracellular $Ca^{2+}$, $Cl^{-}$, pH and membrane potential in cultured astrocytes using a fluorescence plate reader. Journal of Neuroscientific Methods, 91, 73-81.

Mizel, S.B. and Wilson, L. (1972). Inhibition of the transport of several hexoses in mammalian cells by cytochalasin B. Journal of Biological Chemistry, 247, 4102-4105.

Montcourrier, P., Silver, I., Farnoud, R., Bird, I. and Rochefort,H. (1997). Breast cancer cells have a high capacity to acidify extracellular milieu by a dual mechanism. Clinical and Experimental Metastasis, 15, 382-392.

Montero, M., Lobaton, C.D., Gutierrez-Fernandez, S., Moreno, A. and Alvarez, J. (2003). Modulation of histamine-induced $Ca^{2+}$ release by protein kinase C: effects on cytosolic and mitochondrial [$Ca^{2+}$] peaks. Journal of Biological Chemistry, 278, 49972-49979.

Moy, A.B., Winter, M., Kamath, A., Blackwell, K., Reyes, G., Giaever, I., Keese, C. and Shasby, D.M. (2000). Histamine alters endothelial barrier function at cell-cell and cell-matrix sites. American Journal of Physiology: Lung Cellular and Molecular Physiology 278, L888-L898.

Murphy, T.H., Schnaar, R.L. and Coyle, J.T. (1990). Immature cortical neurons are uniquely sensitive to glutamate toxicity by inhibition of cystine uptake. The FASEB Journal: Official Publication of the Federation of American Societies for Experimental Biology, 4, 1624-1633.

Otto, A.M., Brischwein, M., Niendorf, A., Henning, T., Motrescu, E. and Wolf, B. (2003). Microphysiological testing for chemosensitivity of living tumor cells with multiparametric microsensor chips. Cancer Detection and Prevention, 27, 291-296.

Owicki, J.C. and Parce, J.W. (1992). Biosensors based on the energy metabolism of living cells: The physical chemistry and cell biology of extracellular acidification. Biosensors and Bioelectronics, 7, 255-272.

Parys, J.B., Sienaert ,I., Vaningen, S, Callewaert, G., Smet, P,D., Missiaen, L. and Smedt, H.D. "Regulation of inositol 1,4,5-triphospahte induced $Ca^{2+}$ release by $Ca^{2+}$ in: Calcium. The Molecular Basis of Calcium Action in Biology and Medicine. R. Pochet (2000). Kluwer Academic Publishers, Dordrecht.

Pereira, C.F. and Oliveira, C.R.D. (2000). Oxidative glutamate toxicity involves mitochondrial dysfunction and perturbation of intracellular $Ca^{2+}$ homeostasis. Neuroscience Research, 37, 227-236.

Petch, D. and Butler, M. (1994). Profile of energy metabolism in a murine hybridoma: glucose and glutamine utilization. Journal of Cellular Physiology, 161, 71-76.

Peters, L.J. and Fletcher, G.H. (1983). Causes of failure of radiotherapy in head and neck cancer. Radiotherapy and Oncology, 1, 53-63.

Pfister, D.G., McCaffrey, J., Zahalsky, A.J., Schwartz, G.K., Lis, E., Gerald, W., Huvos, A., Shah, J., Kraus, D., Shaha, A., Singh, B., Wolden, S., Zelefsky, M. and Palgi, I. (2002). A phase II trial of bryostatin-1 in patients with metastatic or recurrent squamous cell carcinoma of the head and neck. Investigational New Drugs, 20, 123-127.

Pulselli, R., Amadio, L., Fanciulli, M., and Floridi, A. (1996). Effect of lonidamine on the mitochondrial potential in situ in Ehrlich ascites tumor cells. Anticancer Research 16, 419-423.

Richter, C., Schweizer, M., Cossarizza, A. and Franceschi, C. (1996). Control of apoptosis by the cellular ATP level. FEBS Letters, 378, 107-110.

Rozhin, J., Sameni, M., Ziegler, G. and Sloane, B.F. (1994). Pericellular pH affects distribution and secretion of cathepsin B in malignant cells. Cancer Research, 54, 6517-6525.

Sanchez-Alcazar, J.A., Ruiz-Cabelo, J., Hernandez-Munoz.I., Pobre, P.S., de,laTore,P., Siles-Rivas, E., Garcia, I., Kaplan, O., Munoz-Hague, M.T. and Solis-Heruzzo, J.A. (1997). Tumor necrosis factor-alpha increases ATP content in metabolically inhibited L929 cells preceding cell death. Journal of Biological Chemistry, 272, 30167-30177.

Sauve, R., Diarra, A., Chahine, M., Simoneau, C., Morier, N. and Roy, G. (1991). $Ca^{2+}$ oscillations induced by histamine H1 receptor stimulation in Hela cells: Fura-2 and patch clamp analysis. Cell Calcium, 12, 165-176.

Schrüfer, E. (1995). Elektrische Messtechnick 6 Edition. Hanser publishing company.

Schwan, H.P. (1963). Determination of biological impedances. In Nastuk, W.L. (Ed) Physical Techniques in Biological Research. Electrophysiological Methods, part B. Academic Press, New York 6, 323-408.

Secomb, T.W., Hsu, R., Ong, E.T., Gross, J.F. and Dewhirst, M.W. (1995). Analysis of the effects of oxygen supply and demand on hypoxic fraction in tumors. Acta Oncologica (Stockholm, Sweden) 34, 313-316.

Semenza, G.L. (2000). Expression of hypoxia-inducible factor 1: Mechanism and consequences. Biochemical Pharmacology, 59, 47-53.

Serafino, A., Sinibaldi, V., Lazzarino, G., Tavazzi, B., Di, P., Rasi, G. and Ravagnan, G. Modifications of mitochondria in human tumor cells during anthracycline-induced apoptosis. Anticancer Research, 20, 3383-3394.

Sjaastad, M.D., Angres, B., Lewis, R.S., Nelson, W.J. (1994). Feedback regulation of cell-substratum adhesion by integrin-mediated intracellular $Ca^{2+}$ signaling. Proceedings of the National Academy of Science of the United States of America, 1691:17, 8214-8218.

Skog, S., Tribukait, B. and Sundius,G. (1982). Energy metabolism and ATP turnover time during the cell cycle of Ehrlich ascites tumour cells. Experimental Cell Research, 141, 23-29.

Slater, K. (2001). Cytotoxicity tests for high-throughput drug discovery. Current Opinion in Biotechnolgy, 12, 70-74.

Sood, C. and O'Brien, P.J. (1993). Molecular mechanisms of chloroacetaldehyde-induced cytotoxicity in isolated rat hepatocytes. Biochemical Pharmacology, 46, 1621-1626.

Stubbs, M., McSheehy, P.M.J. and Griffiths, J.R. (1999). Causes and consequences of acidic pH in tumors: A magnetic resonance study. Advances in Enzyme Regulation, 39, 13-30.

Tacev, T., Skricka, T., Zaloudik, J. and Pacovsky, Z. (2002). Preoperative hypoxyradiotherapy of colorectal carcinoma. Strahlenther Onkology, 178, 676-681.

Teicher, B.A. (1994). Hypoxia and drug resistance. Cancer Metastasis Reviews, 13, 139-168.

Thomas, R.C. (1989). Bicarbonate and pHi response. Nature, 337, 601.

Thompson, E.W., Paik, S., Brünner, N., Sommers, C.L., Zugmaier, G., Clarke, R., Shima, T.B., Torri, J., Donahue, S., Lippman, M.B., Martin, G.R. and Dickson, R.B. (1992). Association of increased basement membrane invasiveness with absence of estrogen receptor and expression of vimentin in human breast cancer cell lines. Journal of Cell Physiology, 150, 534-544.

Vanek, P.G. and Tunon, P. (2002): High Throughput Single-Cell Tracking in Real Time. Genetic Engineering News, 22, 34-38.

Vaupel, P.W.(1997). The influence of tumor blood flow and microenvironmental factors on the efficacy of radiation, drugs and localized hyperthermia. Klinische Pediatrie, 209, 243-249.

Vaupel, P. and Hockel, M. (2000). Blood supply, oxygenation status and metabolic micromilieu of breast cancers: characterization and therapeutic relevance. International Journal of Oncology, 17, 869-879.

Vaupel, P., Kelleher, D. and Hockel, M. (2001). Oxygenation status of malignant tumors: Pathogenesis of hypoxia and significance for tumor therapy. Seminars in Oncology, 28, 29-35.

Violin, J.D., Zhang, J., Tsien, R.Y. and Newton, A.C. (2003). A genetically encoded fluorescent reporter reveals oscillatory phosphorylation by protein kinase C. Journal of Cell Biology, 161, 899-909.

Walenta, S., Snyder, S., Haroon, Z.A., Braun, R.D., Amin, K., Brizel, D., Mueller-Klieser, W., Chance, B. and Dewhirst, M.W. (2001). Tissue gradients of energy metabolites mirror oxygen tension gradients in a rat mammary carcinoma model. International Journal of Radiation Oncology Biology Physics, 51, 840-848.

Walmsey A.R., Lowe, A.G. and Henderson, P.J. (1994). The kinetics and thermodynamics of the binding of cytochalasin B to sugar transporters. Eurpean Jornal of Biochemistry/FEBS 221, 513-229.

Warburg, O. (1930). The Metabolism of Tumors. London, Constable.

Wen, J., You, K.R., Lee, S.Y., Song, C.H. and Kim, D.G. (2002). Oxidative Stress-mediated Apoptosis. Journal of Biological Chemistry, 277, 38954-38964.

Wodnicka, M., Guarino R., Hemperly, J., Timmins, M., Stitt, D. and Bruce Pitner J. (2000): Novel fluorescent technology platform for high throughput cytotoxicity and proliferation assays. Journal of Biomolecular Screening, 5, 141-52.

Wolf, B., Kraus, M., Brischwein, M., Ehret, R., Baumann, W. and Lehman, M. (1998). Biofunctional hybrid structures - Cell-silicon-hybrids for application in biomedicine and bioinformatics. Bioelectrochemistry and Bioenergetics, 46, 215-225.

Zimmer, M. (2002). Green fluorescent protein (GFP): Applications, structure and related photophysical behavior. Chemical Reviews, 102, 759-81.

www.probes.com (web page-Molecular Probes)